Investigation of Mixed Mode Crack Initiation Angels under Different Loading Conditions

by

Shafique Mohammad Ahmed Khan

A Thesis Presented to the

FACULTY OF THE COLLEGE OF GRADUATE STUDIES

KING FAHD UNIVERSITY OF PETROLEUM & MINERALS

DHAHRAN, SAUDI ARABIA

In Partial Fulfillment of the
Requirements for the Degree of

MASTER OF SCIENCE

In

MECHANICAL ENGINEERING

December, 1999

INFORMATION TO USERS

This manuscript has been reproduced from the microfilm master. UMI films the text directly from the original or copy submitted. Thus, some thesis and dissertation copies are in typewriter face, while others may be from any type of computer printer.

The quality of this reproduction is dependent upon the quality of the copy submitted. Broken or indistinct print, colored or poor quality illustrations and photographs, print bleedthrough, substandard margins, and improper alignment can adversely affect reproduction.

In the unlikely event that the author did not send UMI a complete manuscript and there are missing pages, these will be noted. Also, if unauthorized copyright material had to be removed, a note will indicate the deletion.

Oversize materials (e.g., maps, drawings, charts) are reproduced by sectioning the original, beginning at the upper left-hand corner and continuing from left to right in equal sections with small overlaps.

Photographs included in the original manuscript have been reproduced xerographically in this copy. Higher quality 6" x 9" black and white photographic prints are available for any photographs or illustrations appearing in this copy for an additional charge. Contact UMI directly to order.

Bell & Howell Information and Learning
300 North Zeeb Road, Ann Arbor, MI 48106-1346 USA
800-521-0600

Investigation of Mixed Mode Crack Initiation Angles Under Different Loading Conditions

BY

Shafique Mohammad Ahmed Khan

A Thesis Presented to the

DEANSHIP OF GRADUATE STUDIES

KING FAHD UNIVERSITY OF PETROLEUM & MINERALS

DHAHRAN, SAUDI ARABIA

In Partial Fulfillment of the
Requirements for the Degree of

MASTER OF SCIENCE

In

MECHANICAL ENGINEERING

December 1999

KING FAHD UNIVERSITY OF PETROLEUM AND MINERALS

DHAHRAN, SAUDI ARABIA

DEANSHIP OF GRADUATE STUDIES

This thesis, written by

SHAFIQUE MOHAMMAD AHMED KHAN

under the direction of his Thesis Advisor and approved by his Thesis Committee, has been presented to and accepted by the Dean of the College of Graduate Studies, in partial fulfillment of the requirements for the degree of

MASTER OF SCIENCE IN MECHANICAL ENGINEERING

Thesis Committee

Dr. Marwan K. Khraisheh (Chairman)

Dr. Necar Merah (Member)

Dr. Mohammad N. Hamdan (Member)

22/12/1999

Dr. AbdulGhani A. Al-Farayedhi
Chairman, Mechanical Engineering

22-12-99

Dr. AbdAllah M. Al-Shehri
Dean, College of Graduate Studies

to my

grandparents

parents

sisters

and

brothers

Acknowledgements

I am extremely grateful to Allah, who alone made this accomplishment possible.

Acknowledgement is due to King Fahd University of Petroleum and Minerals for the support in carrying out this research.

I would like to express my deepest gratitude to my thesis advisor, Dr. Marwan K. Khraisheh for his constant help and guidance during the course of this work. The experience that I got while working with him is going to influence my future life. Thanks are due to members of my thesis committee, Dr. Necar Merah and Dr. Nader Hamdan for their cooperation and valuable suggestions.

I would like to thank Dr.Al-Farayedhi, Chairman ME, faculty members and graduate students of the department. Special thanks go to Mr. Farhan Hamid and Mr. Owais Iqbal.

Finally, I am grateful to my family for their extreme moral support, encouragement and patience during the course of my studies.

Contents

2. ANALYSIS OF MIXED MODE CRACK INITIATION ANGLES UNDER VARIOUS LOADING CONDITIONS

3. EFFECT OF THE CRACK TIP CORE REGION ON CRACK INITIATION ANGLES

List of Figures

List of Tables

Nomenclature

a	Half crack length
E	Elastic modulus
G	Modulus of rigidity
K	Stress intensity factor
I, II, III	Subscripts denoting mode of loading
I_1, I_2	First and second stress invariant respectively
r, θ	Polar co-ordinates at the crack tip
x, y	Cartesian co-ordinates at the crack tip
x', y'	Cartesian co-ordinates for applied stress
$\mathscr{G}$	Energy release rate
M	Stress triaxiality ratio
S	Strain energy density factor
T_v	Dilatational strain energy
T_D	Distortional strain energy
β	Crack inclination angle
θ_o	Crack initiation angle
α	Loading ratio for proportional tension-torsion loading
λ	Loading ratio for biaxial loading
μ	Ratio of stress intensity factors
ν	Poisson's ratio
σ_H	Hydrostatic stress
σ_{eq}	Equivalent stress

σ_n, τ_n	Normal & tangential stress at crack face
$\sigma_x, \sigma_y, \tau_{xy}$	Stresses at the crack tip
$\sigma_{x'}, \sigma_{y'}, \tau_{x'y'}$	Stresses applied to the cracked plate
σ_{YS}	Tensile yield strength
τ_{YS}	Shear yield strength
r_P	Radius of Mises elastic-plastic boundary
R_P	Non-dimensionlized radius of Mises elastic-plastic boundary
$r_{P,H}$	Radius of Hill's anisotropic elastic-plastic boundary
$R_{P,H}$	Non-dimensionlized radius of Hill's anisotropic elastic-plastic boundary
$f_{K_I}(\beta), f_{K_{II}}(\beta)$	Dimensionless function of β

ABSTRACT

Name	Shafique Mohammad Ahmed Khan
Thesis Title	Investigation of mixed mode crack initiation angles under different loading conditions
Major Field	Mechanical Engineering
Date of Degree	December 1999

With the recent advances in computation technology researchers around the globe are working to simulate the crack propagation. One of the key issues in predicting crack propagation path is the knowledge of the crack initiation angle. The study of crack initiation angles is also as much important in dealing with arresting the crack. A detailed analysis of mixed mode I-II crack initiation angles under different loading conditions is presented using different criteria, including the maximum tangential stress (MTS) criterion, minimum strain energy density (S) criterion, maximum dilatational strain energy (T) criterion, and the maximum triaxial stress (M) criterion. In addition, the MTS-criterion, which was proposed originally for brittle materials, is modified such that it can be used for ductile materials. A variable radius for the core region based on the von Mises yield function is introduced and incorporated in the formulation of the MTS-criterion.

The effects of the characteristics of the crack tip core region on the crack initiation angles are also investigated in details. A relation for the non-dimensional core region radius under mixed mode I-II has been developed, and the core region shapes are plotted for various loading conditions. The crack initiation angles, as predicted by different well-based criteria, show the trend of following the minima of the core region. Based on this observation a new criterion, the R-criterion, is proposed which shows better fit to the available experimental data. In addition, the R-criterion is also extended for anisotropic materials, by introducing Hill's anisotropic yield function. The limited available experimental data exhibits large scatter, and presents a need for standardization of the experimental setups. Therefore, the available experimental setups are summarized and some points are highlighted for future experimental investigations.

Master of Science Degree

King Fahd University of Petroleum and Minerals

Dhahran, Saudi Arabia

December 1999

الخلاصة

الاسم شفيق محمد أحمد خان

عنوان الرسالة استقصاء في نشأة تشقق ذات زوايا بشكل ممزوج عند حمولات مختلفة

التخصص هندسة ميكانيكية

تاريخ الشهادة ديسمبر ١٩٩٩

مع التطورات الحديثة التي تشهدها تقنية الحاسوب، عكف الباحثون في أنحاء المعمورة على بحث محاكاة انتشار التشقق. من أهم مصادر معرفة انتشار التشقق هي معرفة بداية زوايا التشقق. و تحظى دراسة بداية زوايا التشقق بنفس الاهتمام لإيقاف التشقق. نقدم هنا تفصيلاً بحثيا لنشأة زوايا التشقق بشكل ممزوج I-II عند حمولات مختلفة باستعمال عدة معايير منها معيار إجهاد التماس الأعظم، معيار كثافة طاقة التوتر الصغرى، معيار طاقة التمدد القصوى، و معيار الإجهاد الثلاثي المحاور الأعظم. بالإضافة، فانّ إجهاد التماس الأعظم الذي اقترح على المواد القصية حوّل بحيث أنه يمكن استعماله في المواد اللينة القابلة للتمطط. أدخل قطر متغير في لب المنطقة لدالة فون ميسس و أخذ بعين الاعتبار في صياغة معيار إجهاد التماس الأعظم.

كما بحث بالتفصيل آثار خواص التشقق عند طرف لب المنطقة و طورت علاقة بدون وحدات لقطر لب المنطقة بشكل ممزوج I-II، ورسمت أشكال اللب لعدة حمولات مختلفة. إن زوايا التشقق كما استنتجت بعدة معايير تدل على مزاولة الصغرى للب المنطقة. بناء على هذه الملاحظة يمكننا اقتراح معيار جديد، معيار R والذي يستحوذ على كل الأرقام الرقمية و المعدة سلفاً. بالإضافة يمكن امتداد هذا المعيار إلى مواد متباينة الخواص بإدخال دالة هيل المتباينة الخواص. إن البيانات السابقة تمثل تباينا كبيراً و علية فلا بد من وضع معايرة أو وحدة مقاييس بالنسبة للتجربة. و بناء علية فإنه ثم تلخيص التجارب المعملية و شرحت أهم الخطوات لعمليات تجريبية مستقبلية.

درجة الماجستير في العلوم

جامعة الملك فهد للبترول والمعادن

الظهران، المملكة العربية السعودية

ديسمبر ١٩٩٩

Chapter 1

PREAMBLE

1.1 Introduction

The field of fracture mechanics have been developed as a result of technological advancement in other fields of science and engineering. Whenever a man-made structure fails, a question arises: why did it fail? Has the structure completed its service life? or is it a premature failure? Several reasons can attribute to premature failure; poor design and fabrication, negligence during operation, and introduction of a new design or material.

A new design or material is applied to give better service, but some potential problems may be overlooked during design. An example of such a design is the failure of many Liberty ships during World War II. These were built with an all-welded hull, as opposed to the existing riveted construction at that time. Three factors attributed to the failure of Liberty ships; poor workmanship, local stress concentration at welds, and poor toughness of the steel used.

The concept of fracture mechanics developed during early research were applicable only to linear elastic materials, i.e., materials obeying Hooke's law. The branch is known as Linear Elastic Fracture Mechanics (LEFM). Later on, research was made to extend LEFM to include non-linear effects such as plasticity, viscoelasticity, viscoplasticity, and dynamic effects.

First of all it is necessary to understand fracture at the atomic level. A material fractures when the applied stress exceeds the cohesive strength between the atoms of the material. Cohesive strength σ_c is represented as(Anderson, 1991; Hertzberg, 1996):

$$\sigma_c = \sqrt{\frac{E\gamma_s}{a_o}} \tag{1.1}$$

where E is the Young's modulus, a_o is the equilibrium atomic spacing, and γ_s is the surface energy, defined as the energy required for the formation of one surface. Fracture energy is defined as the energy required for a fracture to occur. Since two new surfaces are created when a material fractures, so the fracture energy is equal to $2\gamma_s$. Eq. 1.1 shows the cohesive strength of a material, but experimental fracture strengths are typically three to four order of magnitude below this value.

Griffith(1921) was the first person who explained the discrepancy between theoretical and experimental results by assuming the existence of cracks or defects in the material. Griffith invoked the first law of thermodynamics and based his model on a global energy balance. It states that fracture will occur when the energy stored in the structure

overcomes the surface energy of the material. According to Griffith model, fracture stress σ_f is given by:

$$\sigma_f = \sqrt{\frac{2E\gamma_s}{\pi a}} \tag{1.2}$$

where a is the half crack length. This equation is valid only for through thickness crack in an infinitely wide plate of an ideally brittle solid subjected to a remote tensile stress. Griffith verified the theoretical prediction through experiments on glass. Griffith equation can be generalized to be applicable to other materials by replacing γ_s by w_f (Anderson, 1991):

$$\sigma_f = \sqrt{\frac{2Ew_f}{\pi a}} \tag{1.3}$$

where w_f is the fracture energy, that may include plastic, viscoelastic or viscoplastic effects.

The concept of the energy release rate $\mathcal{G}$ and the stress intensity factor K has been widely used in LEFM to study the behavior of cracks. The energy release rate $\mathcal{G}$ is defined as the measure of the energy available for an increment of crack extension. If the crack extends by an amount da under a load displacement δ, then the work done by an external body force P is $Pd\delta$, and the release of strain energy is dV, then: (Hertzberg, 1996)

$$\mathcal{G} = \frac{dU}{da} = P\frac{d\delta}{da} - \frac{dV}{da} \tag{1.4}$$

where U is the potential energy of body with crack. $\mathcal{G}$ is independent of the type of load application, e.g., fixed grip, constant load. The term rate as it is used in this context does not refer to a derivative with respect to time; $\mathcal{G}$ is the rate of change in potential energy with crack area.

Stress intensity factor K is developed in order to find closed form expressions for the stresses at the crack tip. The general form of stress field in a linear elastic cracked body is given by:(Anderson)

$$\sigma_{ij} = \left(\frac{k}{\sqrt{r}}\right) f_{ij}(\theta) + \text{other terms} \qquad (1.5)$$

where $K = k\sqrt{2\pi}$, k is a constant, σ_{ij} is the stress tensor, r and θ are the polar co-ordinate with origin at the crack tip, and f_{ij} is a dimensionless function of θ. Higher order terms are geometry dependent, but the leading term always contains $1/\sqrt{r}$. As $r \to 0$, $\sigma_{ij} \to \infty$, thus Eq. 1.5 represents a stress singularity in absence of other terms, which remain finite or approach zero. The stress intensity factor defines the amplitude of the crack tip singularity. This means that the stresses near the crack tip are proportional to stress intensity factor, and it completely defines the crack tip conditions in LEFM. K is given a subscript I, II, III to denote the mode of loading. The three modes of loading are (Fig. 1.1):

Mode I: The opening mode, where the load is applied normal to the crack plane, and it tends to open the crack.

Mode II: The sliding mode, where in-plane shear loading is applied to the crack and it tends to slide the crack surfaces over one another in a direction perpendicular to the leading edge of the crack.

Mode III: The tearing mode, where out-of-plane shear loading is applied to the crack and it tends to move the crack surfaces relative to one another and parallel to the leading edge of the crack.

$\mathcal{G}$ describes global behavior and K is a local parameter. For linear elastic materials, K and $\mathcal{G}$ are uniquely related. For mode I:

$$\mathcal{G} = \frac{K_I^2}{E} \tag{1.6}$$

Recently Awaji(1998) has extended Griffith criterion for mode II loading, and obtained following relationship:

$$\mathcal{G} = \frac{3K_{II}^2}{2E} \tag{1.7}$$

After defining a stress-field at the crack tip using the stress intensity factors, the next step is to study crack behavior under this stress field. Under which conditions does a crack start to grow? What is the initial angle of crack extension? What is the subsequent path until fracture? Can a crack be arrested at a stage of its growth? If not, then what is the critical crack length? Among these the most important is the initiation of a crack growth. With the advances in computation technology, researchers around the globe are working to simulate the crack propagation path. This is being done using numerical methods such

as FEM, BEM in conjunction with computer. One cannot predict the fracture path without studying the initial crack extension angle. The study of the crack initiation angles is also as much important in dealing with arresting the crack. Much work has been done to predict the crack initiation angle under mixed-mode loading for uniaxial loading. However there is not much work in terms of different loading conditions. Moreover, discrepancies are present between the experimental data and the theoretical prediction.

1.2 Statement of the Problem

Stress field and stress-intensity factors play a vital role in linear elastic fracture mechanics, and several researchers have worked in this respect to define these for different crack configurations. Williams(1957) was the first to demonstrate the universal nature of the $1/\sqrt{r}$ singularity for the elastic crack problems, although the results for specific configurations were already found. Williams started by considering stresses at the corner of a plate, with various included angles. The specific case when included angle of the plate corner is zero, gives the solution for a crack.

Kassir and Sih(1966) and Hartranft and Sih(1977) got the stress distribution at the crack front in 3D space. By using proper choice of the co-ordinates, Hartranft and Sih showed that a much simplified stress function can be obtained in 3D.

Several criteria have been proposed for predicting the crack initiation angles. All of these available criteria can be classified on the basis of the critical parameter used to define the criterion. This parameter may be critical value of stress, energy, or strain. Using stress as a critical parameter, the maximum tangential stress criterion (MTS-criterion) is the first criterion proposed by Erdogan and Sih(1963). In order to support their theory, Erdogan

and Sih(1963) performed experiments using brittle plexiglass plates. Their results show a good agreement with theoretical predictions for the uniaxial loading. Maiti and Smith(1983) criticized the MTS-criterion and gave the concept of zero shear stress. Both these criteria are equivalent if the singular elastic stress field at the crack tip is used. Kong et al.(1995) proposed the maximum triaxial stress criterion (M-criterion). Kong et al.(1995) performed experiments using steel specimen at low temperature to ensure K-controlled fracture. Griffith(1921) was the first person who proposed his classical model based on energy, but it assumes the direction of crack initiation as a priori. Hussain et al.(1974) extended the G-criterion for mixed mode I-II based on Griffith-Irwin energy principal, and described it using the maximum value of the energy release rate, $\mathcal{G}$. Sih(1973,1974) presented the strain energy density criterion (S-criterion). It also shows good agreement with the experimental results obtained earlier by Erdogan and Sih(1963) for brittle plexiglass specimen. S-criterion depends on the Poisson's ratio. The T-criterion was proposed by Theocaris et al.(1982) and it uses the maximum value of dilatational strain energy to define the crack initiation angle. Theocaris et al.(1982) performed experiments using polycarbonate (PCBA) specimen to get results for ductile fracture. Their experimental results shows good agreement with the theoretical prediction. Ukadgaonker and Awasare(1995) presented the T-criterion in a new form using the first and second stress invariants. Vallejo(1987) performed experiments under uniaxial compression using kaolinite clay, and showed that the MTS-criterion matches well with the experimental data for brittle fracture under compression. Zengtao(1994) has pointed out that for criteria depending upon the material properties, the difference in such

properties between the material at the crack tip and the matrix should be taken into account.

All of these criteria use Linear Elastic Fracture Mechanics (LEFM) and assumed a core region at the crack tip. The core region represents a highly strained region, and the stress state cannot be defined in this region using LEFM. Hence the boundary of the core region serves to separate the outside material assumed to behave elastically from the inside material whose physical behavior is unknown. There are two possible ways to assume the shape of the core region, use a constant radius or variable radius. The MTS, M, and the S-criterion assume constant crack tip core region and the T-criterion and the criterion presented by Ukadgaonker and Awasare(1995) assume a variable radius for the crack tip core region. Several investigators (Williams and Ewing, 1972; Ewing and Williams, 1974; Maiti and Smith, 1983) have shown the dependence of the crack initiation angles on the radius of the core region. Theocaris et al.(1982) and Ukadgaonker and Awasare(1995) used the variable radius for the core region based on von Mises yield function. However, there is not enough discussion on characteristics of the core region and its relation to crack initiation angles.

While comparing the different available criteria with the limited available experimental data, we find no one perfect criteria that fits the experimental results. The T-criterion, based on a variable core region radius, is derived for ductile fracture, whereas the M-criterion, based on a constant core region radius, is derived for brittle fracture, however, the predictions by both criteria match exactly. This needs clarification. No or very little effort has been done to investigate the available criteria under different loading conditions. The experimental data from two different sources (Theocaris et al., 1982;

Kong et al., 1995) and two different material behavior (ductile and brittle) show scatter in the same region. A detailed experimental investigation is much needed. In addition, the effect of the characteristics such as the actual size and shape of the core region at the crack tip also needs attention.

1.3 Objectives

The main goal of this research is to investigate certain issues that have not been addressed in analyzing mixed mode crack initiation angles. As observed through literature review a number of criteria are proposed, however these have not been compared rigorously under different loading conditions. In addition, the correlation of crack tip core region with crack initiation angles has not been investigated thoroughly under various loading conditions.

The main objectives of this research are:

1) Investigate the different criteria for mixed mode crack initiation angles under various loading conditions including uniaxial, pure shear, biaxial, and proportional tension-torsion loading.

2) Investigate the effect of crack tip core region on the mixed mode crack initiation angles under several loading conditions.

3) Develop a new/better criterion that is based on the physics of the crack tip condition.

4) Investigate the possible extension of new criterion towards including anisotropic behavior of materials.

5) Examine the experimental set ups and the problems associated with the design of experiments for measuring the mixed mode crack initiation angle.

1.4 Thesis Layout

The thesis has been divided into six chapters. The first chapter describes the objectives of this study.

The second chapter analyzes the different available criteria for mixed mode crack initiation angles under various loading conditions, including uniaxial, pure shear, biaxial, and proportional tension torsion loading. Detailed discussion of each criterion is presented. The study includes how to derive and solve the equations for each criterion. The different criteria are compared with available experimental data for uniaxial and pure shear loading. The MTS-criterion, that was originally defined using a constant core region, is modified using a variable radius for the crack tip core region.

The third chapter presents the investigation of the crack tip core regions, under various loading conditions, using von Mises yield flow rule. Detailed discussion is presented on how to develop the relation for the dimensionless crack tip core region radius under mixed mode (I-II) loading. The core region shapes for various loading conditions are compared with the predicted crack initiation angles by different criteria, based on which a new criterion is presented. This new criterion, the R-criterion is based on the physics of the crack tip core region. The R-criterion is presented for both the plane stress and plane strain cases.

The fourth chapter discusses the application of the R-criterion to the anisotropy. The anisotropic R-criterion is presented for both the plane stress and plane strain case. The

results are presented with the crack tip core region shapes, for different magnitudes of anisotropy.

The fifth chapter examines the experimental setups used for studying the crack initiation angles under mixed mode loading. A comparison is made between different experimental techniques used by different researchers. Some suggestions are presented that are believed to enhance the credibility of the experimental results.

The sixth chapter presents the conclusions and recommendations of this research.

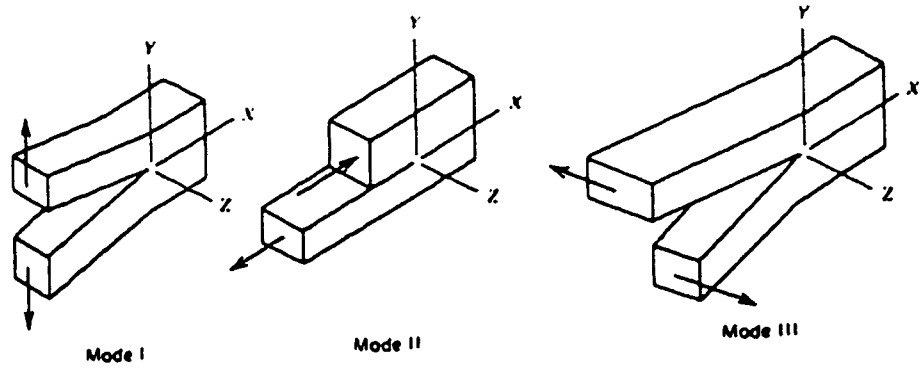

Figure 1.1: The three modes of loading

Chapter 2

Analysis of Mixed Mode Crack Initiation Angles under Various Loading Conditions

2.1 Introduction

The problem involving mixed mode fracture has been extensively investigated during the past three decades, and several criteria have been proposed for predicting crack initiation angles. The criteria presented so far can be grouped under three headings: stress-based criteria, energy-based criteria, and strain-based criteria. The critical condition refers to one of the extremum of the stated parameter, i.e., stress, energy, or strain. The most commonly used criteria are the ones based on stress and energy as the critical parameter, hence we are going to use these criteria only, for our analysis.

The first criterion for fracture initiation was proposed by Griffith(1921). It states that fracture occurs when the energy stored in the structure overcomes the surface energy of the material. This criterion is defined for mode-I loading only and it assumes the direction of crack initiation as a priori. Hussain et al.(1974) extended the G-criterion for

mixed mode I-II based on the Griffith-Irwin energy principle, and showed that crack initiation occurs in the direction of the maximum value of the energy release rate. However, Hussain et al.(1974) based the G-criterion on the assumption that the crack under combined loading moves along its own initial plane, and assumed that the combined energy release rate $\mathcal{G}$ is given by:

$$\mathcal{G} = \frac{1}{E}\left(K_I^2 + K_{II}^2\right) \tag{2.1}$$

which is obviously fictitious as also indicated by Sih(1974). Awaji(1998) have presented energy release rate under combined mode loading, and extended the Griffith energy criterion to mode II fracture (See Eq. (1.7)).

Using the stress as a parameter, the maximum tangential stress ($\sigma_{\theta,max}$) criterion was first presented by Erdogan and Sih(1963). They are the first who studied the slant crack problem for mixed mode (I-II) loading. A through thickness crack is assumed to render $K_{III} = 0$. This criterion states that a crack initiates in a direction corresponding to the direction of maximum tangential stress (MTS-criterion) along a constant radius around the crack tip. The MTS-criterion is based on the assumption that the material behaves ideally brittle.

Erdogan and Sih(1963) also performed uniaxial tensile experiments to support their theory. They used plexiglass specimen, which is a good approximation to a homogeneous, isotropic, and linearly elastic brittle material. The results show a good agreement between the theoretical predictions and the experimental results. Vallejo(1987) performed mixed mode fracture experiments under uniaxial compression, for both brittle

and ductile states. Vallejo(1987) used kaolinite clay samples and stated that a sample with water content less than 20% behaves in a brittle manner. Vallejo showed strong agreement between the theoretical predictions by MTS-criterion and the experimental data for brittle material under uniaxial compression. Selcuk et al.(1994) employed the MTS-criterion for their study of interfacial crack path using a direct boundary integral approach. They performed experiments on anodically bonded silicon/Pyrex glass compact-tension specimen, which is a brittle material. Recently, Plank and Kuhn(1999) have also used the MTS-criterion for their study of fatigue crack propagation under non-proportional mixed mode loading. However, they performed experiments on aluminum alloys, which are ductile materials.

Maiti and Smith(1983) criticized the MTS-criterion and gave the concept of zero shear stress ($\tau_{r\theta} = 0$) . Both criteria (MTS and zero shear stress) are equivalent for the first term representation of the stress function given by Williams(1957). Since we will use the same first term representation of the function, therefore, the MTS and zero shear stress criterion will give the same results, and only the MTS-criterion will be considered in present analysis.

The second stress criterion is the maximum stress triaxiality criterion (M-criterion) presented by Kong et al.(1995). It states that the direction of initial crack extension coincides with the direction of maximum stress triaxiality along a constant radius around the crack tip. Stress triaxiality is defined as the ratio of the hydrostatic stress to the equivalent stress. Although Kong et al.(1995) defined it as "triaxial stress", however, it must be defined as "stress triaxiality ratio". Kong et al.(1995) also performed experiments

to check the theoretical predictions. They used steel specimen at low temperature (-140°C), with high loading speed (50 mm/sec) to ensure K-controlled brittle fracture.

Sih(1973,1974) presented the minimum strain energy density criterion (S-criterion). It states that the direction of crack initiation coincides with the direction of minimum strain energy density, along a constant radius around the crack tip. The region within this constant radius is known as the core region, and it is assumed that LEFM does not hold in this core region. S-criterion is the only one that shows dependence of crack initiation angle on the material elastic properties represented by the Poisson's ratio, ν and the state of the stress. It shows good agreement with the experimental data for brittle plexiglass material(Sih, 1973; Erdogan and Sih, 1963) for $\nu = 1/3$. Kipp and Sih(1975) applied the S-criterion to notched elastic solids. They considered plane elliptical crack under remote tension and compression, and determined the fracture trajectories. Gdoutos(1984) compiled a book that discusses the application of the S-criterion to various crack configurations.

The T-criterion was proposed by Theocaris et al.(1982). They modified the S-criterion by using a variable radius for the core region. They assumed the core region to be a local plastic region around the crack tip and used r-Mises as the elastic-plastic-boundary. Since distortional strain energy is constant along r-Mises, this criterion states that crack initiates in the direction of maximum dilatational strain energy along the contour of constant distortional strain energy. Although the T-criterion is obtained by modifying the S-criterion, it does not depend on the material elastic properties (Poisson's ratio ν) or the state of the stress. In order to support their criterion, Theocaris et al.(1982) also

performed experiments on polycarbonate (PCBA) specimen. The theoretical predictions based on the T-criterion are in good agreement with the experimental data for ductile fracture. Ukadgaonker and Awasare(1995) presented the T-criterion in a new form using the first and the second stress invariants.

When the different criteria are compared with the limited available experimental results for uniaxial and pure shear loading cases, none of the criterion can fit the experimental data for all the cases. Moreover, the T-criterion and the M-criterion match exactly, however both were derived on different theoretical basis. In addition, these available criteria have not been discussed under different loading conditions rigorously. In this chapter, we present a detailed analysis of mixed mode crack initiation angles under different loading conditions using available criteria, and compare the results with the available experimental data. Different loading conditions include: uniaxial tension, uniaxial compression, pure shear, biaxial, and proportional tension-torsion. In addition, the MTS criterion is modified by including a variable radius core region at the crack tip to make it applicable for ductile materials.

2.2 Analysis

The basic angled crack problem is shown in Fig. 2.1. The crack is oriented at an angle β (inclination angle) measured clockwise to the direction of the load. The crack initiation is assumed to occur at an angle $-\theta_o$, measured clockwise. The length of the crack is $2a$. All the criteria that we are going to analyze depend on the stress field existing just before the onset of crack propagation. Defining r and θ as in Fig. 2.2a, the stress field at the crack tip in Cartesian co-ordinates is defined as (refer to Anderson, 1991)

$$\sigma_x = \frac{1}{\sqrt{2\pi r}}\left[\left\{K_I \cos\frac{\theta}{2}\left(1-\sin\frac{\theta}{2}\sin\frac{3\theta}{2}\right)\right\}-\left\{K_{II}\sin\frac{\theta}{2}\left(2+\cos\frac{\theta}{2}\cos\frac{3\theta}{2}\right)\right\}\right]$$

$$\sigma_y = \frac{1}{\sqrt{2\pi r}}\left[\left\{K_I \cos\frac{\theta}{2}\left(1+\sin\frac{\theta}{2}\sin\frac{3\theta}{2}\right)\right\}+\left\{K_{II}\sin\frac{\theta}{2}\cos\frac{\theta}{2}\cos\frac{3\theta}{2}\right\}\right]$$

$$\tau_{xy} = \frac{1}{\sqrt{2\pi r}}\left[\left\{K_I \cos\frac{\theta}{2}\sin\frac{\theta}{2}\cos\frac{3\theta}{2}\right\}+\left\{K_{II}\cos\frac{\theta}{2}\left(1-\sin\frac{\theta}{2}\sin\frac{3\theta}{2}\right)\right\}\right] \qquad (2.2)$$

$$\sigma_z = \nu(\sigma_x + \sigma_y) \quad \text{For plane strain}$$

$$\sigma_z = 0 \quad \text{For plane stress}$$

Referring to Fig. 2.2b, the stress field at the crack tip in polar co-ordinates is defined as (refer to Williams, 1984)

$$\sigma_\theta = \frac{1}{\sqrt{2\pi r}}\left[\left\{\frac{K_I}{2}\cos\frac{\theta}{2}(1+\cos\theta)\right\}-\left\{\frac{3K_{II}}{2}\sin\frac{\theta}{2}(1+\cos\theta)\right\}\right]$$

$$\sigma_r = \frac{1}{\sqrt{2\pi r}}\left[\left\{\frac{K_I}{2}\cos\frac{\theta}{2}(3-\cos\theta)\right\}-\left\{\frac{K_{II}}{2}\sin\frac{\theta}{2}(1-3\cos\theta)\right\}\right] \qquad (2.3)$$

$$\tau_{r\theta} = \frac{1}{\sqrt{2\pi r}}\left[\left\{\frac{K_I}{2}\sin\frac{\theta}{2}(1+\cos\theta)\right\}-\left\{\frac{K_{II}}{2}\cos\frac{\theta}{2}(1-3\cos\theta)\right\}\right]$$

2.2.1 Crack Initiation Criteria

2.2.1.1 MTS-criterion (Sih, 1963)

MTS-criterion is the simplest of all, and it states that direction of crack initiation coincides with the direction of the maximum tangential stress along a constant radius around the crack tip. It can be stated mathematically as:

$$\frac{\partial\sigma_\theta}{\partial\theta} = 0$$

$$\frac{\partial^2\sigma_\theta}{\partial\theta^2} < 0 \qquad (2.4)$$

Using the stress field (Eq. (2.3)) in polar co-ordinates and applying the MTS-criterion, we get the following equation:

$$\begin{aligned} &\tan^2\frac{\theta}{2}-\frac{\mu}{2}\tan\frac{\theta}{2}-\frac{1}{2}=0 \\ &-\frac{3}{2}\left[\left(\frac{1}{2}\cos^3\frac{\theta}{2}-\cos\frac{\theta}{2}\sin^2\frac{\theta}{2}\right)+\frac{1}{\mu}\left(\sin^3\frac{\theta}{2}-\frac{7}{2}\sin\frac{\theta}{2}\cos^3\frac{\theta}{2}\right)\right]<0 \end{aligned} \tag{2.5}$$

where μ is defined as:

$$\mu=\frac{K_I}{K_{II}} \tag{2.6}$$

The zero shear stress criterion (Maiti and Smith, 1983) will give the same results for the singular elastic solution used (Eq. (2.3)).

2.2.1.2 M-*criterion (Kong et al., 1995)*

M-criterion states that the direction of crack initiation coincides with the direction of maximum stress triaxiality ratio along a constant radius around the crack tip. M-criterion can be stated mathematically as:

$$\begin{aligned} &\frac{\partial M}{\partial\theta}=0 \\ &\frac{\partial^2 M}{\partial\theta^2}<0 \end{aligned} \tag{2.7}$$

Where M is the Stress triaxiality ratio, defined as:

$$M=\frac{\sigma_H}{\sigma_{eq}} \tag{2.8}$$

where σ_H is the hydrostatic stress and σ_{eq} is the equivalent stress. Kong et al.(1995) used von Mises equivalent stress.

The hydrostatic stress is given by: (using the stress field in Eq. (2.2) for plane strain condition)

$$\sigma_H = \frac{\sigma_x + \sigma_y + \sigma_z}{3} = \frac{2(1+\nu)}{3\sqrt{2\pi r}}\left[K_I \cos\frac{\theta}{2} - K_{II}\sin\frac{\theta}{2}\right] \tag{2.9}$$

The von Mises equivalent stress for plane strain condition at the crack tip, is given by:

$$\begin{aligned}\sigma_{eq} &= \left[\frac{(\sigma_x-\sigma_y)^2+(\sigma_y-\sigma_z)^2+(\sigma_z-\sigma_x)^2+6\tau_{xy}^2}{2}\right]^{\frac{1}{2}} \\ &= \frac{1}{\sqrt{2}\sqrt{2\pi r}}\left[\left(\frac{3}{2}K_I^2-\frac{9}{2}K_{II}^2\right)\sin^2\theta+\left(2(1-2\nu)^2K_I^2+6K_{II}^2\right)\cos^2\frac{\theta}{2}+\right. \\ &\qquad \left. 8(1-\nu+\nu^2)K_{II}^2\sin^2\frac{\theta}{2}+K_IK_{II}\left(3\sin 2\theta-2(1-2\nu)^2\sin\theta\right)\right]^{\frac{1}{2}}\end{aligned} \tag{2.10}$$

Applying the M-criterion, we get the following equation:

$$\begin{aligned}&\tan^4\frac{\theta}{2}-3\mu\tan^3\frac{\theta}{2}-(1-2\mu^2)\tan^2\frac{\theta}{2}+\frac{1}{2}(1-\mu^2)\mu\tan\frac{\theta}{2}-\frac{1}{2}(1+\mu^2)=0 \\ &[2(\mu^2+5)]\sin\frac{\theta}{2}+[27(\mu^2+1)]\sin\frac{3\theta}{2}+[5(5\mu^2-3)]\sin\frac{5\theta}{2} \\ &\quad -[2(\mu^2+5)\mu]\cos\frac{\theta}{2}-[9(\mu^2+1)\mu]\cos\frac{3\theta}{2}-[5(\mu^2-7)\mu]\cos\frac{5\theta}{2}<0\end{aligned} \tag{2.11}$$

where μ is defined in Eq. (2.6). Although plane strain formulation is done here, yet plane stress formulation gives the same results.

2.2.1.3 S-criterion (Sih, 1973,1974)

S-criterion states that the direction of crack initiation coincides with the direction of minimum strain energy density along a constant radius around the crack tip. In mathematical form, S-criterion can be stated as:

$$\frac{\partial S}{\partial \theta} = 0 \qquad \frac{\partial^2 S}{\partial \theta^2} > 0 \tag{2.12}$$

Where S is the strain energy density factor, defined as:

$$S = r_o \frac{dW}{dV} \tag{2.13}$$

where dW/dV is the strain energy density function per unit volume, and r_o is a finite distance from the point of failure initiation. For slit cracks, the crack tip is assumed to be the point of failure initiation. Using the stress field (Eq. (2.2)) in Cartesian co-ordinates, we can obtain the strain energy density function per unit volume, and then using Eq. (2.13), we can write the strain energy density function as:

$$S = a_{11}K_I^2 + 2a_{12}K_I K_{II} + a_{22}K_{II}^2 \tag{2.14}$$

where the factors a_{ij} are functions of the angle θ, and are defined as:

$$a_{11} = \frac{1}{16G\pi}[(1+\cos\theta)(\kappa-\cos\theta)]$$
$$a_{12} = \frac{1}{16G\pi}\sin\theta[2\cos\theta-(\kappa-1)] \qquad (2.15)$$
$$a_{22} = \frac{1}{16G\pi}[(\kappa+1)(1-\cos\theta)+(1+\cos\theta)(3\cos\theta-1)]$$

where G is the modulus of Rigidity, and κ is a constant depending upon stress state, and is defined as:

$$\kappa = \frac{(3-\nu)}{(1+\nu)} \quad \text{for plane stress} \qquad (2.16a)$$

$$\kappa = (3-4\nu) \quad \text{for plane strain} \qquad (2.16b)$$

From Eqs. (2.12, 2.14, 2.15) we get:

$$[2(1+\kappa)\mu]\tan^4\frac{\theta}{2}+[2\kappa(1-\mu^2)-2\mu^2+10]\tan^3\frac{\theta}{2}-24\mu\tan^2\frac{\theta}{2}$$
$$+[2\kappa(1-\mu^2)+6\mu^2-14]\tan\frac{\theta}{2}+2(3-\kappa)\mu=0 \qquad (2.17)$$
$$[2(\kappa-1)\mu]\sin\theta-8\mu\sin 2\theta+[(\kappa-1)(1-\mu^2)]\cos\theta+[2(\mu^2-3)]\cos 2\theta>0$$

where μ is defined as in Eq. (2.6).

2.2.1.4 T-criterion (Theocaris et al., 1982)

T-criterion states that direction of crack initiation coincides with the direction of maximum dilatational strain energy density along the contour of constant distortional strain energy around the crack tip. T-criterion uses elastic plastic boundary as given by von Mises flow rule, to define the radius of the core region at the crack tip. In mathematical form, T-criterion can be stated as:

$$\frac{\partial T_v}{\partial \theta} = 0$$
$$\frac{\partial^2 T_v}{\partial \theta^2} < 0 \tag{2.18}$$

where T_v is the dilatational strain energy, defined as:

$$T_v = \frac{(1-2\nu)}{6E}(\sigma_x + \sigma_y)^2 \tag{2.19}$$

The distortional strain energy T_D, is given by:

$$T_D = \frac{(1+\nu)}{3E}(\sigma_x^2 + \sigma_y^2 - \sigma_x\sigma_y + 3\tau_{xy}^2) \tag{2.20}$$

The relations for T_v and T_D are used for plane stress condition, however the results are the same for plane strain condition.

Now defining $f_x(\theta), f_y(\theta), f_{xy}(\theta)$ as:

$$f_x(\theta) = \left[\left\{K_I \cos\frac{\theta}{2}\left(1 - \sin\frac{\theta}{2}\sin\frac{3\theta}{2}\right)\right\} - \left\{K_{II}\sin\frac{\theta}{2}\left(2 + \cos\frac{\theta}{2}\cos\frac{3\theta}{2}\right)\right\}\right]$$
$$f_y(\theta) = \left[\left\{K_I \cos\frac{\theta}{2}\left(1 + \sin\frac{\theta}{2}\sin\frac{3\theta}{2}\right)\right\} + \left\{K_{II}\sin\frac{\theta}{2}\cos\frac{\theta}{2}\cos\frac{3\theta}{2}\right\}\right] \tag{2.21}$$
$$f_{xy}(\theta) = \left[\left\{K_I \cos\frac{\theta}{2}\sin\frac{\theta}{2}\cos\frac{3\theta}{2}\right\} + \left\{K_{II}\cos\frac{\theta}{2}\left(1 - \sin\frac{\theta}{2}\sin\frac{3\theta}{2}\right)\right\}\right]$$

We get the stress field in Cartesian co-ordinates:

$$\sigma_x = \frac{1}{\sqrt{2\pi r}} f_x(\theta)$$
$$\sigma_y = \frac{1}{\sqrt{2\pi r}} f_y(\theta) \qquad (2.22)$$
$$\sigma_{xy} = \frac{1}{\sqrt{2\pi r}} f_{xy}(\theta)$$

Using this notation, we obtain from Eq. (2.19,2.20), respectively:

$$T_v = \frac{(1-2\nu)}{12\pi E r}\left(f_x + f_y\right)^2 \qquad (2.23)$$

$$T_D = \frac{(1+\nu)}{6\pi E r}\left(f_x^2 + f_y^2 - f_x f_y + 3f_{xy}^2\right) \qquad (2.24)$$

Since the distortional strain energy is constant along the Mises elastic plastic boundary, $T_{D,o}$ can be considered as a material constant. Combining Eqs. (2.23, 2.24), we get:

$$r = \frac{(1+\nu)}{6\pi E T_{D,o}}\left(f_x^2 + f_y^2 - f_x f_y + 3f_{xy}^2\right) \qquad (2.25)$$

$$T_v = \frac{(1-2\nu)T_{D,o}}{2(1-\nu)} \frac{\left(f_x + f_y\right)^2}{\left(f_x^2 + f_y^2 - f_x f_y + 3f_{xy}^2\right)} \qquad (2.26)$$

Applying the T-criterion, to Eq. (2.26), we get:

$$\tan^5\frac{\theta}{2} - 4\mu\tan^4\frac{\theta}{2} + \left(5\mu^2 - 1\right)\tan^3\frac{\theta}{2} + \frac{\left(3-5\mu^2\right)\mu}{2}\tan^2\frac{\theta}{2} + \frac{\left(\mu^4 - 2\mu^2 - 1\right)}{2}\tan\frac{\theta}{2} + \frac{\left(1+\mu^2\right)\mu}{2} = 0 \qquad (2.27)$$

$$\left[1 - 20\mu^2 - 5\mu^4\right]\cos\theta + \left[8\left(3 + 2\mu^2 - \mu^4\right)\right]\cos 2\theta - \left[3\left(3 - 12\mu^2 + \mu^4\right)\right]\cos 3\theta + \left[2\left(13 + 5\mu^2\right)\mu\right]\sin\theta + \left[32\left(1+\mu^2\right)\mu\right]\sin 2\theta - \left[6\left(5 - 3\mu^2\right)\mu\right]\sin 3\theta < 0$$

where μ is defined as in Eq. (2.6).

2.2.1.5 I_P-criterion (Ukadgaonker and Awasare, 1995)

Although Ukadgaonker and Awasare(1995) suggested that they have presented a new criterion, however their formulation is only a new representation of the T-criterion in terms of the first and the second stress invariants. They defined I_P as:

$$I_P = \left[I_1^2 - 2I_2\right] \tag{2.28}$$

where I_1 and I_2 are the first and the second stress invariants. I_P-criterion postulates that crack will propagate along the direction defined by a maximum value of I_P along the elastic-plastic boundary defined by von Mises. Mathematically, I_P-criterion can be stated as:

$$\frac{\partial I_P}{\partial \theta} = 0 \qquad \frac{\partial^2 I_P}{\partial \theta^2} < 0 \tag{2.29}$$

When this criterion is applied, the final equation comes out to be the same as for the T-criterion (Eq. (2.27)). So this criterion will not be shown in results in the following sections.

2.2.2 Stress Intensity Factors

To solve the equations for the crack initiation angles defined above (Eqs. (2.5, 2.11, 2.17, 2.27)), we need to have expressions for the stress intensity factors for the angled crack

problem for different loading conditions. General forms of stress intensity factors are given by:

$$K_I = \sigma_n \sqrt{\pi a}$$
$$K_{II} = \tau_n \sqrt{\pi a} \tag{2.30}$$

Where σ_n and τ_n are the normal and the tangential stresses to the crack plane respectively, as illustrated in Fig. 2.3. To obtain expressions for σ_n and τ_n for the slant crack problem, the most general loading case is considered (Fig. 2.3):

$$\sigma_n = \sigma_{x'} \cos^2 \beta + \sigma_{y'} \sin^2 \beta - \tau_{x'y'} \sin 2\beta$$
$$\tau_n = \frac{(\sigma_{y'} - \sigma_{x'})}{2} \sin 2\beta - \tau_{x'y'} \cos 2\beta \tag{2.31}$$

Eqs. (2.30, 2.31) will be used to get the stress intensity factors for various loading conditions as explained below.

2.2.2.1 Uniaxial Loading

For uniaxial loading (Fig. 2.1 and 2.3)

$$\sigma_{x'} = 0 \qquad \sigma_{y'} = \sigma \qquad \tau_{x'y'} = 0$$

From Eq. (2.31):

$$K_I = \sigma \sin^2 \beta \sqrt{\pi a}$$
$$K_{II} = \sigma \sin \beta \cos \beta \sqrt{\pi a} \tag{2.32}$$

These expressions for uniaxial case are the same as represented by Sih et al.(1962), so we can safely extend our analysis to other loading conditions, using the general representation in Eq. (2.31).

Using these stress intensity factors for uniaxial loading, Fortran programs are developed to find the roots of the equation for each criterion. The real roots are separated from complex roots, and tested for extremum condition. These roots are then written in separate files.

Since the equation for the MTS-criterion is of second degree, two roots are obtained. The roots that yield maximum tangential stress are for uniaxial tension case. Whereas the roots that yield minimum tangential stress are for uniaxial compression case, since for uniaxial compression, σ is to be replaced by $-\sigma$ (in this case positive roots will also yield maximum tangential stress). The roots for uniaxial tension are negative, and those for uniaxial compression are positive.

For the S-criterion, we get four roots; two are complex conjugates and two are real. One set of the real roots (negative ones) is for uniaxial tension, and the other set of the real roots (positive ones) is for uniaxial compression. Both roots for uniaxial tension and compression yield minimum strain energy density. This is contrary to the MTS-criterion, where one set of the roots yields maximum value and the other set yields minimum value. Since the quantity S depends on σ^2, the solution is for both uniaxial tension $(+\sigma)$ and uniaxial compression $(-\sigma)$, as indicated by Sih(1974).

Since stress triaxiality ratio also depends on σ (involved in σ_H) and not on σ^2, therefore, the same reasoning in interpreting the roots is also valid for the M-criterion as for the MTS-criterion. The negative real roots yield maximum stress triaxiality ratio and the positive real roots yield minimum stress triaxiality ratio. The other two roots are complex conjugate.

For the T-criterion, we obtain five roots; two complex conjugate and three real roots. Out of the real roots, one set (negative ones) is for uniaxial tension. Another set (positive ones) is for uniaxial compression. Since T_v depends upon σ^2, hence both roots for uniaxial tension and compression yield maximum dilatational strain energy (T_v). The third real root does not present data of engineering significance.

Same reasoning for interpreting the roots for each criterion will be extended to other loading cases.

2.2.2.2 Pure Shear

For pure shear (Fig. 2.3)

$$\sigma_{x'} = 0 \qquad \sigma_{y'} = 0 \qquad \tau_{x'y'} = \tau$$

and

$$\begin{aligned} K_I &= -\tau \sin 2\beta \sqrt{\pi a} \\ K_{II} &= -\tau \cos 2\beta \sqrt{\pi a} \end{aligned} \qquad (2.33)$$

We get two sets of valid real roots for each of the four criteria. For the MTS and M criteria, one set of the real roots yields maximum value, and the other set yields minimum

value of the tangential stress and stress triaxiality ratio, respectively. Whereas for the S and T criteria, both sets of the real roots yield minimum strain energy density and maximum dilatational strain energy, respectively. This is due to the same reason explained in the case of uniaxial loading, that the expressions for the MTS and M criteria involve σ, and the expressions for the S and T criteria involve σ^2. Negative roots are for the shear stress direction shown in Fig. 2.3 and 2.6, whereas positive roots are for the case shown in Fig. 2.7, where the direction of the shear stress is reversed. The sign of Eq. (2.33) will be both positive, if we use the other sign convention for shear stresses.

2.2.2.3 Biaxial Loading

For proportional biaxial loading (Fig. 2.3)

$$\sigma_{yy} = \lambda\sigma \qquad \sigma_{xx} = \sigma \qquad \tau_{xy} = 0$$

and

$$\begin{aligned} K_I &= \sigma\left(\sin^2\beta + \lambda\cos^2\beta\right)\sqrt{\pi a} \\ K_{II} &= \sigma(1-\lambda)\sin\beta\cos\beta\sqrt{\pi a} \end{aligned} \tag{2.34}$$

$\lambda = 0$ implies uniaxial tension

$\lambda > 0$ implies biaxial tension

$\lambda < 0$ implies tension on y-axis and compression on x-axis

As with the case of pure shear loading, two sets of valid real roots for each of the four criteria are obtained. These sets of roots yield either maximum or minimum values of the related quantity for the criterion (e.g., tangential stress, stress triaxiality ratio, strain

energy density, dilatational strain energy) that depend upon whether the quantity involves σ or σ^2. The negative real roots are for the directions of stress shown in Fig. 2.3, whereas the positive real roots are for the case where the directions of all the stresses are reversed in Eq. (2.34). The directions of all stresses are shown with each plot to avoid confusion.

2.2.2.4 Proportional Tension-Torsion Loading

Assuming proportional normal and shear strain loading (Fig. 2.3) $\varepsilon = \eta\gamma$, we get $\tau = \frac{G}{\eta E}\sigma$, where E and G are the modulus of elasticity and modulus of rigidity, respectively, and η is the proportionality constant. So for proportional tension-torsion loading, we get:

$$\sigma_{x'} = 0 \qquad \sigma_{y'} = \sigma \qquad \tau_{x'y'} = \alpha\sigma \qquad \alpha = G/\eta E$$

and

$$\begin{aligned} K_I &= \sigma(\sin^2\beta - \alpha \sin 2\beta)\sqrt{\pi a} \\ K_{II} &= \sigma(\sin\beta\cos\beta - \alpha\cos 2\beta)\sqrt{\pi a} \end{aligned} \tag{2.35}$$

For each criteria, we get two sets of valid real roots. The negative real roots are for the direction shown in Fig. 2.3, and the positive real roots are for the case where the signs of the applied stresses are reversed in Eq. (2.35). These roots for different criteria may yield maximum or minimum values in a similar manner as for other loading cases depending on the involvement of σ or σ^2.

2.3 Results and Discussion

The results obtained for different loading cases are shown in Fig. 2.4 through Fig. 2.17. The results for the S-criterion are for Poisson's ratio of 1/3. The results for the M- and T-criteria match exactly for all the loading cases, although the T-criterion is believed to be for ductile materials and the M-criterion for brittle materials. This is due to the similarity in the equations of M and T_V for the two criteria. If we take the square of M (Eq. (2.8)) and ignore the constants (since these are going to be zero after differentiation) then the RHS of both equations for M and T_V becomes the same. Since the M-criterion is based on a constant radius core region, and the T-criterion is based on a variable (Mises) radius core region, and the results of both criteria match exactly, one may wrongly conclude that there is no effect of the crack tip core region on crack initiation angles. However, this is not true as different studies (Maiti and Smith, 1983; Williams and Ewing, 1972; Ewing and Williams, 1974) have shown dependence of crack initiation angles on crack tip core region. The discrepancy can be cleared out by considering the formulation of the M-criterion. For the M-criterion, the radius r (one of polar co-ordinates) cancels out (Eq. (2.8)), and since both criteria use von Mises flow rule, similar results were obtained. The difference between M and T-criteria shown by Kong et al.(1995) in their paper, is because they didn't plotted the theoretical results for the M-criterion, and they plotted experimental results for their work.

Fig. 2.4 shows the results for uniaxial tension. Three sets of experimental data are also plotted for comparison. The data from Erdogan and Sih(1963) is for brittle material, and it shows good agreement with both MTS and S-criteria (plane stress and plane strain) for crack inclination angles greater than 30°, whereas the data from Kong et al.(1995) is also

for brittle material, and it shows better agreement with the M and T-criteria. Yet another set of experimental data from Williams and Ewing(1972) (not shown here for clarity) is also for brittle material and it also shows favor to M and T-criteria. The experimental points for crack initiation angle tends to be -90° at $\beta = 0^\circ$. Williams and Ewing(1972) used polymethylmethacrylate (PMMA) sheets for tests for which Poisson's ratio is 0.43(Ewing et al., 1976). The S-criterion gives $\theta_o = -90^\circ$ for plane strain and $\theta_o = -83.6^\circ$ for plane stress at $\beta = 0^\circ$ and $\nu = 0.5$. So the experimental data also shows agreement with the S-criterion at low inclination angles. Kong et al.(1995) performed experiments on steel at low temperature(-140°). Poisson's ratio for steels is usually between 0.3-0.35, yet the experimental data shows the same behavior as for PMMA(Williams and Ewing, 1972). The only experimental data available for ductile material under uniaxial tension is for polycarbonate (PCBA) by Theocaris et al.(1982). This data also shows scatter in the same area. Since Poisson's ratio for PCBA is 0.38, it also shows agreement with the S-criterion at lower limits. So the experimental data available so far does not favor any criterion especially at low inclination angles. Experimental data and techniques need to be scrutinized carefully.

Fig. 2.5 shows the results for uniaxial compression. There is not much experimental data available, and the shown data is from Vallejo(1987), who performed experiments using kaolinite clay. Water content greater than 20% implies ductile behavior. The MTS-criterion is in excellent agreement between $\beta = 0^\circ \sim 65^\circ$ with the experimental points for brittle material only. For ductile behavior, the experimental points shift towards lower crack initiation angles. However, the theoretical results (M and T-criteria) shift towards higher crack initiation angles.

Fig. 2.6 shows the results for pure shear case. At an inclination angle of 45°, the resultant shear stress τ_n vanishes on the crack face, and only the principal stress σ_n is acting. If this stress is tensile, then the crack will open and if this stress is compressive then the crack will close. Due to symmetry, the initiation angles at $\beta = 0^{\circ}$ and $\beta = 90^{\circ}$ are the same, this shows that the present theoretical analysis is correct. The validity of present analysis can also be checked with the results shown by Ewing and Williams(1974) and by Sih(1974), for $\beta = 0^{\circ}$. The only experimental data available is from Ewing and Williams(1974) for experiments performed using PMMA specimen. The experimental points are very much scattered and do not favor any criterion for $0^{\circ}<\beta<45^{\circ}$. For $45^{\circ}<\beta<90^{\circ}$ these points favor the M and T-criteria. Although the M and T-criteria are for ductile behavior and PMMA is a brittle material, yet the experimental data favors the M and T criteria.

In order to understand the non-symmetry observed for pure shear results (Fig. 2.6 and 2.7), it is important to understand the behavior under uniaxial loading case. For uniaxial tension, both the resultant stresses σ_n and τ_n, normal and parallel to the crack face, are positive, whereas for uniaxial compression case, both the resultant stresses are negative. For the results of pure shear case, the behavior for $0^{\circ}<\beta<45^{\circ}$ is the same as for uniaxial tension, since both σ_n and τ_n have the same sign, whereas from $45^{\circ}<\beta<90^{\circ}$, only τ_n changes sign, so the behavior goes like mirrored uniaxial compression. Fig. 2.7 shows the other set of roots obtained for pure shear case, when the direction of the applied shear stress is reversed. The two cases are interchangeable depending on the sign convention used for tangential stress.

The results for biaxial loading are comparable with the results shown by Chang(1982) for biaxial loading for $\lambda = -10 \sim +10$. Fig. 2.8 shows the results for biaxial loading with $\lambda = -0.5$. At $\beta = 0^o$, the crack tends to close as the compressive stress becomes normal to the crack plane. At $\beta = 90^o$, the crack tends to open due to the tensile stress. The behavior is similar to uniaxial tension for $35^o<\beta<90^o$, and similar to mirrored uniaxial compression for $0^o<\beta<35^o$. This can be explained as follows. First, the sign of both σ_n and τ_n become positive after $\beta \cong 35^o$, and for $\beta < 35^o$ σ_n is negative. Second, since the tensile stress is more than the compressive stress in magnitude, it has stronger influence over larger range of β than the compressive stress. Fig. 2.9 shows the other set of roots. For this case, the crack opens at $\beta = 0^o$ and closes at $\beta = 90^o$. Also for the range $0^o<\beta<35^o$, the behavior is like mirrored uniaxial tension, and for $\beta>35^o$ it is like mirrored uniaxial compression.

Fig. 2.10 and Fig. 2.11 show the results for biaxial loading for $\lambda = -1.0$. These are similar to the results for $\lambda = -0.5$ except that the graph is shifted towards lower initiation angles. Also the transition between tensile and compressive behavior occurs at $\beta = 45^o$, which is quite obvious for equal tension and compression stresses. This angle is unique for a particular value of β, and at this inclination angle the values for crack initiation angles are the same as for uniaxial tension or uniaxial compression at $\beta = 0^o$.

Fig. 2.12 and Fig. 2.13 show the results for biaxial loading for $\lambda = 0.5$. The maximum initiation angle occurs at $\beta = 35^o$. This is due to the same reason as for biaxial loading for $\lambda = -0.5$. If both stresses (σ_n and τ_n) are tensile then the crack opens at $\beta = 0^o$ and 90^o, whereas if both stresses are compressive then the crack closes at $\beta = 0^o$ and 90^o.

For $\lambda = 1.0$, employing equal tension or equal compression, the crack will always open at 0^o for equal tension and will always close for equal compression, for any inclination angle. This is due to the fact that in both cases, shear stress at the crack face is always zero, and normal stress is either σ (for tensile case) or $-\sigma$ (for compressive case).

Fig. 2.14 shows the results for proportional tension-torsion loading for $\alpha = -0.5$. These results are similar to pure shear case, but the line of zero shear stress has moved to $\beta = 67.5^o$, due to the inclusion of a tensile stress. For $0^o<\beta<67.5^o$, both σ_n and τ_n have the same sign, hence similar to uniaxial tension, and for $67.5^o<\beta<90^o$, τ_n changes sign so the results are similar to mirrored uniaxial compression. Fig. 2.15 shows the results obtained for the other set of roots.

Fig. 2.16 and Fig. 2.17 show the results obtained for proportional tension-torsion loading with $\alpha = 0.5$. The position of zero shear stress has been moved to $\beta = 22.5^o$.

2.4 Modified MTS-criterion

Many researchers (e.g., Selcuk et al., 1994; Plank and Kuhn, 1999) used the MTS-criterion to determine the crack initiation angle for the study of crack propagation without giving any regard to the nature of the materials used in the study. The MTS-criterion have been found to be good for brittle fracture. Plank and Kuhn(1999) performed experiments on Aluminum alloys and used the MTS-criterion. It seems necessary to modify the MTS-criterion to make it applicable to ductile materials. In order to achieve that a variable radius for the plastic core region will be introduced and incorporated in the formulation

of the criterion. The von Mises yield criterion will be used for determining the variable radius.

Using the stress field (Eq. (2.3)) in polar co-ordinates, we get:

$$\begin{aligned}\sigma_\theta &= \frac{1}{2\sqrt{2\pi r}} f_\theta(\theta) \\ \sigma_r &= \frac{1}{2\sqrt{2\pi r}} f_r(\theta) \\ \tau_{r\theta} &= \frac{1}{2\sqrt{2\pi r}} f_{r\theta}(\theta)\end{aligned} \tag{2.36}$$

where

$$\begin{aligned}f_\theta(\theta) &= \left[\left\{K_I \cos\frac{\theta}{2}(1+\cos\theta)\right\} - \left\{3K_{II}\sin\frac{\theta}{2}(1+\cos\theta)\right\}\right] \\ f_r(\theta) &= \left[\left\{K_I \cos\frac{\theta}{2}(3-\cos\theta)\right\} - \left\{K_{II}\sin\frac{\theta}{2}(1-3\cos\theta)\right\}\right] \\ f_{r\theta}(\theta) &= \left[\left\{K_I \sin\frac{\theta}{2}(1+\cos\theta)\right\} - \left\{K_{II}\cos\frac{\theta}{2}(1-3\cos\theta)\right\}\right]\end{aligned} \tag{2.37}$$

Using the von Mises yield criterion with Eqs. (2.36, 2.37), we get:

$$r = \frac{(1+\nu)}{24\pi E T_{D,o}}\left(f_r^2 + f_\theta^2 - f_r f_\theta + 3f_{r\theta}^2\right) \tag{2.38}$$

where r is the radius of the core region and $T_{D,o}$ is the distortional strain energy that is constant along the elastic plastic boundary. Using this equation with the equation for the tangential stress (Eq. (2.36)), we get:

$$\sigma_\theta = \sqrt{\frac{3ET_{D,o}}{(1+\nu)}} \frac{f_\theta}{\left(f_r^2 + f_\theta^2 - f_r f_\theta + 3f_{r\theta}^2\right)^{1/2}} \tag{2.39}$$

Applying the MTS-criterion to Eq. (2.39), we get the equation for the modified MTS-criterion,

$$\begin{aligned} &12\tan^6\frac{\theta}{2} - 24\mu\tan^5\frac{\theta}{2} + \left[3+16\mu^2\right]\tan^4\frac{\theta}{2} - \left[\left(5+4\mu^2\right)\mu\right]\tan^3\frac{\theta}{2} \\ &\qquad + 3\mu^2\tan^2\frac{\theta}{2} - \frac{\left[\left(7+5\mu^2\right)\mu\right]}{2}\tan\frac{\theta}{2} - \frac{\left[9+5\mu^2\right]}{2} = 0 \\ &\left[177+49\mu^2\right]\sin\frac{\theta}{2} + \left[1269+621\mu^2\right]\sin\frac{3\theta}{2} - \left[255-425\mu^2\right]\sin\frac{5\theta}{2} \\ &+ \left[189-147\mu^2\right]\sin\frac{7\theta}{2} - \left[\left(305+49\mu^2\right)\mu\right]\cos\frac{\theta}{2} - \left[\left(423+207\mu^2\right)\mu\right]\cos\frac{3\theta}{2} \\ &\qquad + \left[\left(595-85\mu^2\right)\mu\right]\cos\frac{5\theta}{2} - \left[\left(315-21\mu^2\right)\mu\right]\cos\frac{7\theta}{2} < 0 \end{aligned} \tag{2.40}$$

Four out of the six roots obtained from Eq. (2.40) are complex conjugate, and the two real roots are analyzed in the same manner as for the MTS-criterion.

The modified MTS-criterion is plotted for all loading cases in Fig. 2.4 through Fig. 2.17. The crack initiation angles shift towards higher values as compared to the original MTS-criterion, when variable radius is applied for the plastic core region. This behavior is similar to that of the T-criterion in comparison with the S-criterion, since the T-criterion was obtained by introducing a variable radius for the core region in the formulation of the S-criterion. The radius r appears in the denominator for equations of critical parameter (such as strain energy or tangential stress) for all the criteria. When a dimensionless function of polar angle θ is introduced in place of radius r, it causes the absolute values of crack initiation angles to rise. For uniaxial tension and compression, the difference

between the MTS and the Modified MTS-criteria is more pronounced. For uniaxial tension, the modified MTS-criterion gives a better fit to the experimental data for ductile materials, especially at small inclination angles. For pure shear case, the modified MTS-criterion proves itself to be a better candidate to fit the experimental data as compared to the MTS-criterion. However, since there is a large scatter in the limited available experimental data, no definite conclusions can be drawn without extensive experimental studies on brittle and ductile materials.

2.5 Conclusions

A detailed analysis of mixed mode crack initiation angles under various loading conditions as encountered in real problems is presented in this study. The following can be concluded:

1. The limited available experimental data is very much scattered and sometimes contradictory as for ductile and brittle behavior. The experimental results do not favor any criterion over the other for all loading conditions. A detailed experimental investigation is very much needed. For uniaxial tension, the experimental results are in somewhat good agreement with most criteria for higher crack inclination angles. For low inclination angles, no particular criterion is favored. For uniaxial compression, the MTS criterion seems suitable for brittle materials, but there is an anomaly for ductile behavior between experimental and theoretical results. No experimental data is available for other loading condition (except a single experimental study for pure shear) and one cannot decide in favor of a particular criterion.

2. The crack behavior under various loading conditions was explained based on the understanding of the crack behavior under uniaxial loading. The crack's initial extension mainly depends on the direction of the resultant stresses, normal and tangential to the crack face.

3. The MTS-criterion was modified by incorporating a variable-radius plastic core region at the crack tip. The von Mises flow rule was used. The proposed modified MTS criterion can be used for ductile materials. For uniaxial tension and pure shear loading cases, the modified MTS-criterion presented a better fit to the experimental data than the original MTS-criterion. However, the original MTS-criterion presented a better fit than the modified one for uniaxial compression.

4. After thorough examination of the available criteria, there are "variables" that we believe have a strong influence on crack initiation angles, but were not considered. These may include: elastic properties of the material (except for Poisson's ratio which is considered in the S-criterion) and the initial crack length (in mixed mode fracture, the ratio of stress intensity factors is used and the effect of crack length does not appear in the final equation for crack initiation angles).

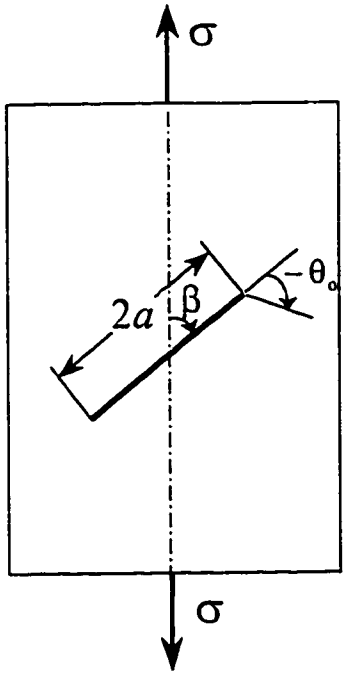

Fig. 2.1: Uniaxial loading

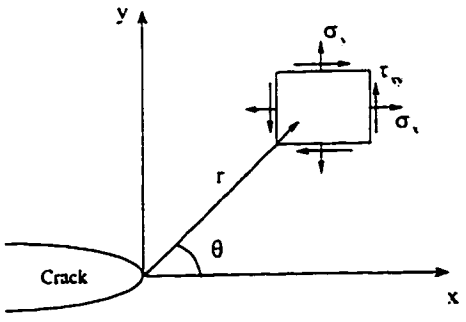

Fig. 2.2a: Stress field in Cartesian co-ordinate system

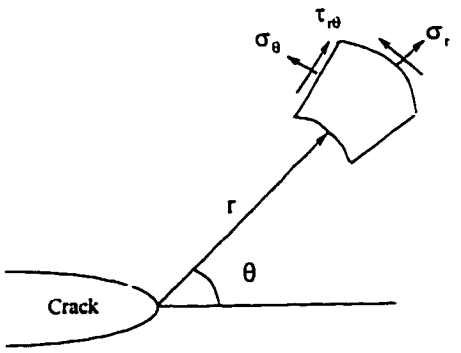

Fig. 2.2b: Stress field in polar co-ordinate system

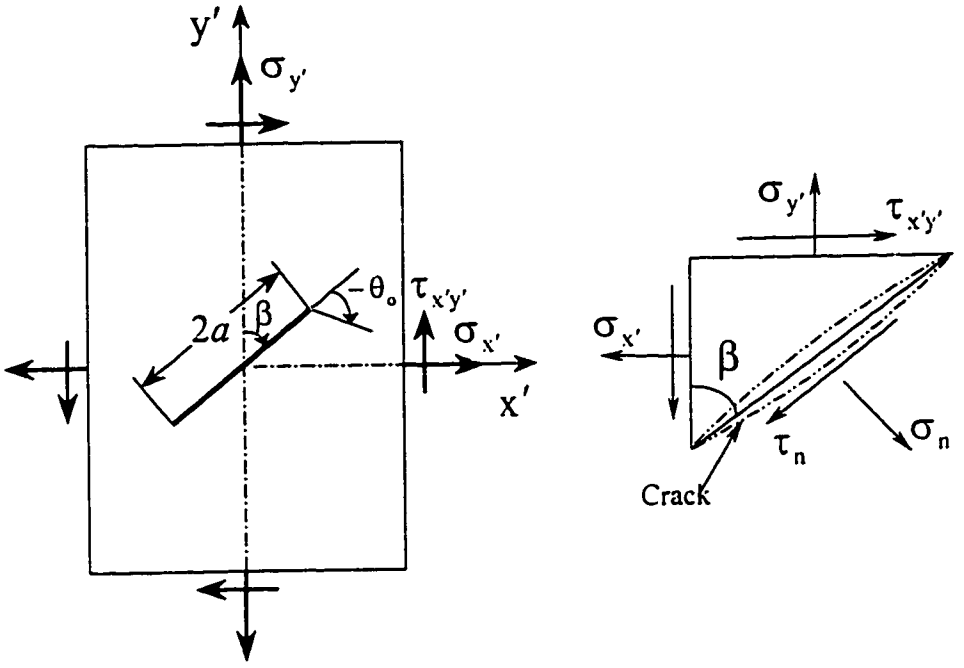

Fig. 2.3: General loading condition for angled crack

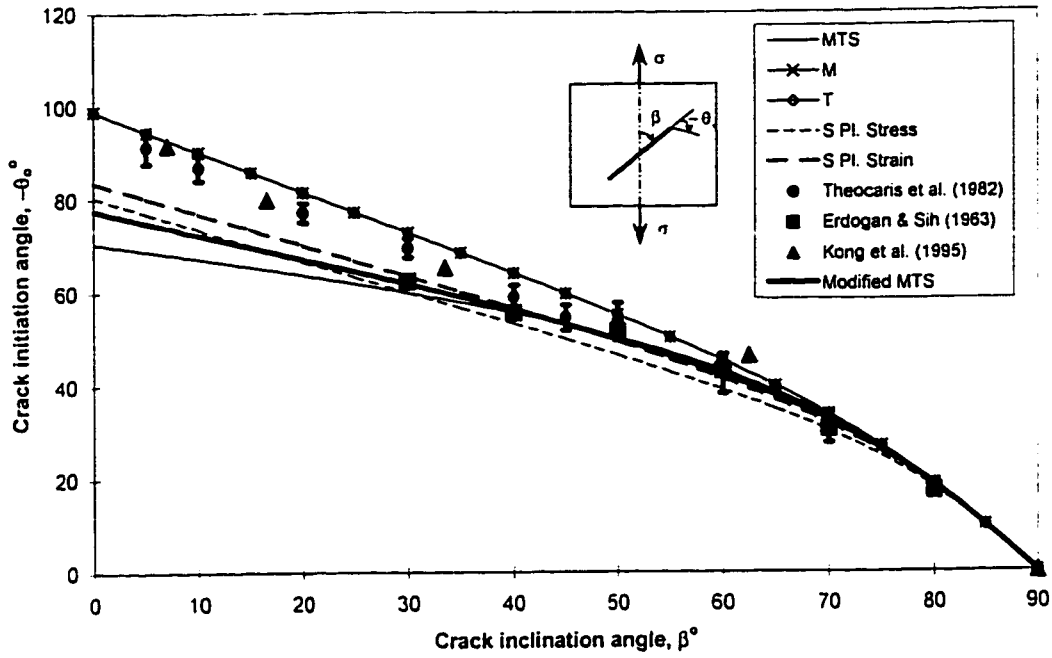

Fig. 2.4: Uniaxial tension (negative roots)

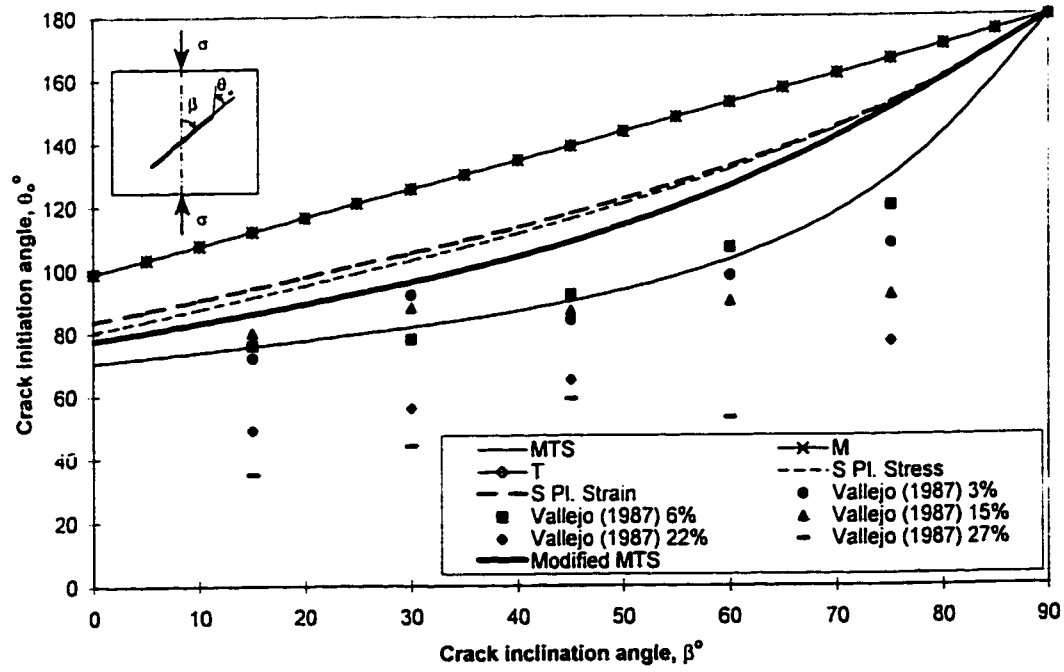

Fig. 2.5: Uniaxial compression (positive roots)

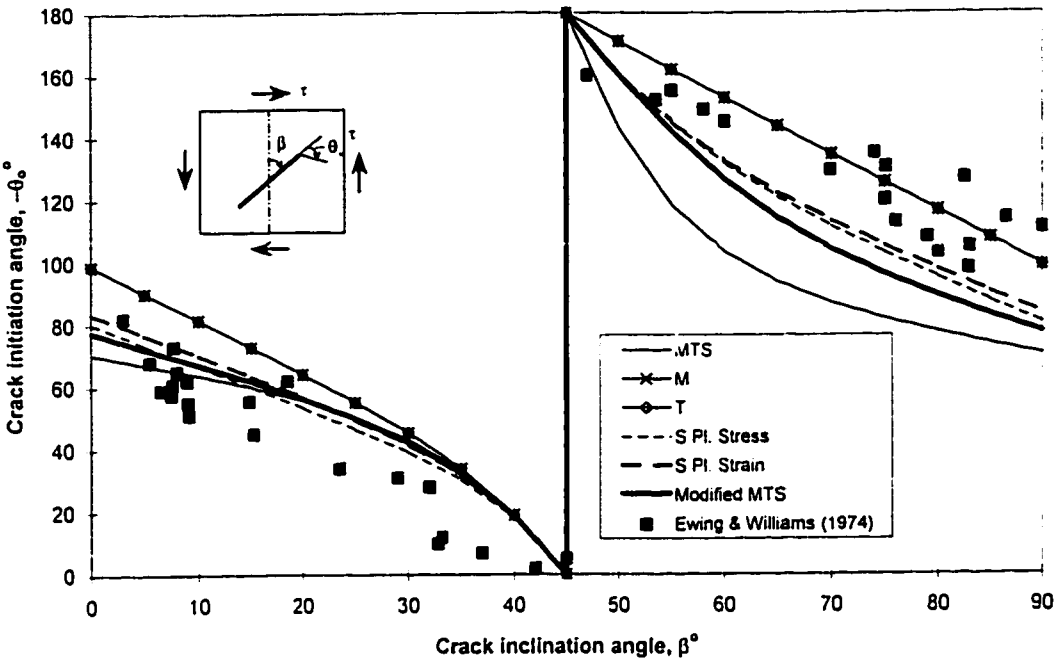

Fig. 2.6: Pure shear loading, negative roots

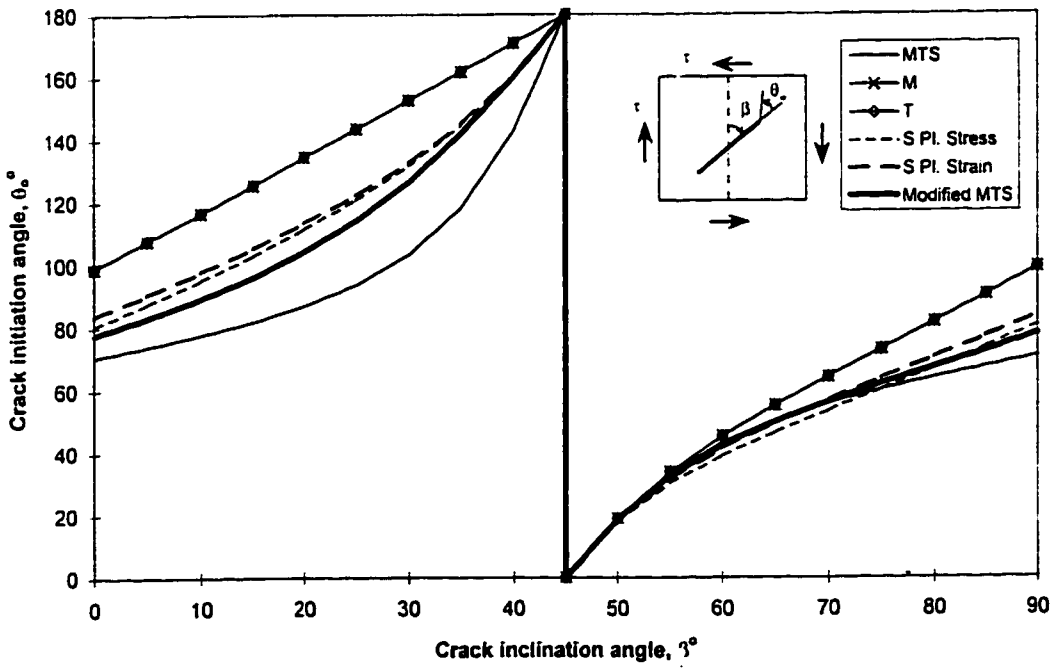

Fig. 2.7: Pure shear loading, positive roots

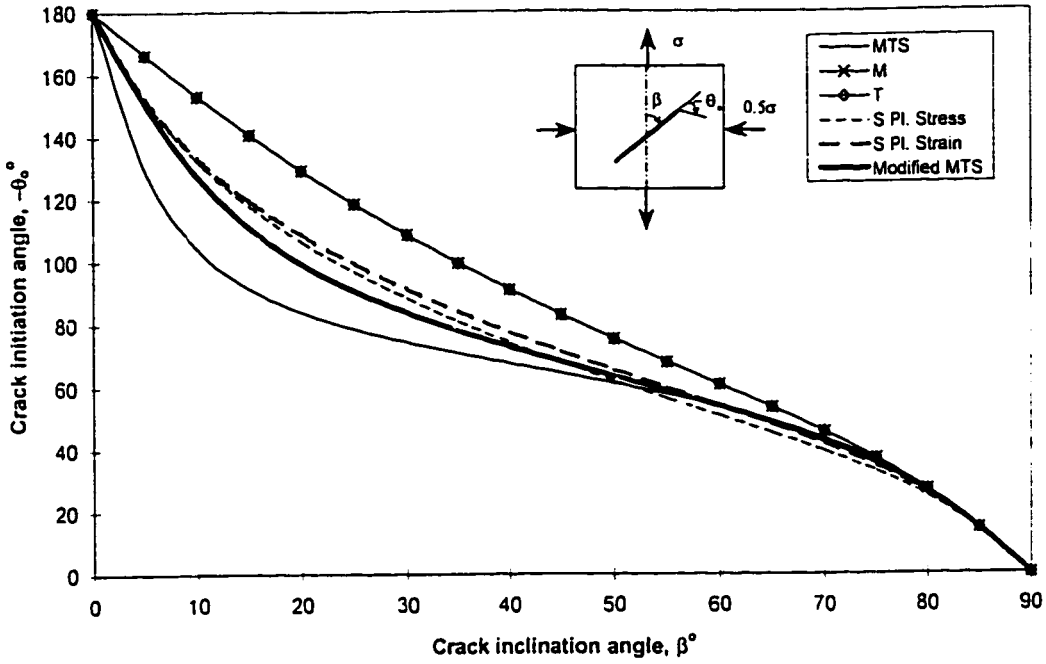

Fig. 2.8: Biaxial loading $\lambda = -0.5$, negative roots

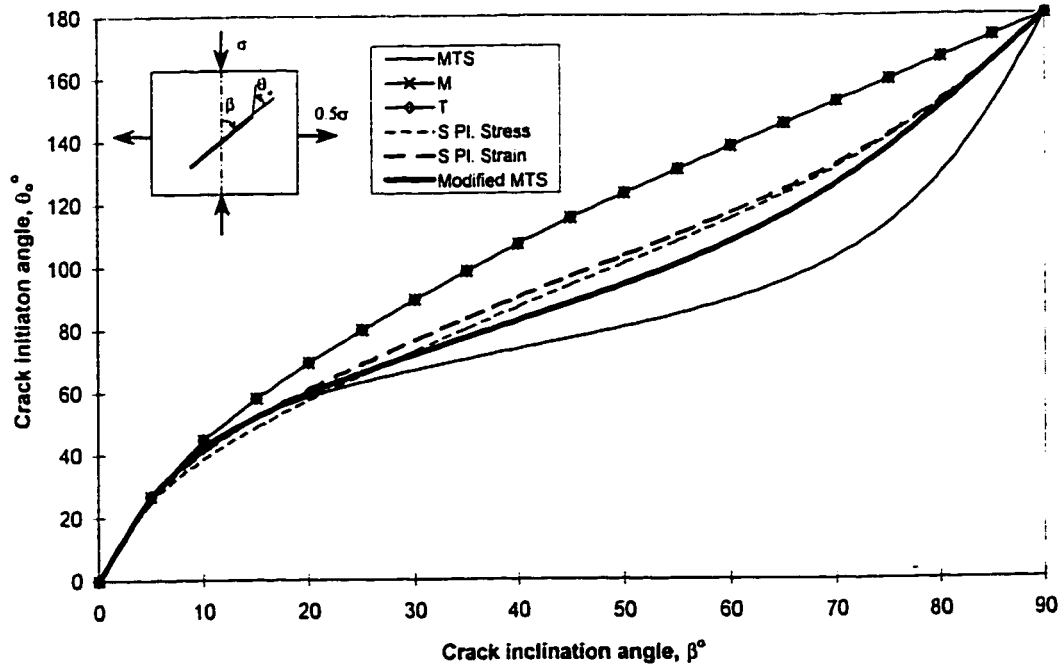

Fig. 2.9: Biaxial loading $\lambda = -0.5$, positive roots

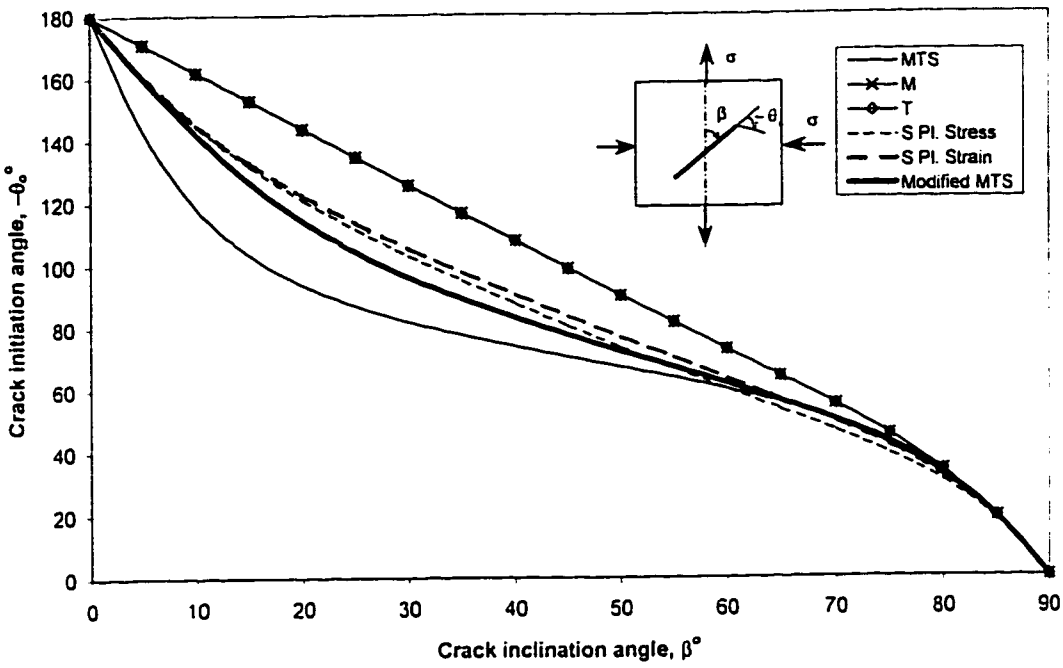

Fig. 2.10: Biaxial loading $\lambda = -1.0$, negative roots

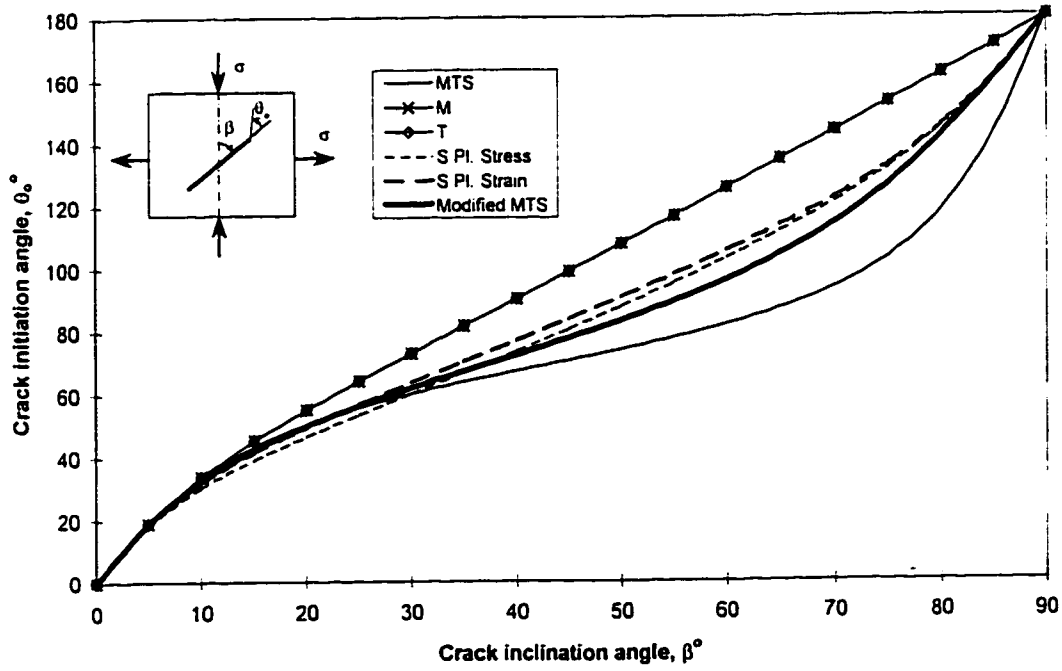

Fig. 2.11: Biaxial loading $\lambda = -1.0$, positive roots

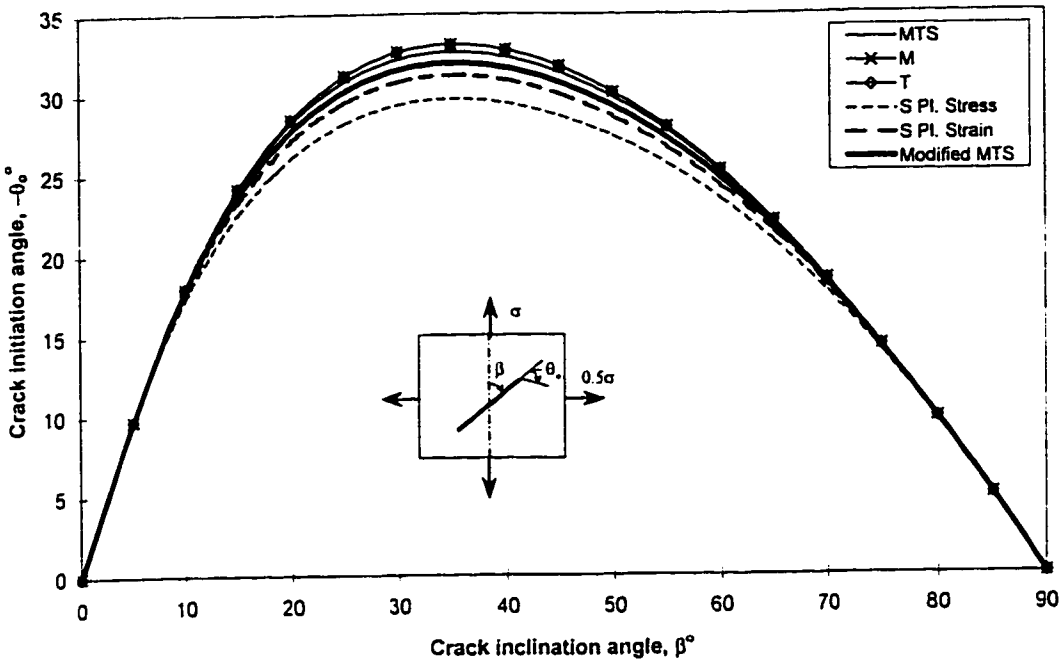

Fig. 2.12: Biaxial loading $\lambda = 0.5$, negative roots

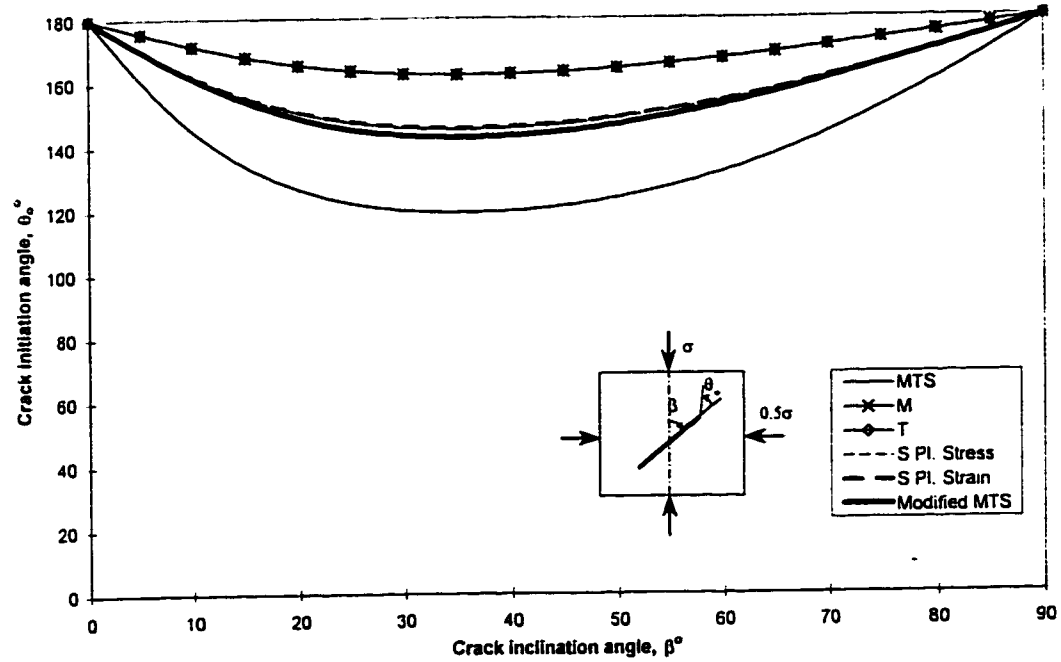

Fig. 2.13: Biaxial loading $\lambda = 0.5$, positive roots

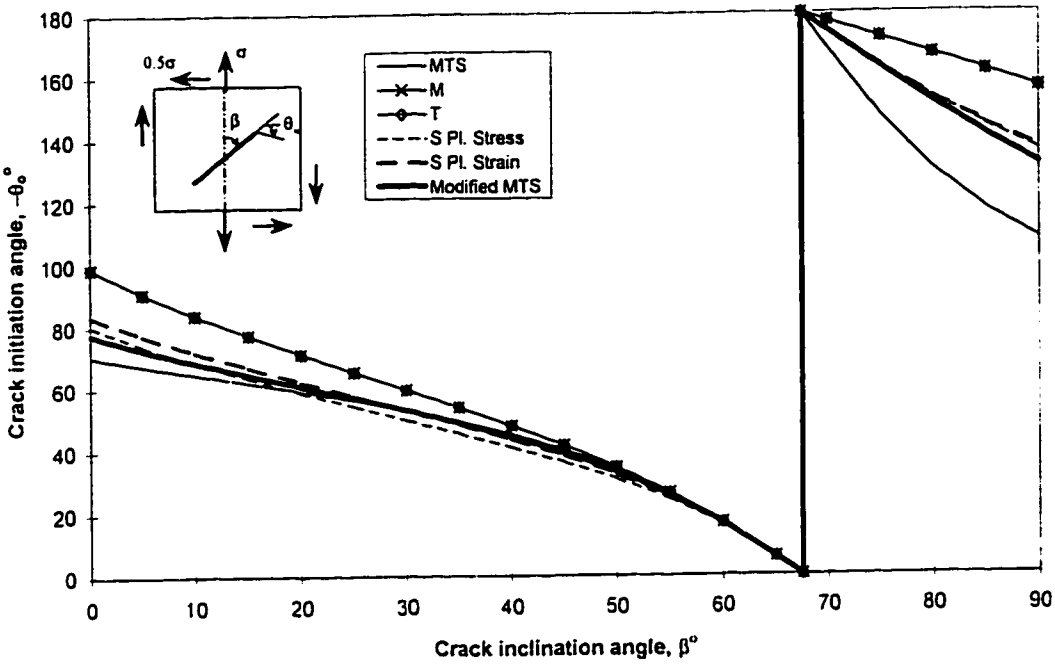

Fig. 2.14: Proportional tension-torsion loading α = -0.5, negative roots

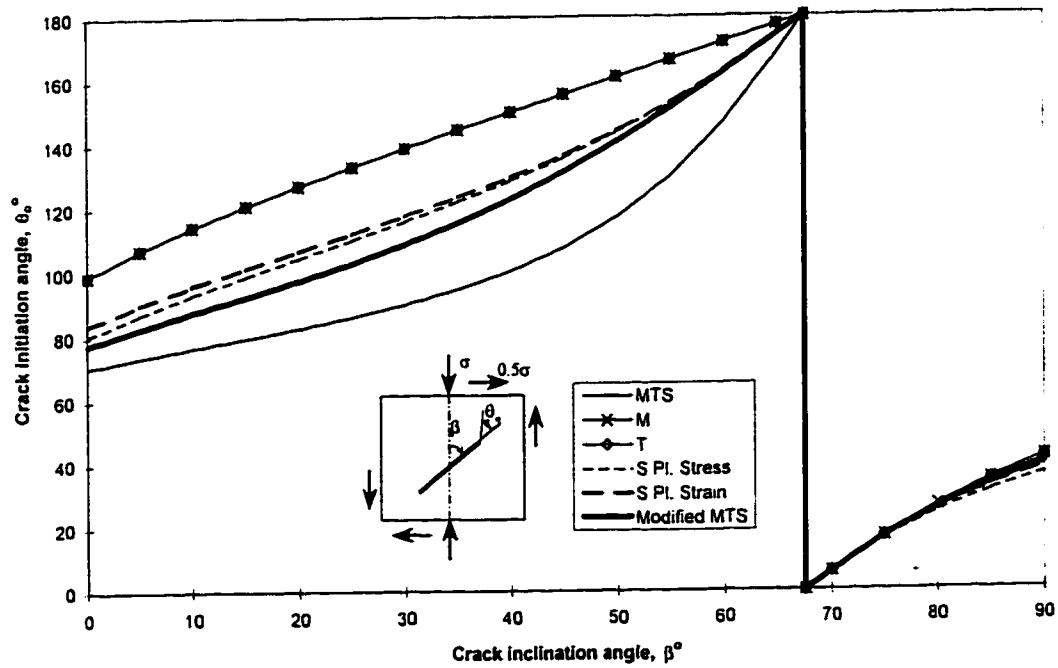

Fig. 2.15: Proportional tension-torsion loading α = -0.5, positive roots

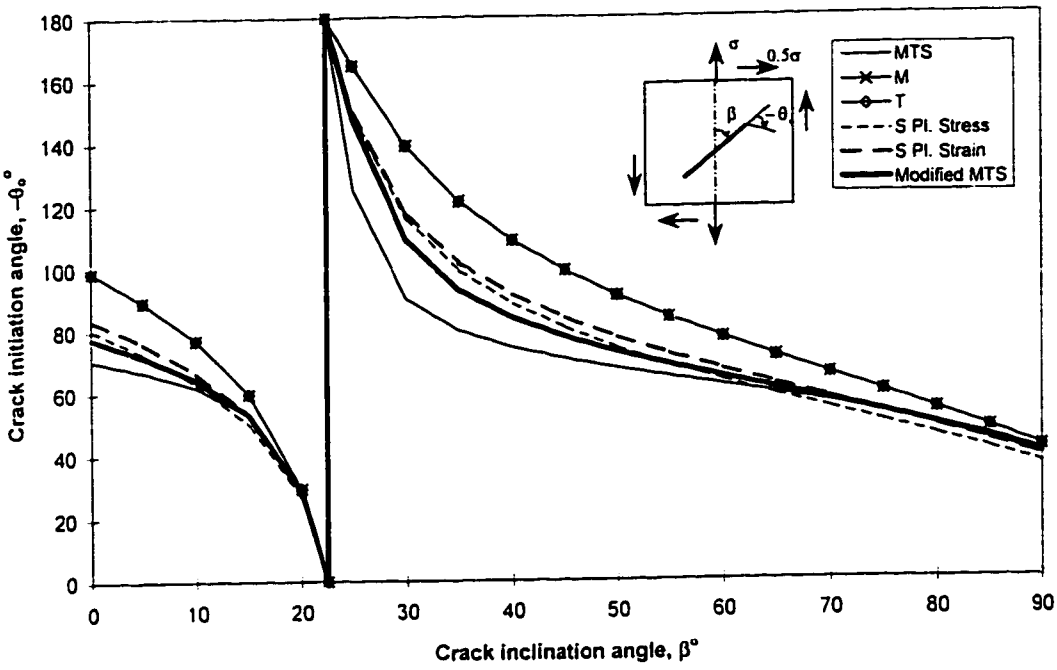

Fig. 2.16: Proportional tension-torsion loading $\alpha = 0.5$, negative roots

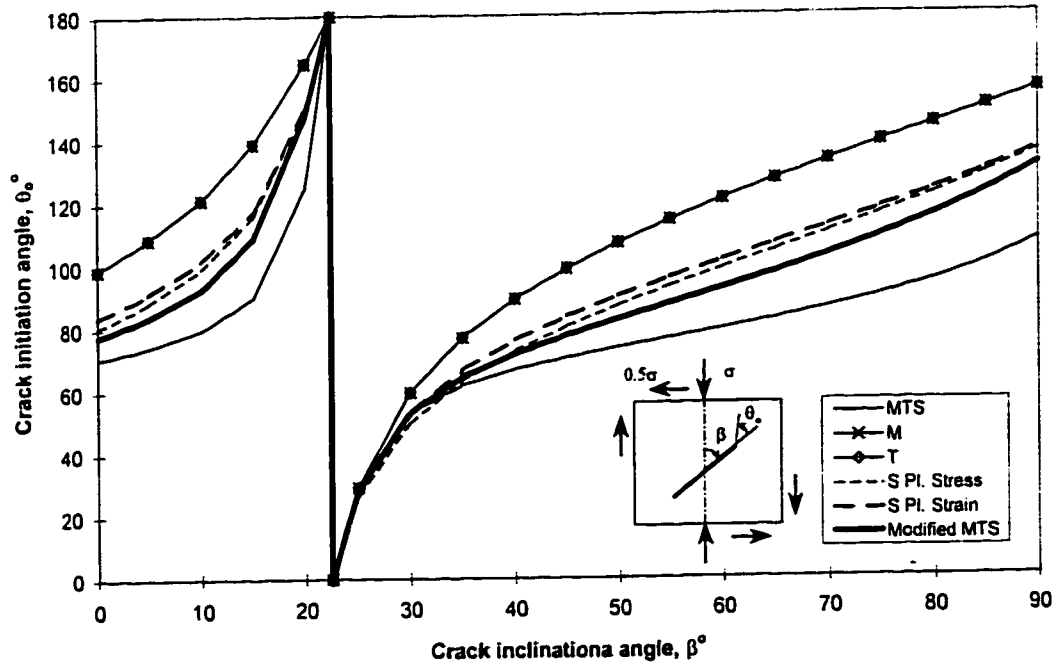

Fig. 2.17: Proportional tension-torsion loading $\alpha = 0.5$, positive roots

Chapter 3

Effect of the Crack Tip Core Region on Crack Initiation Angles

3.1 Introduction

Erdogan and Sih (1963) were the first to use the angled crack problem to study the mixed mode crack initiation. They proposed the first criterion for crack initiation under mixed mode loading, the maximum tangential stress (MTS) criterion, based on stress as a critical parameter for crack initiation. Since then, several criteria (Sih, 1973 and1974; Theocaris et al., 1982; Kong et al., 1995; Ukadgaonker and Awasare, 1995) have been proposed for mixed mode crack initiation. These criteria use linear elastic fracture mechanics (LEFM), and assume a core region at the crack tip. The inability of LEFM to accurately define the stress state in the immediate vicinity of the crack, forces one to assume a core region at the crack tip. The boundary of the core region serves to separate the outside material assumed to behave elastically from the inside material whose physical behavior is unknown. Hence we can use the continuum mechanics approach

outside the core region only, and the critical value of the quantity, defined for crack initiation must be determined on or outside the boundary of the core region. Out of the available criteria, the maximum tangential stress criterion (MTS-criterion, Erdogan and Sih, 1963), the minimum strain energy density criterion (S-criterion, Sih, 1973 and 1974), and the maximum triaxial stress criterion (Kong et al., 1995) assume a constant core region radius. The maximum dilatational strain energy criterion (T-criterion, Theocaris et al., 1982) and the criterion proposed by Ukadgaonker and Awasare (1995) use a variable core region radius. From a mathematical point of view, for criteria based on constant radius, the value of 'r' does not affect the crack initiation angle, when the singular elastic stress field at the crack tip is used. When non-singular terms (independent of r) are added to singular elastic field or the exact stress field is used, the value of 'r' affects the angle θ (Williams and Ewing, 1972; Ewing and Williams, 1974; Maiti and Smith, 1983). Williams and Ewing (1972) added a non-singular term to the elastic stress field and used the experimental results to validate the MTS-criterion, regarding mixed mode crack initiation experiments under uniaxial tension performed on polymethylmethacrylate (PMMA) specimen. They presented a relationship between the constant core region radius (r) to the half crack length (a) as $(2r/a)^{1/2}$. A value of 0.0 to this ratio employs singular elastic field. They suggested that a value of 0.1 to this ratio gives a better fit to the experimental data as compared to a value of 0.0. Later Ewing and Williams (1974) performed mixed mode crack initiation experiments in torsion, and after verifying the results using both the MTS and S-criterion, came up with the same conclusion. Maiti and Smith (1983) used the exact solution of the stress field at the crack tip, and while using different available criteria, studied the effect of the radius ratio (r/a) on crack initiation

angles. They analyzed the MTS, S, and the maximum tangential strain criteria, and suggested that a radius ratio between 0.001~0.1 gives accurate prediction of the angle of initial crack extension. These observations clearly show that crack initiation angle depends on the radius of the core region. Although, 'r' does not affect the crack initiation direction when a singular elastic field is used, yet it seems necessary to use r, radius of the core region as a function of polar angle θ since it effects the crack initiation angle. Theocaris et al. (1982) used the radius as a function of angle θ by employing von Mises yield criterion. They defined the crack initiation angle on the basis of the strain energy at the Mises elastic-plastic boundary, and analyzed the results for uniaxial case. However, they did not discuss the effect of the core region on crack initiation angles. Ukadgaonker and Awasare (1995) also used Mises elastic-plastic radius to define the core region, and presented a criterion in terms of the first and second stress invariants (I_1 and I_2) that agrees with the T-criterion. Although, they presented core region shapes for different loading conditions, yet they did not presented any discussion about the relation between the core region and the crack initiation angles. Yan et al. (1992) presented 'r' as a function of θ using Nadai yield criterion, and modified the MTS and S-criteria. The effect of strength anisotropy can be studied using these modified criteria.

In general, it is well established that the nature of the core region at the crack tip plays an important role in determining the initial direction of crack propagation. Different criteria are based on different definitions of the core region. However, there exists no direct correlation between the size and shape of the core region and the crack initiation angles for various loading conditions. Therefore, it is the purpose of present study to closely examine the role of the core region in the determination of initial crack extension

direction. A criterion based on the shape of the core region will be presented and analyzed for different loading conditions.

Experimental results (Jendoubi et al., 1991; Ranganathan et al., 1994) show that the elastic plastic boundary at the crack tip is qualitatively similar to the boundary defined by von Mises yield function. Moreover, the photo-elastic patterns obtained (Broek, 1982) also favor the Mises elastic-plastic boundary. Hence, von Mises yield function will be used to define the core region boundary.

There have been an exhaustive discussion between Yehia, Theocaris and Andrianopolous (Theocaris, 1986; Andrianopolous, 1986; Andrianopolous and Theocaris, 1988; Yehia, 1990; Andrianopolous, 1992) on the application of T-criterion in fracture mechanics, and its ability to predict fracture load for a propagating crack under load increments. The original T-criterion (Theocaris et al., 1982) defines critical load to be obtained from critical value of dilatational strain energy. Yehia and Shephard (1987) said that the critical value of dilatational strain energy is independent of applied load and modified the T-criterion to use the critical value of plastic core region to determine the fracture load (Yehia and Shephard, 1987). Theocaris and Andrianopolous (1988) rejected this conclusion and modification to the T-criterion. Later Yehia (1986) discussed the possibility of defining a criterion completely based on elastic-plastic core region, to remove the consistency problem in modified T-criterion. However, the Y-criterion presented by Yehia (1991) needs some clarification in terms of quantity used for determining crack initiation angle. First the Y-criterion is defined (Yehia, 1991) based on elastic-plastic core region, however the energy form obtained on "re-arrangement" of parameters is defined using minimum distortional strain energy. Distortional strain

energy cannot be minimized on the Mises elastic-plastic boundary since it is constant along it. Therefore, Yehia (1991) used a constant radius for the Y-criterion.

3.2 Analysis for Formulation of Non-dimensional Core Radius

For an isotropic cracked body under mixed mode (I-II) condition, the singular linear elastic stress field at the crack tip is given by Eq. (2.2). This stress field involves two field variables, r and θ. When this stress field is used to apply any crack initiation criterion based on LEFM, the angle θ_o defines the crack initiation angle, and r defines the radius of the core region. This radius can be approached in two different ways: assuming as constant or as variable. A variable radius is always based on some yield function. As discussed in the introduction, the von Mises yield function shows a qualitative similarity to the experimental results, therefore we will use this yield function. Von Mises criterion for a general state of stress at the crack tip, is given by:

$$U_{D,o} = U_D \tag{3.1}$$

Where $U_{D,o}$ is the critical value of the distortional strain energy in uniaxial tension, and U_D the distortional strain energy in a general state of stress. U_D depends on the condition at the crack tip, whether plane stress or plane strain, which in turn depends on the thickness of the cracked plate. In general, we have from Eq. (3.1):

$$\sigma_{YS}^2 = \frac{(\sigma_x - \sigma_y)^2 + (\sigma_y - \sigma_z)^2 + (\sigma_z - \sigma_x)^2 + 6\tau_{xy}^2}{2} \tag{3.2}$$

Where σ_{YS} is the tensile yield strength of the material. By substituting Eq. (2.2) in Eq. (3.2) we can find a relationship for plastic core radius, r_p. This relationship, however,

depends on the loading conditions. To obtain a generalized relation for plastic core radius independent of the half crack length and the applied stress, we have to define a non-dimensional radius. Broek (1982) and Anderson (1991) show the shape and size of the core region, for pure modes (I or II or III), using a non-dimensional Mises core radius. In such pure loading modes, the respective stress intensity factor is used for non-dimensional purpose, for example, for pure mode I, we have (Broek, 1982; Anderson, 1991):

$$R_{P_I}(\theta) = \frac{r_p(\theta)}{\frac{1}{\pi}\left[\frac{K_I}{\sigma_{YS}}\right]^2} = \frac{1}{4}\left[1 + \cos\theta + \frac{3}{2}\sin^2\theta\right] \tag{3.3}$$

Where R_{P_I} is the non-dimensional mode I core radius, and $K_I = \sigma\sqrt{\pi a}$.

When a crack is under pure loading of any one of the modes, only one stress intensity factor (K_I, K_{II}, K_{III}) appears in the equations and it is used to non-dimensionlize the core radius. However, in the case of mixed mode (I-II) loading, both K_I and K_{II} appear in the equations (Eq. (2.2)), and question arises, which one should be used for non-dimensionlizing purpose? One wonders why this issue has not received due attention in the open literature. Although some studies (Theocaris et al., 1982; Ukadgaonker and Awasare, 1995) show the core region plots, but there is no indication of exactly what function is plotted. The core region plots shown provide only the "relative" shape and size for different configurations. Since K_I and K_{II} are functions of the crack inclination angle β, and core radius itself is also a function of crack inclination angle β, none of these can be used above for non-dimensionlizing purpose. Therefore, in order to study the

characteristics of the core region in an effective manner, it is important to define a standard way to obtain a non-dimensional core radius for mixed mode loading.

Consider the case of an infinite plate with a central crack of length $2a$ inclined at an angle β, with the y′-axis under general loading, as shown in Fig. 2.3. For any particular loading condition, we represent the stress intensity factors as:

$$K_i = \sigma_{app}\sqrt{\pi a} f_{K_i}(\beta) \quad i = I, II, \text{ or } III \tag{3.4}$$

where σ_{app} is the applied stress, which may be tensile, compressive, shear stress, or a combination of these, $f_{K_i}(\beta)$ is a function of the crack inclination angle, β, and the loading condition (will be defined later for different loading conditions). For mode I and mode II stress intensity factors, we get:

$$\begin{aligned} K_I &= \sigma\sqrt{\pi a} f_{K_I}(\beta) \\ K_{II} &= \sigma\sqrt{\pi a} f_{K_{II}}(\beta) \end{aligned} \tag{3.5}$$

Using Eq. (3.5) in Eq. (2.2), we get:

$$\sigma_x = \frac{\sigma_{app}\sqrt{a}}{\sqrt{2r}}\left[\left\{f_{K_I}(\beta)\cos\frac{\theta}{2}\left(1-\sin\frac{\theta}{2}\sin\frac{3\theta}{2}\right)\right\}-\left\{f_{K_{II}}(\beta)\sin\frac{\theta}{2}\left(2+\cos\frac{\theta}{2}\cos\frac{3\theta}{2}\right)\right\}\right]$$
$$= \frac{\sigma_{app}\sqrt{a}}{\sqrt{2r}} f_x(\theta, f_{K_I})$$
$$\sigma_y = \frac{\sigma_{app}\sqrt{a}}{\sqrt{2r}}\left[\left\{f_{K_I}(\beta)\cos\frac{\theta}{2}\left(1+\sin\frac{\theta}{2}\sin\frac{3\theta}{2}\right)\right\}+\left\{f_{K_{II}}(\beta)\sin\frac{\theta}{2}\cos\frac{\theta}{2}\cos\frac{3\theta}{2}\right\}\right] \qquad (3.6)$$
$$= \frac{\sigma_{app}\sqrt{a}}{\sqrt{2r}} f_y(\theta, f_{K_I})$$
$$\tau_{xy} = \frac{\sigma_{app}\sqrt{a}}{\sqrt{2r}}\left[\left\{f_{K_I}(\beta)\cos\frac{\theta}{2}\sin\frac{\theta}{2}\cos\frac{3\theta}{2}\right\}+\left\{f_{K_{II}}(\beta)\cos\frac{\theta}{2}\left(1-\sin\frac{\theta}{2}\sin\frac{3\theta}{2}\right)\right\}\right]$$
$$= \frac{\sigma_{app}\sqrt{a}}{\sqrt{2r}} f_{xy}(\theta, f_{K_I})$$

Where $f_x(\theta, f_{K_I})$, $f_y(\theta, f_{K_I})$, and $f_{xy}(\theta, f_{K_I})$ are defined as:

$$f_x(\theta, f_{K_I}) = \left\{f_{K_I}(\beta)\cos\frac{\theta}{2}\left(1-\sin\frac{\theta}{2}\sin\frac{3\theta}{2}\right)\right\}-\left\{f_{K_{II}}(\beta)\sin\frac{\theta}{2}\left(2+\cos\frac{\theta}{2}\cos\frac{3\theta}{2}\right)\right\}$$
$$f_y(\theta, f_{K_I}) = \left\{f_{K_I}(\beta)\cos\frac{\theta}{2}\left(1+\sin\frac{\theta}{2}\sin\frac{3\theta}{2}\right)\right\}+\left\{f_{K_{II}}(\beta)\sin\frac{\theta}{2}\cos\frac{\theta}{2}\cos\frac{3\theta}{2}\right\} \qquad (3.7)$$
$$f_{xy}(\theta, f_{K_I}) = \left\{f_{K_I}(\beta)\cos\frac{\theta}{2}\sin\frac{\theta}{2}\cos\frac{3\theta}{2}\right\}+\left\{f_{K_{II}}(\beta)\cos\frac{\theta}{2}\left(1-\sin\frac{\theta}{2}\sin\frac{3\theta}{2}\right)\right\}$$

By substituting Eq. (3.6) in Eq. (3.2), we get the non-dimensional elastic-plastic core region radius R_P for mixed mode loading. For plane stress,

$$R_P(\theta, f_{K_I}) = \frac{r_p(\theta, f_{K_I})}{a\left[\frac{\sigma_{app}}{\sigma_{YS}}\right]^2} \qquad (3.8a)$$
$$= \frac{1}{2}\left[f_x^2(\theta, f_{K_I}) + f_y^2(\theta, f_{K_I}) - f_x(\theta, f_{K_I}) f_y(\theta, f_{K_I}) + 3f_{xy}^2(\theta, f_{K_I})\right]$$

and, for plane strain

$$R_P(\theta, f_{K_I}) = \frac{r_p(\theta, f_{K_I})}{a\left[\frac{\sigma_{app}}{\sigma_{YS}}\right]^2} = \frac{1}{2}\left[(\nu^2 - \nu + 1)(f_x(\theta, f_{K_I}) + f_y(\theta, f_{K_I}))^2 - 3(f_x(\theta, f_{K_I}) f_y(\theta, f_{K_I}) - f_{xy}^2(\theta, f_{K_I}))\right] \tag{3.8b}$$

Equation (3.8b) reduces to Eq. (3.8a) for $\nu = 0$.

Using Eq. (3.7) in Eq. (3.8), we get the non-dimensional plastic core radius R_P, in the form:

$$R_P(\theta, f_{K_I}) = \frac{r_p(\theta, f_{K_I})}{a\left[\frac{\sigma_{app}}{\sigma_{YS}}\right]^2} = f_{K_I}^2(\beta) g_1(\theta) + f_{K_{II}}^2(\beta) g_2(\theta) + f_{K_I}(\beta) f_{K_{II}}(\beta) g_{12}(\theta) \tag{3.9a}$$

for plane stress, and

$$R_P(\theta, f_{K_I}) = \frac{r_p(\theta, f_{K_I})}{a\left[\frac{\sigma_{app}}{\sigma_{YS}}\right]^2} = f_{K_I}^2(\beta)(g_1(\theta) + h_1(\theta, \nu)) + f_{K_{II}}^2(\beta)(g_2(\theta) + h_2(\theta, \nu)) + f_{K_I}(\beta) f_{K_{II}}(\beta)(g_{12}(\theta) + h_{12}(\theta, \nu)) \tag{3.9b}$$

for plane strain, where g_1, g_2, g_{12} are functions of angle θ, and h_1, h_2, h_{12} are functions of θ and ν, defined as:

$$g_1(\theta) = \frac{7 + 4\cos\theta - 3\cos 2\theta}{16}$$
$$g_2(\theta) = \frac{19 - 4\cos\theta + 9\cos 2\theta}{16} \tag{3.10a}$$
$$g_{12}(\theta) = \frac{-2\sin\theta + 3\sin 2\theta}{4}$$

$$
\begin{aligned}
h_1(\theta) &= \nu(\nu-1)(1+\cos\theta) \\
h_2(\theta) &= \nu(\nu-1)(1-\cos\theta) \\
h_{12}(\theta) &= -2\nu(\nu-1)\sin\theta
\end{aligned}
\tag{3.10b}
$$

These equations show that the shape of the core region is a function of two angles, θ and β. The function of the angle β in turn depends on the loading conditions, for example, uniaxial, pure shear, biaxial, or proportional tension-torsion loading. The shape of the core region is also a function of the Poisson's ratio in case of plane strain condition at the crack tip. Two parameters control the actual size of the core region: the initial half crack length a, and the ratio of the applied stress to the tensile yield strength of the material. The size of the core region is proportional to the initial half length of the crack, and to the square of the ratio σ_{app}/σ_{YS} .

3.3 Loading Conditions and Core Regions

3.3.1 Uniaxial Loading

Referring to the angled crack problem under uniaxial stress (Fig. 2.3), the stress intensity factors are given by:

$$
\begin{aligned}
K_I &= \sigma \sin^2\beta\sqrt{\pi a} \\
K_{II} &= \sigma \sin\beta\cos\beta\sqrt{\pi a}
\end{aligned}
\tag{3.11}
$$

It follows from Eq. (3.5) and Eq. (3.11):

$$
\begin{aligned}
f_{K_I}(\beta) &= \sin^2\beta \\
f_{K_{II}}(\beta) &= \sin\beta\cos\beta \\
\sigma_{app} &= \sigma
\end{aligned}
\tag{3.12}
$$

Where σ is the applied stress in y′ direction. Using Eq. (3.12) with Eq. (3.9), the Mises elastic-plastic radius is obtained for uniaxial loading for both plane stress and plane strain condition at the crack tip as:

$$R_p(\theta,\beta)=\frac{r_p(\theta,\beta)}{a\left[\frac{\sigma}{\sigma_{YS}}\right]^2}=\sin^4\beta g_1(\theta)+\sin^2\beta\cos^2\beta g_2(\theta)+\sin^3\beta\cos\beta g_{12}(\theta) \tag{3.13a}$$

for plane stress, and

$$R_p(\theta,\beta)=\frac{r_p(\theta,\beta)}{a\left[\frac{\sigma}{\sigma_{YS}}\right]^2}=\sin^4\beta(g_1(\theta)+h_1(\theta,\nu))+\sin^2\beta\cos^2\beta(g_2(\theta)+h_2(\theta,\nu)) + \sin^3\beta\cos\beta(g_{12}(\theta)+h_{12}(\theta,\nu)) \tag{3.13b}$$

for plane strain.

The shape and size of the core region is shown in Fig. 3.1a and Fig. 3.1b for plane stress and plane strain condition at the crack tip, respectively, for $\beta=30°,60°,90°$. Crack inclination angle $\beta=90°$ implies pure mode I loading, and the size and shape is same as in Broek (1982) and Anderson (1991).

If the applied uniaxial stress is less than the tensile yield strength of the material then the ratio σ/σ_{YS} will be less than one, and its square will even have smaller value. Consequently, the actual size of the core region will be smaller. One can safely use the available criteria for the crack initiation prediction, since these are based on LEFM for small scale yielding. But for applied stress greater than tensile yield strength, the actual

size of the core region may go considerably larger, and may cause general yielding of the material.

The size of the plastic core region for plane strain condition is less then the size in the case of plane stress condition at the crack tip. For plane strain condition, the strain in z-direction is kept at zero, due to the constraint by the surrounding elastic material, hence, the plastic core region is smaller. For plane stress condition, yielding can take place freely in the thickness direction, so a larger size of the plastic core region exists. Same trend is observed between plane stress and plane strain conditions at the crack tip for other loading conditions, however, the plots for other loading conditions will be shown only for plane stress condition at the crack tip.

3.3.2 Pure Shear Loading

For pure shear loading, the stress intensity factors are given by:

$$\begin{aligned} K_I &= -\tau \sin 2\beta \sqrt{\pi a} \\ K_{II} &= -\tau \cos 2\beta \sqrt{\pi a} \end{aligned} \tag{3.14}$$

It follows from Eq. (3.5) and Eq. (3.14):

$$\begin{aligned} f_{K_I}(\beta) &= -\sin 2\beta \\ f_{K_{II}}(\beta) &= -\cos 2\beta \\ \sigma_{app} &= \tau \end{aligned} \tag{3.15}$$

where τ is the applied shear stress in the direction shown in Fig. 2.3. Combining Eq. (3.15) and Eq. (3.9), the Mises elastic plastic radius is obtained for pure shear loading as:

$$R_p(\theta,\beta)=\frac{r_p(\theta,\beta)}{a\left[\frac{\tau}{\sqrt{3}\tau_{YS}}\right]^2}=\sin^2 2\beta g_1(\theta)+\cos^2 2\beta g_2(\theta)+\sin 2\beta\cos 2\beta g_{12}(\theta) \tag{3.16a}$$

for plane stress, and

$$R_p(\theta,\beta)=\frac{r_p(\theta,\beta)}{a\left[\frac{\tau}{\sqrt{3}\tau_{YS}}\right]^2}=\sin^2 2\beta(g_1(\theta)+h_1(\theta,\nu))+\cos^2 2\beta(g_2(\theta)+h_2(\theta,\nu)) + \sin 2\beta\cos 2\beta(g_{12}(\theta)+h_{12}(\theta,\nu)) \tag{3.16b}$$

for plane strain.

Figure 3.2 shows the core regions for $\beta=30°,45°,60°$ for plane stress condition at the crack tip. While considering the actual size of the core region, it is important to note that σ_{YS} in Eq. (3.9) is replaced with equivalent τ_{YS} in Eq. (3.16), the shear yield strength of the material. The von Mises relationship between σ_{YS} and τ_{YS} is given as:

$$\sigma_{YS}=\sqrt{3}\tau_{YS} \tag{3.17}$$

3.3.3 Biaxial Loading

For proportional biaxial loading $(\sigma_{x'}=\lambda\sigma_{y'})$, the stress intensity factors are given by:

$$\begin{aligned} K_I &= \sigma(\sin^2\beta+\lambda\cos^2\beta)\sqrt{\pi a} \\ K_{II} &= \sigma(1-\lambda)(\sin\beta\cos\beta)\sqrt{\pi a} \end{aligned} \tag{3.18}$$

It follows from Eq. (3.5) and Eq. (3.18):

$$f_{K_I}(\beta,\lambda) = (\sin^2\beta + \lambda\cos^2\beta)$$
$$f_{K_{II}}(\beta,\lambda) = (1-\lambda)(\sin\beta\cos\beta) \qquad (3.19)$$
$$\sigma_{app} = \sigma$$

where λ is the biaxial loading ratio and σ is the applied normal stress in the y' direction shown in Fig. 2.3. Using Eq. (3.19) in Eq. (3.9), the Mises elastic plastic radius is obtained for biaxial loading as:

$$R_p(\theta,\beta,\lambda) = \frac{r_p(\theta,\beta,\lambda)}{a\left[\frac{\sigma}{\sigma_{YS}}\right]^2} = (\sin^2\beta + \lambda\cos^2\beta)^2 g_1(\theta) + (1-\lambda)^2\sin^2\beta\cos^2\beta g_2(\theta) + (1-\lambda)\sin\beta\cos\beta(\sin^2\beta + \lambda\cos^2\beta)g_{12}(\theta) \qquad (3.20a)$$

for plane stress, and

$$R_p(\theta,\beta,\lambda) = \frac{r_p(\theta,\beta,\lambda)}{a\left[\frac{\sigma}{\sigma_{YS}}\right]^2} = (\sin^2\beta + \lambda\cos^2\beta)^2 (g_1(\theta) + h_1(\theta,\nu)) + (1-\lambda)^2\sin^2\beta\cos^2\beta(g_2(\theta) + h_2(\theta,\nu)) + (1-\lambda)\sin\beta\cos\beta(\sin^2\beta + \lambda\cos^2\beta)(g_{12}(\theta) + h_{12}(\theta,\nu)) \qquad (3.20b)$$

for plane strain.

The core regions plots are shown in Fig. 3.3a and 3.3b for $\beta = 15°, 30°, 60°$, and for $\lambda =$ 0.5 and $\lambda = -1.0$, respectively under plane stress condition at the crack tip.

3.3.4 Proportional Tension Torsion Loading

For proportional tension torsion loading $(\tau_{x'y'} = \alpha\sigma_{y'})$, the stress intensity factors are given by:

$$K_I = \sigma(\sin^2\beta - \alpha\sin 2\beta)\sqrt{\pi a}$$
$$K_{II} = \sigma(\sin\beta\cos\beta - \alpha\cos 2\beta)\sqrt{\pi a} \qquad (3.21)$$

It follows from Eq. (3.5) and Eq. (3.21):

$$f_{K_I}(\beta,\alpha) = (\sin^2\beta - \alpha\sin 2\beta)$$
$$f_{K_{II}}(\beta,\alpha) = (\sin\beta\cos\beta - \alpha\cos 2\beta) \qquad (3.22)$$
$$\sigma_{app} = \sigma$$

where α is the proportional tension torsion loading ratio and σ is the applied normal stress in the y′ direction shown in Fig. 2.3. Using Eq. (3.22) in Eq. (3.9), the Mises elastic plastic radius is obtained for proportional tension torsion loading as:

$$R_p(\theta,\beta,\alpha) = \frac{r_p(\theta,\beta,\alpha)}{a\left[\frac{\sigma}{\sigma_{YS}}\right]^2} = (\sin^2\beta - \alpha\sin 2\beta)^2 g_1(\theta) + (\sin\beta\cos\beta - \alpha\cos 2\beta)^2 g_2(\theta) + (\sin^2\beta - \alpha\sin 2\beta)(\sin\beta\cos\beta - \alpha\cos 2\beta) g_{12}(\theta) \qquad (3.23a)$$

for plane stress, and

$$R_p(\theta,\beta,\alpha) = \frac{r_p(\theta,\beta,\alpha)}{a\left[\frac{\sigma}{\sigma_{YS}}\right]^2} = (\sin^2\beta - \alpha\sin 2\beta)^2 (g_1(\theta) + h_1(\theta,\nu)) + (\sin\beta\cos\beta - \alpha\cos 2\beta)^2 (g_2(\theta) + h_2(\theta,\nu)) + (\sin^2\beta - \alpha\sin 2\beta)(\sin\beta\cos\beta - \alpha\cos 2\beta)(g_{12}(\theta) + h_{12}(\theta,\nu)) \qquad (3.23b)$$

for plane strain.

The core regions plots are shown in Figs. 3.4a and 3.4b for $\beta = 45°, 60°, 90°$, and for α = 0.5 and $\alpha = -0.5$, respectively under plane stress condition at the crack tip.

3.4 Core Regions and Crack Initiation Angles

Figures 3.5 through 3.8 show the areas on Mises elastic plastic region at the crack tip, in which the crack initiation angles, predicted by four criteria the MTS, M, T and S-criteria, fall for different crack inclination angles. We start by analyzing the uniaxial loading case and then will extend our analysis to other loading conditions. The crack initiation angles for uniaxial tension are negative, i.e., measured clockwise from 0^o on the polar plot of Mises plastic core region, and positive for uniaxial compression i.e. measured counter clockwise from 0^o of the polar plot. For any loading condition, two minima (Fig. 3.5b) along the Mises elastic-plastic boundary can be identified. Out of these, one is the local minimum and the other is the global minimum. Referring to Fig. 3.5, the crack initiation angles for uniaxial tension (-ve values) tend to follow the local minimum of the Mises elastic-plastic boundary, and the crack initiation angles for uniaxial compression (+ve values) tend to follow the global minimum of the Mises elastic plastic boundary. The experimental data for crack initiation angles under uniaxial tension (Erdogan and Sih, 1963; Theocaris et al., 1982; Kong et al., 1995) also show the same trend as by the predicted angles by different well-based available criteria. The experimental data for uniaxial compression (Vallejo, 1987) deviates somewhat from the predicted angles by different criteria, however, it still favors to follow the global minimum of Mises elastic-plastic region. It is important to note that the crack initiation angles will always be negative for uniaxial tension ($+\sigma$), whereas these will always be positive for uniaxial compression ($-\sigma$). For pure shear case Fig. 3.6 (and also for other loading conditions) the sign of crack initiation angles depends on the resultant stresses (σ_n and τ_n) at the crack face and sign convention used for shear stress (for details about sign of crack initiation

angles for different loading conditions, refer to Chapter 2). Hence for $\beta = 30^{o}$, the negative crack initiation angles follow the local minimum and the positive crack initiation angles follow the global minimum. For $\beta = 60^{o}$, negative crack initiation angles follow global minimum, and positive angles follow the local minimum of Mises elastic plastic boundary.

Figures 3.7 and 3.8 show the crack initiation angles predicted by different well-based criteria with the Mises elastic plastic boundary, for biaxial and proportional tension torsion loading, for different loading ratios. The same trend of crack initiation angles, tending towards either the global or the local minimum of the Mises elastic plastic boundary, is observed here, depending upon the state of applied stress and resultant stresses (σ_n and τ_n) at the crack tip.

The analysis and comparison of crack initiation angles predicted by different well-based criteria (plus experimental data for uniaxial loading) with Mises elastic plastic boundary for different loading conditions (Uniaxial tension, uniaxial compression, pure shear, biaxial loading, proportional tension torsion loading) shows a clear trend that the crack initiation angles follow the minima of the elastic plastic boundary. This concept will be utilized to propose a criterion for crack initiation angles based on the crack tip core region.

3.5 The R-criterion

It is shown in the previous section that the crack initiation angles follow either the local or the global minimum of Mises elastic plastic core region depending upon the state of resultant stresses (σ_n and τ_n) at the crack tip (Fig. 2.3). We can get a better

understanding of this phenomenon by considering the physics of the problem. The core region presents a highly strained area. The crack tip has to propagate through this highly strained area to reach the elastically loaded material outside the core radius. In doing so, the crack tip will assume a path towards minimum radius of the core region, since this path offers minimum resistance to propagate through. Hence the R-criterion can now be defined. The direction of crack initiation coincides with the direction of minimum distance to the elastically loaded material around a variable core region, defined by Mises yield function. Mathematically, it can be stated as:

$$\begin{aligned} &\frac{\partial R_P}{\partial \theta} = 0 \\ &\frac{\partial^2 R_P}{\partial \theta^2} > 0 \end{aligned} \tag{3.24}$$

Applying the R-criterion to Eq. (3.8), we get:

$$\begin{aligned} &(2\mu)\tan^4\frac{\theta}{2} + (5-2\mu^2)\tan^3\frac{\theta}{2} - (9\mu)\tan^2\frac{\theta}{2} + (\mu^2-4)\tan\frac{\theta}{2} + \mu = 0 \\ &(1-\mu^2)\cos\theta + 3(\mu^2-3)\cos 2\theta + 2\mu\sin\theta - 12\mu\sin 2\theta > 0 \end{aligned} \tag{3.25}$$

For plane stress, and

$$\begin{aligned} &(4-4\nu+4\nu^2)\mu\tan^4\frac{\theta}{2} + \left((1-4\nu+4\nu^2)(1-\mu^2) - 3(\mu^2-3)\right)\tan^3\frac{\theta}{2} - (18\mu)\tan^2\frac{\theta}{2} \\ &\qquad + \left((1-4\nu+4\nu^2)(1-\mu^2) + 3(\mu^2-3)\right)\tan\frac{\theta}{2} + 2\mu(1+2\nu-2\nu^2) = 0 \\ &(1-\mu^2)(1-4\nu+4\nu^2)\cos\theta + 3(\mu^2-3)\cos 2\theta + 2\mu(1-4\nu+4\nu^2)\sin\theta - 12\mu\sin 2\theta > 0 \end{aligned} \tag{3.26}$$

for plane strain, where:

$$\mu = \frac{K_I}{K_{II}} = \frac{f_{KI}(\beta)}{f_{KII}(\beta)} \tag{3.27}$$

where $K_I, K_{II}, f_{KI}, f_{KII}$ are defined in Eq. (3.6), and μ can be found for different loading conditions from Eqs. (3.11), (3.14), (3.18), and (3.21).

R-criterion is plotted with other criteria (namely MTS, S and T-criteria) in Fig. 3.9 through Fig. 3.12.

3.6 Results and Discussions

Before discussing the results, it is important to mention that the MTS and T-criterion do not depend on the Poisson's ratio, whereas the S-criterion depends on the Poisson's ratio for both plane stress and plane strain conditions at the crack tip. The R-criterion is independent of the Poisson's ratio for plane stress condition at the crack tip, however it depends on it for plane strain condition at the crack tip. A value of 1/3 is taken for the Poisson's ratio, wherever applicable. Also when the terms plane stress and plane strain are used, it is referred to as stress state at the crack tip.

Figure 3.9a, shows the results for uniaxial tension. R-criterion for plane stress matches with S-criterion for plane strain exactly. This is only due to the value of the Poisson's ratio used for S-criterion and this does not mean that these are the same criterion. The predictions of the R-criterion for plane stress are lower than the R-criterion for plane strain, which is the same behavior shown by the S-criterion for plane stress and plane strain. The R-criterion favors the experimental data more than the S and the MTS criteria, for both plane stress and plane strain. The R-criterion for plane strain is closer to experimental data. This can be described on the basis that the crack initiation angle

depends on the state of stress (whether plane stress or plane strain) through dependence on the core region. Due to the effect of ratio of thickness to other dimensions of specimen, the state of stress at the crack tip is usually plane strain, except for very thin specimen. Therefore the R-criterion for plane strain is closer to experimental observations then the R-criterion for plane stress. The experimental data shown is for different materials from three different references (Erdogan and Sih, 1963; Theocaris et al., 1982; Kong et al., 1995)

The only experimental data available for crack initiation under compression is from Vallejo (1987). Vallejo performed experiments on kaolinite clay, and suggested that a specimen with water content greater than 20% is considered as ductile and specimen with water content less than 20% is brittle. The R-criterion deviates from the experimental data like the T and S criteria. The only criterion that fits experimental data for brittle materials under uniaxial compression is the MTS-criterion. More experiments, especially on a ductile material, are needed to compare different criteria for uniaxial compression.

Before discussing other loading cases, it is worth mentioning that it is helpful to refer to Chapter 2 for a detailed discussion of predicted crack initiation angles for other loading conditions. The plots and the non-symmetry found in these plots is discussed based on resultant stresses (σ_n and τ_n) at the crack face.

Considering pure shear case (Fig. 3.10), for $\beta = 0^o$~45^o, the experimental data does not support any particular criterion. Although a little favor is shown for R-criterion at low inclination angles. For $\beta = 45^o$~90^o, the experimental data shows more favor to R-criterion as compared to the S and MTS criteria. In both cases, the R-criterion predicts

higher initiation angles than the S and MTS criteria. The plots for other loading conditions (Fig. 3.11 and 3.12) show the same trend (higher values of crack initiation angles predicted by the R-criterion than by the S or MTS criteria and lower values than the T-criterion). Experiments are needed to verify these theoretical predictions.

3.6.1 Effects of Poisson's Ratio

Only the S-criterion (for both plane stress and plane strain) and the R-criterion (only for plane strain) depend on the Poisson's ratio. These will be compared in this section for different value of Poisson's ratio under uniaxial tension.

Figures 3.13a and 3.13b show the effect of the Poisson's ratio on crack initiation angle as predicted by S-criterion, for both plane strain and plane stress conditions, respectively. Figure 3.14 show the effect of the Poisson's ratio on crack initiation angles as predicted by the R-criterion for plane strain condition, and it also shows the R-criterion for plane stress. The S-criterion for plane strain is spread over a larger range for different values of the Poisson's ratio, whereas this range is very small (less than half of the range for S-criterion) for the R-criterion for plane strain. At $\beta = 0^{\circ}$, the crack initiation angle for the S-criterion under plane strain varies from 70.53°~90°, and for the R-criterion under plane strain it is 83.62°~90°, for different values of the Poisson's ratio. The variation in crack initiation angles for the S-criterion under plane stress for different values of the Poisson's ratio is less that that for the S-criterion under plane strain. However, the R-criterion does not depends on the Poisson's ratio for plane stress condition. Hence the R-criterion shows less dependence on the Poisson's ratio than the S-criterion, for both the plane stress and plane strain conditions at the crack tip.

3.7 Conclusions

The characteristics of the core region at the crack tip and its effects on crack initiation is discussed in detail for different loading conditions (uniaxial tension, uniaxial compression, pure shear, biaxial loading, and proportional tension torsion loading), encountered in real life problems. Following conclusions can be drawn:

1. The shape of the core region is dependent on the crack inclination angle β, and polar co-ordinate θ. In addition, it also depends on Poisson's ratio for plane strain condition, and on loading ratio for biaxial and proportional tension torsion loading.

2. The actual size of the core region is dependent on initial half crack length and the ratio of applied stress to the yield strength of the material. The size of the core region is important in the respect that while performing mixed mode crack initiation experiments using an angled cracked plate problem, the effect of finite width must be given due consideration. For theoretical analysis, it is assumed that stress is applied at infinity. If size of the core region becomes larger as compared to the dimensions of the cracked plate then this assumption may be invalid. For materials with low yield strength, the size of the core region may be considerably larger since it is proportional to the square of σ/σ_{YS}. Thus invalidating the assumption that stress is applied remotely.

3. The crack initiation angles as predicted by different well-based criteria and experimental data tends to follow the global or local minimum of the Mises elastic plastic boundary for various loading conditions considered.

The R-criterion based on the core region is proposed and compared with available criteria under various loading conditions. Following conclusions can be drawn for the R-criterion:

1. The R-criterion shows good agreement with experimental data for uniaxial loading and pure shear loading cases.

2. The derivation for R-criterion is simple as compared to other criterion for ductile materials especially the T-criterion.

3. The R-criterion for plane stress does not depend on the Poisson's ratio, whereas it depends on it in the case of plane strain condition at the crack tip. The variation in the crack initiation angles for the R-criterion is less than for the S-criterion for different values of the Poisson's ratio.

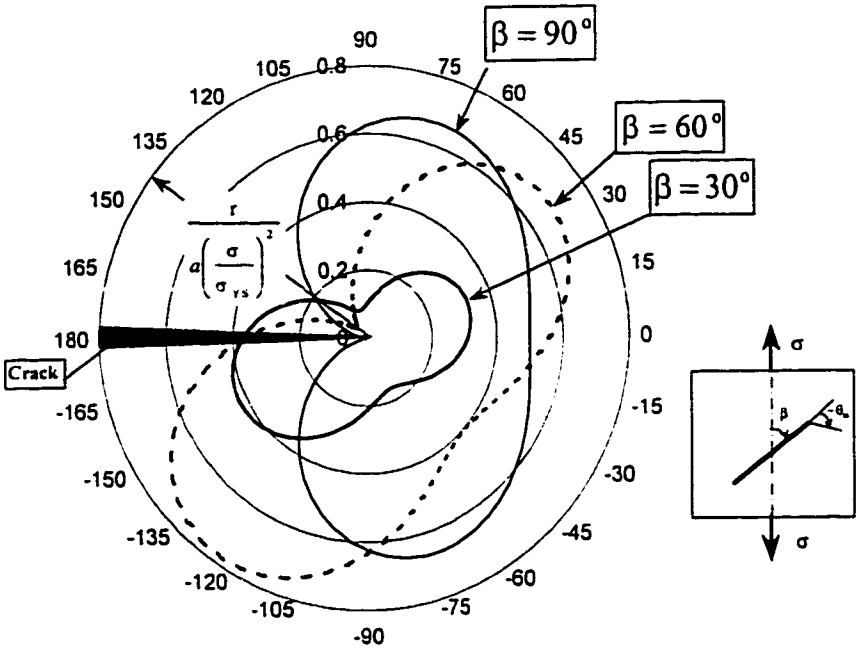

Fig. 3.1a: Mises core region: Uniaxial loading, plane stress

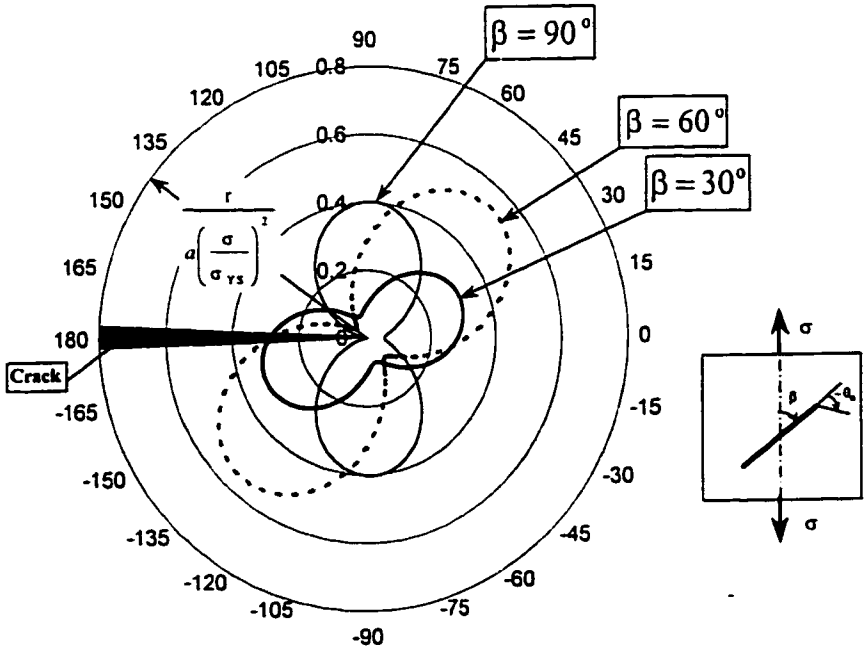

Fig. 3.1b: Mises core region: Uniaxial loading, plane strain

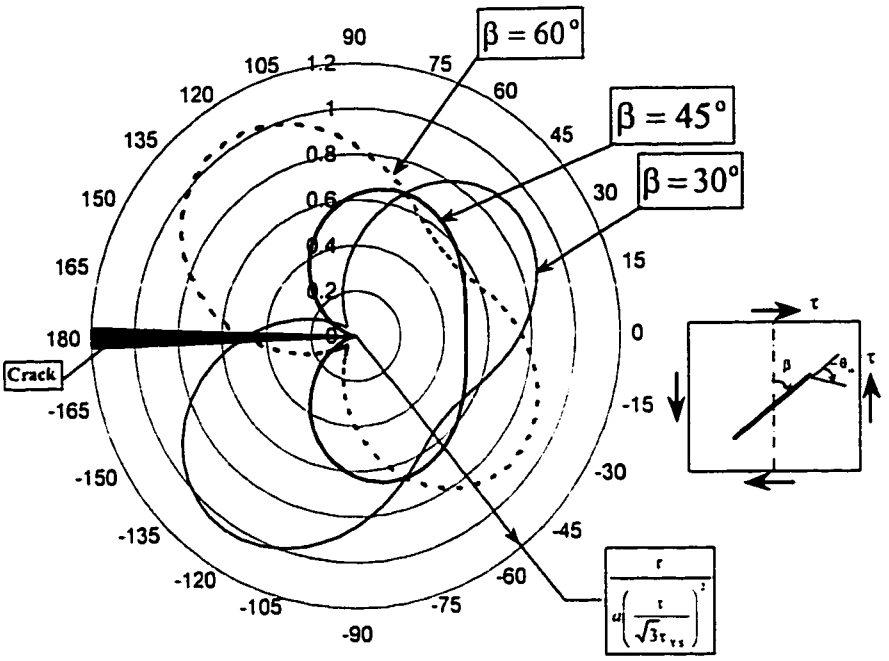

Fig. 3.2: Mises core region: Pure shear loading, plane stress

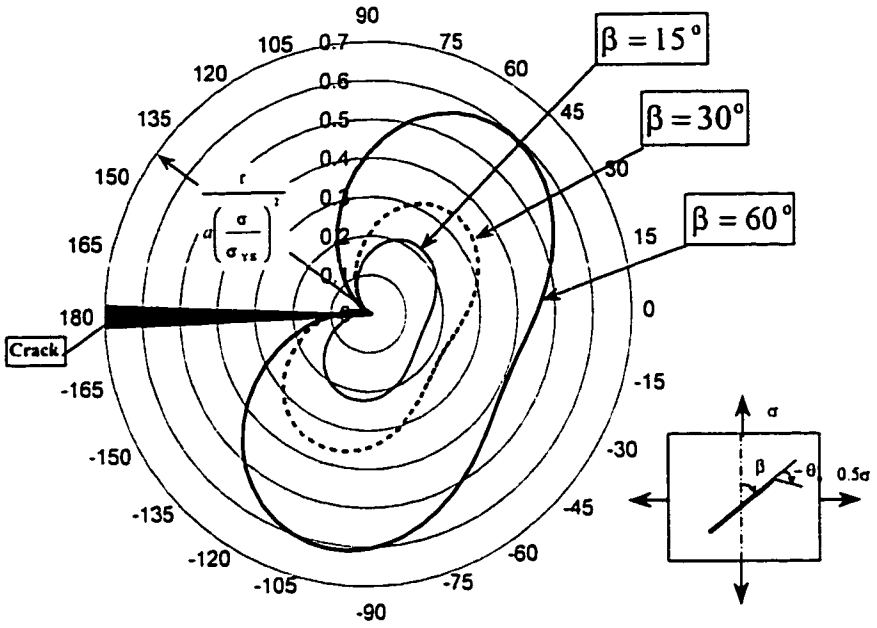

Fig. 3.3a: Mises core region: Biaxial loading, $\lambda = 0.5$, plane stress

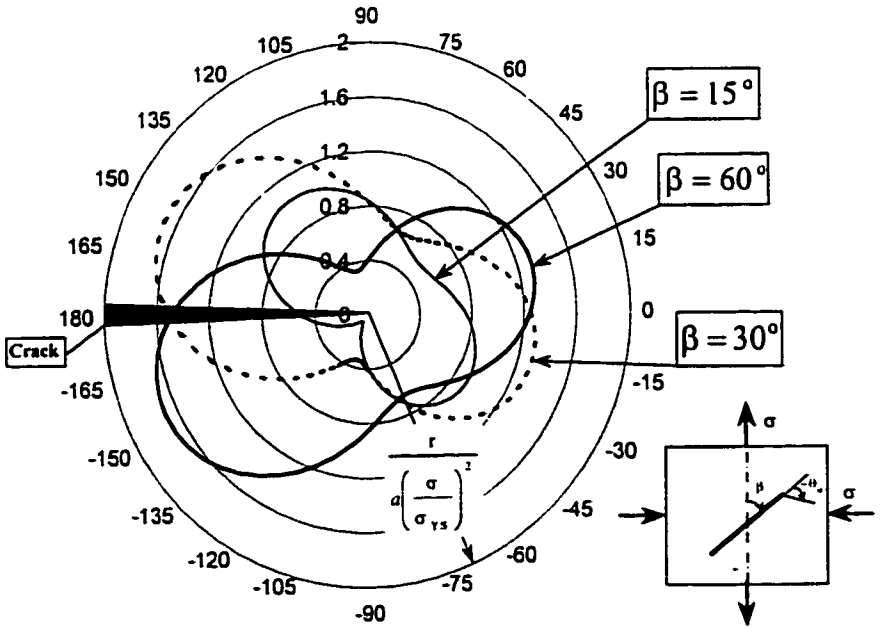

Fig. 3.3b: Mises core region: Biaxial loading, $\lambda = -1.0$, plane stress

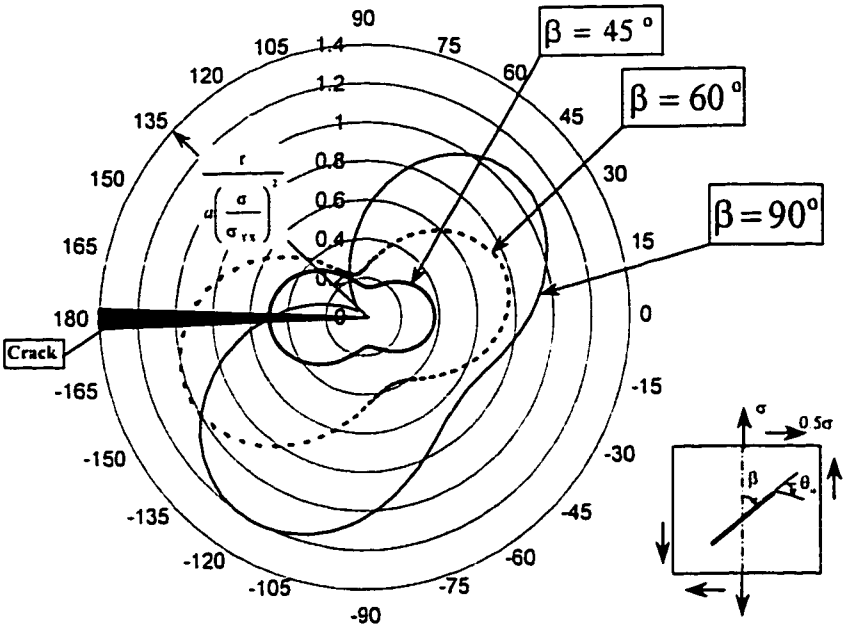

Fig. 3.4a: Mises core region: Proportional tension torsion loading, $\alpha = 0.5$, plane stress

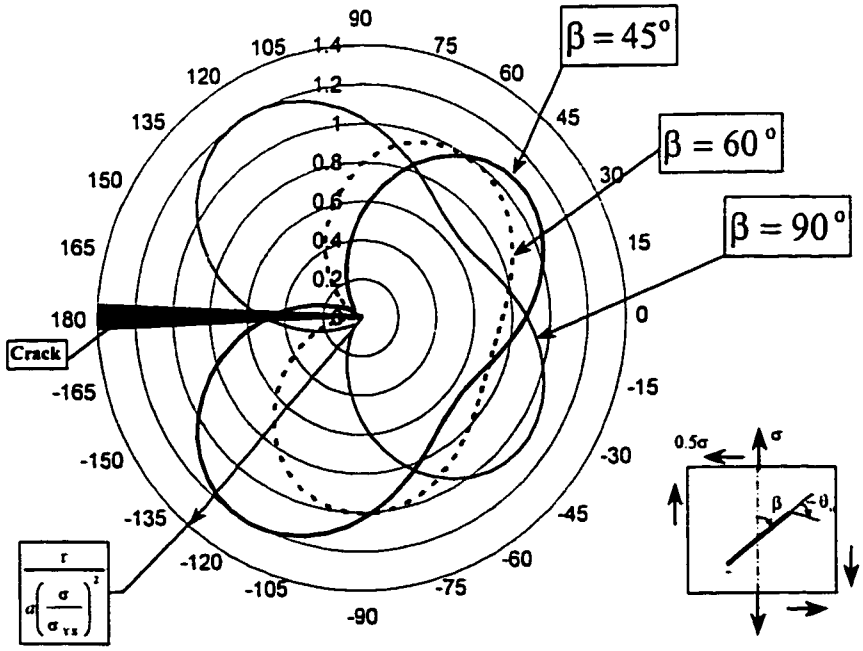

Fig. 3.4b: Mises core region: Proportional tension torsion loading, $\alpha = -0.5$, plane stress

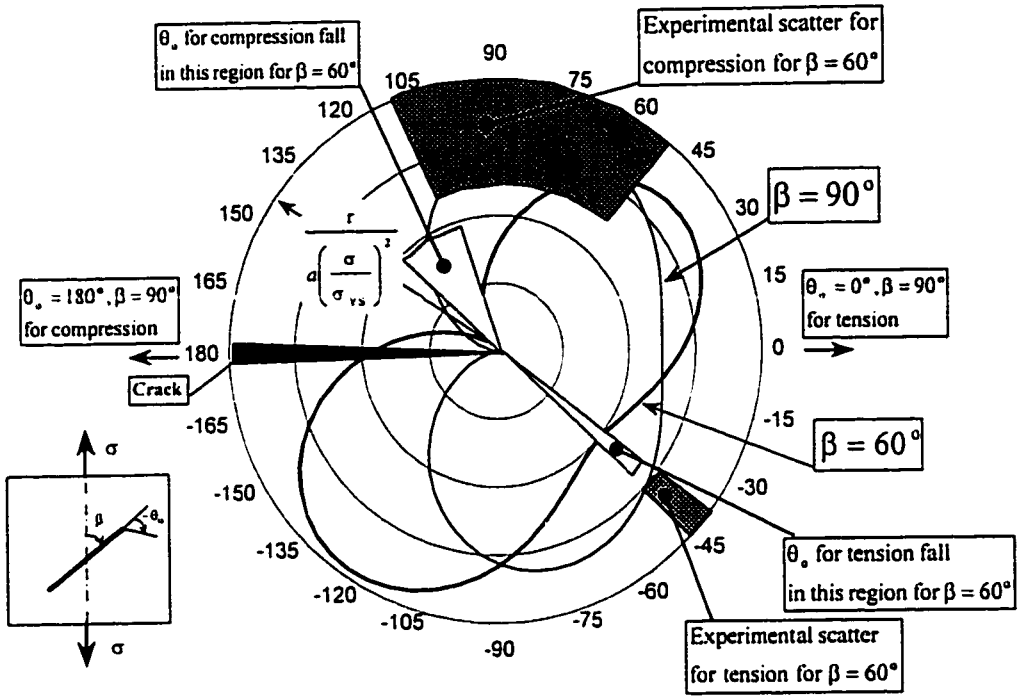

Fig. 3.5a: Crack Initiation angles, Uniaxial loading, plane stress $\beta = 60^{\circ}, 90^{\circ}$

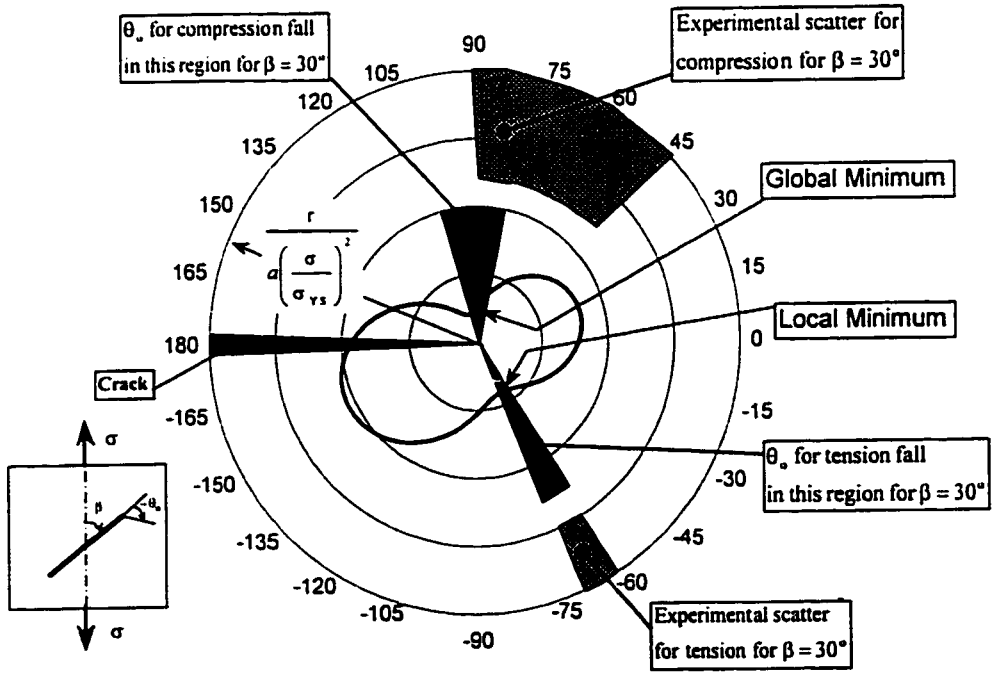

Fig. 3.5b: Crack Initiation angles, Uniaxial loading, plane stress $\beta = 30^{\circ}$

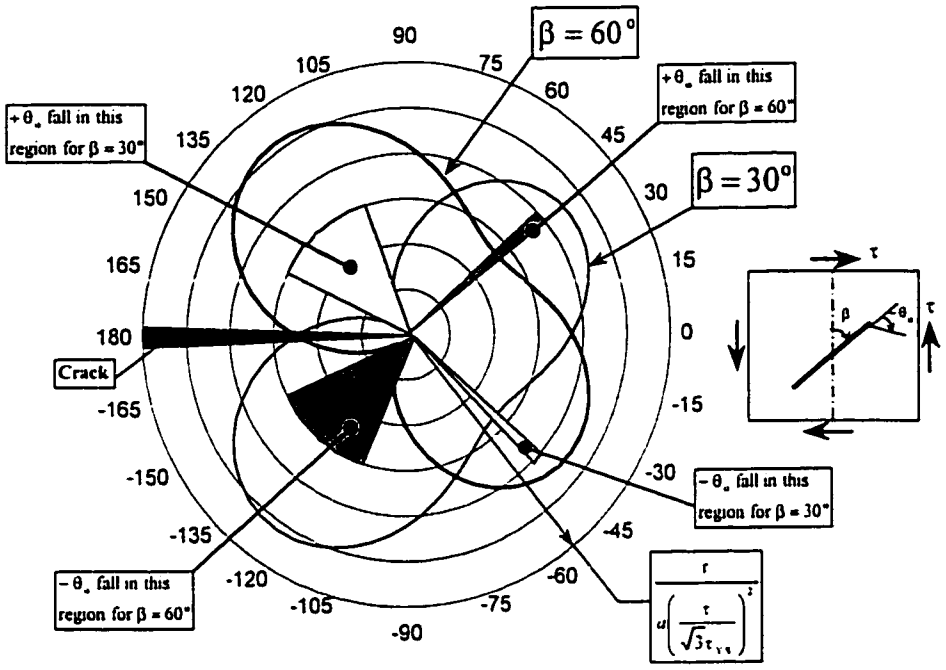

Fig. 3.6: Crack Initiation angles, Pure shear, plane stress

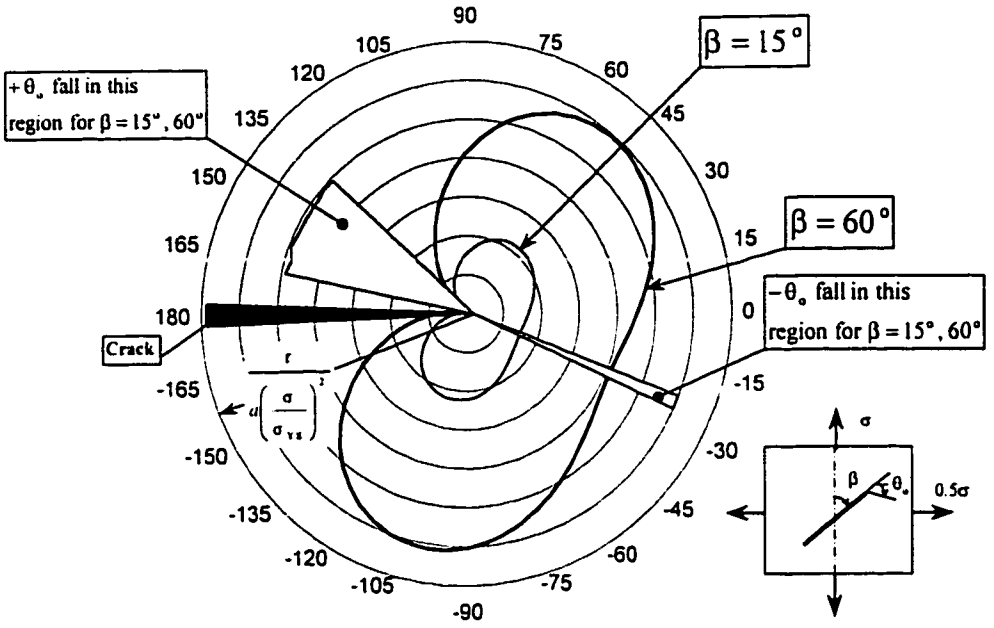

Fig. 3.7a: Crack Initiation angles, Biaxial loading, $\lambda = 0.5$, plane stress

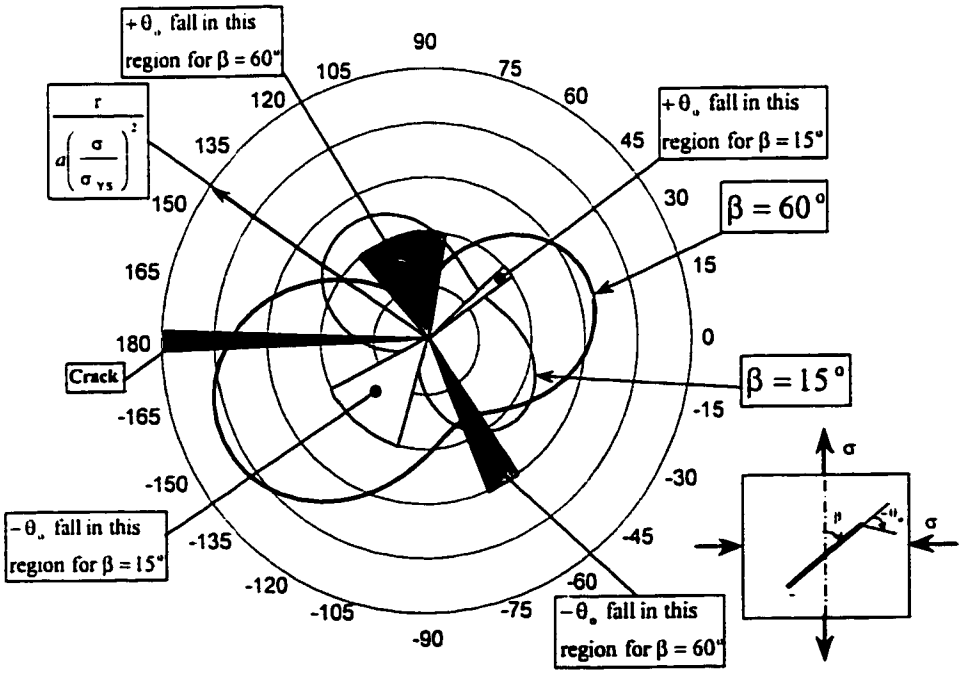

Fig. 3.7b: Crack Initiation angles, Biaxial loading, $\lambda = -1.0$, plane stress

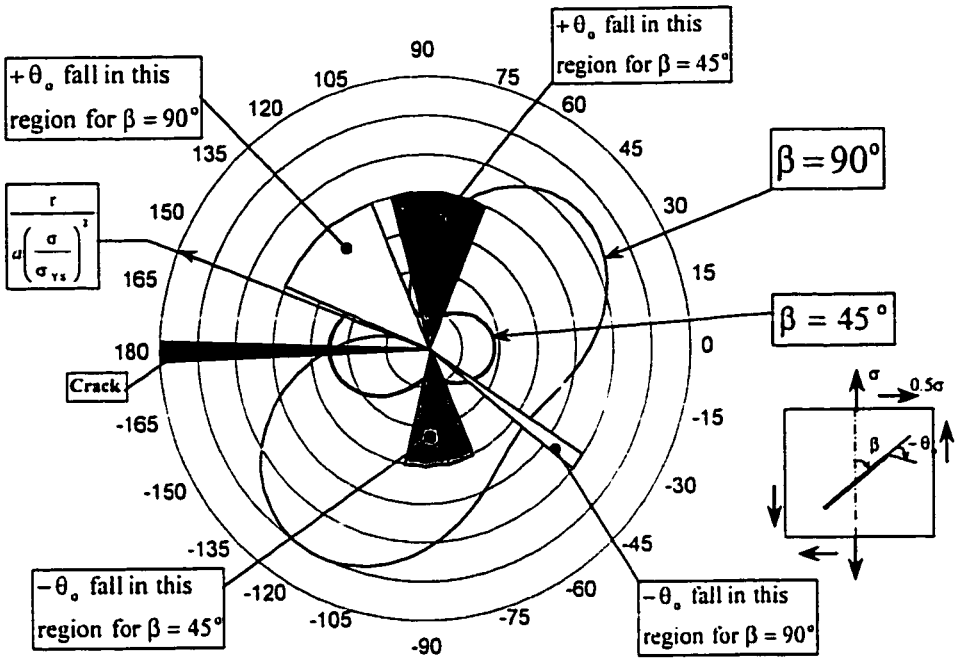

Fig. 3.8a: Crack Initiation angles, Proportional tension torsion loading, $\alpha = 0.5$, plane stress

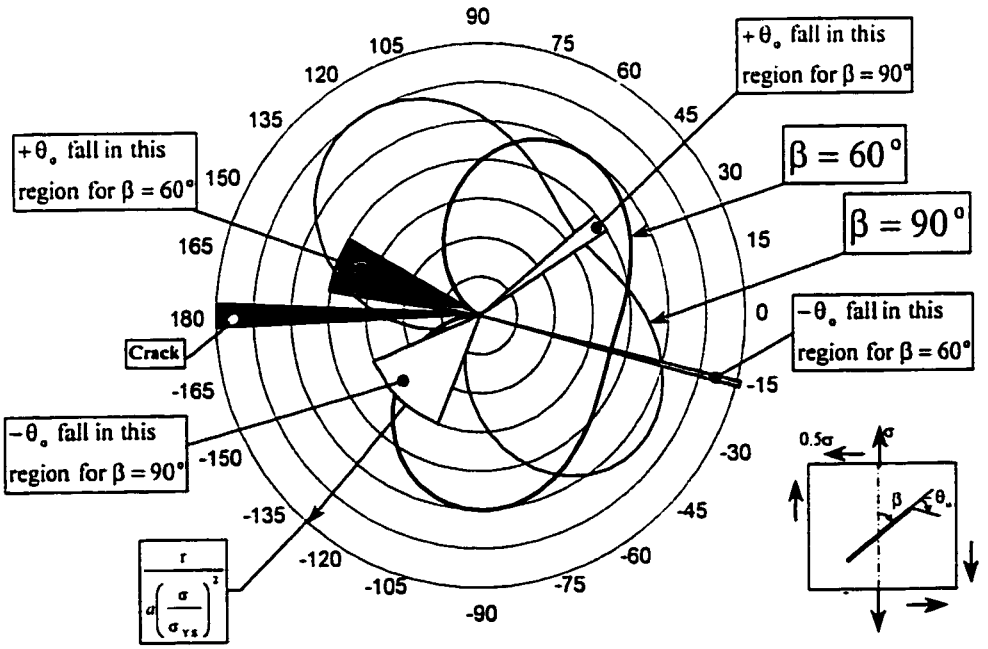

Fig. 3.8b: Crack Initiation angles, Proportional tension torsion loading, $\alpha = -0.5$, plane stress

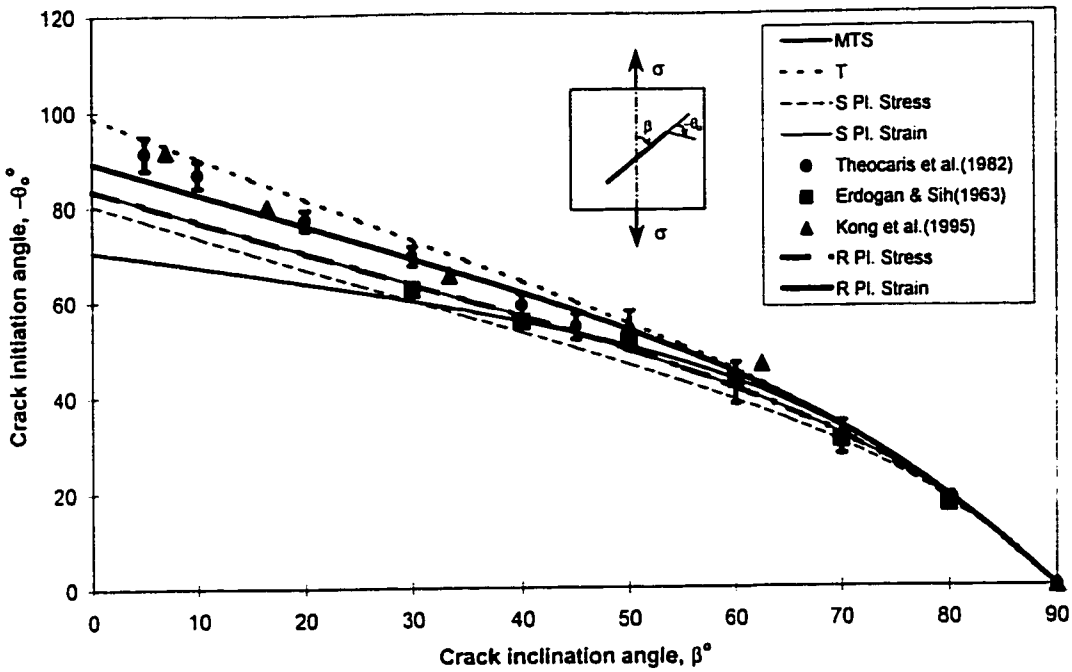

Fig.. 3.9a: Uniaxial tension

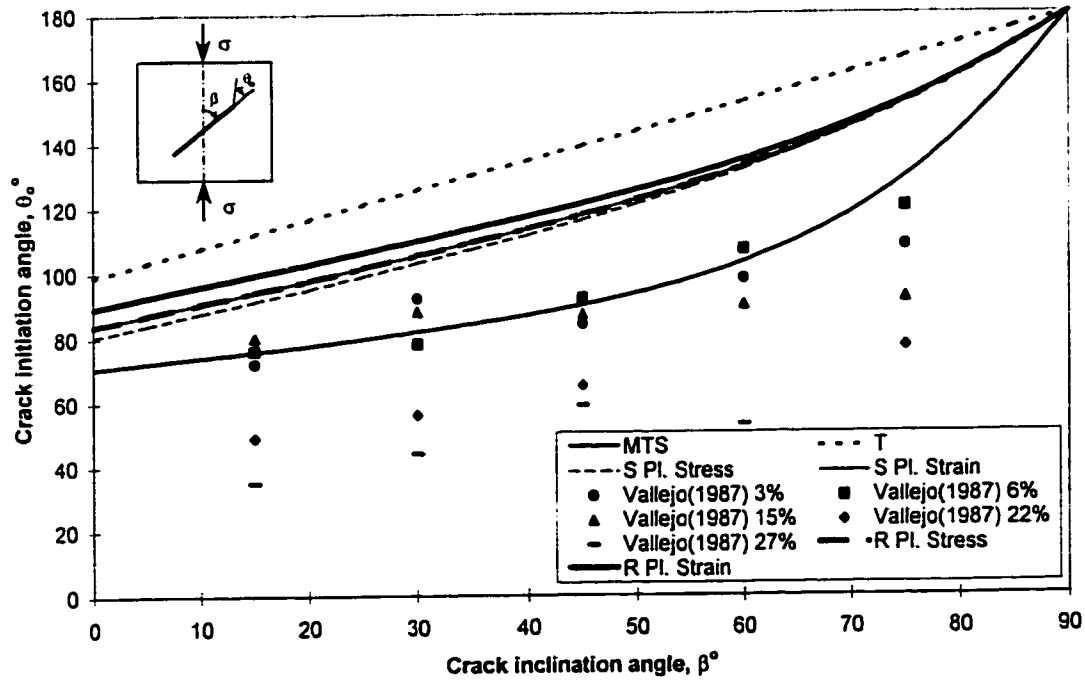

Fig. 3.9b: Uniaxial compression

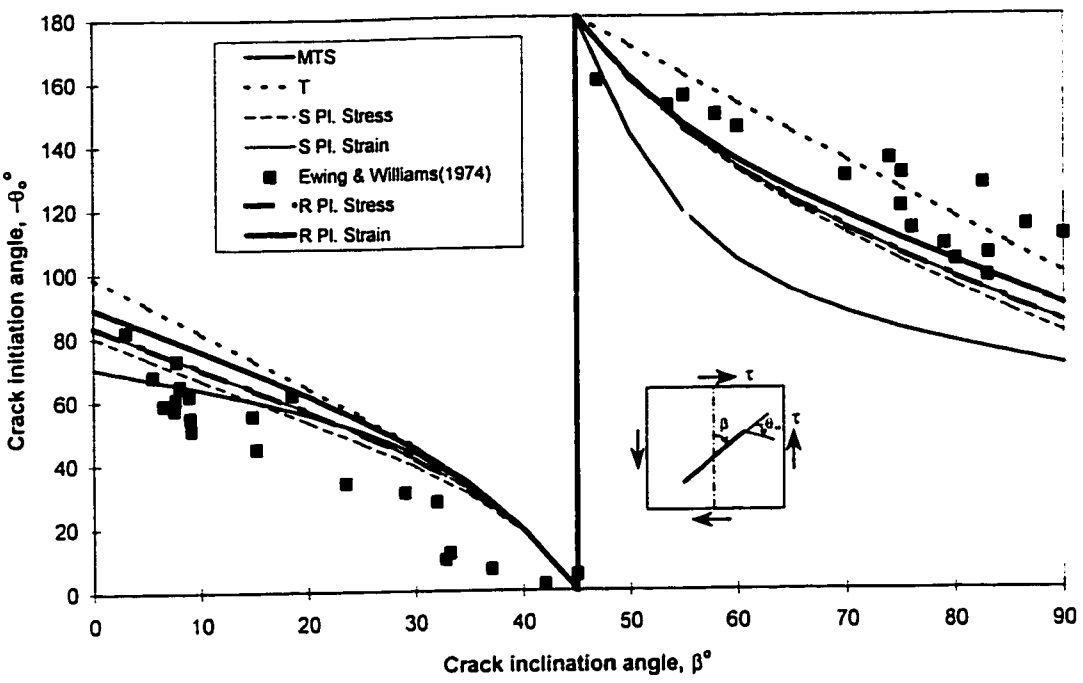

Fig. 3.10: Pure shear loading

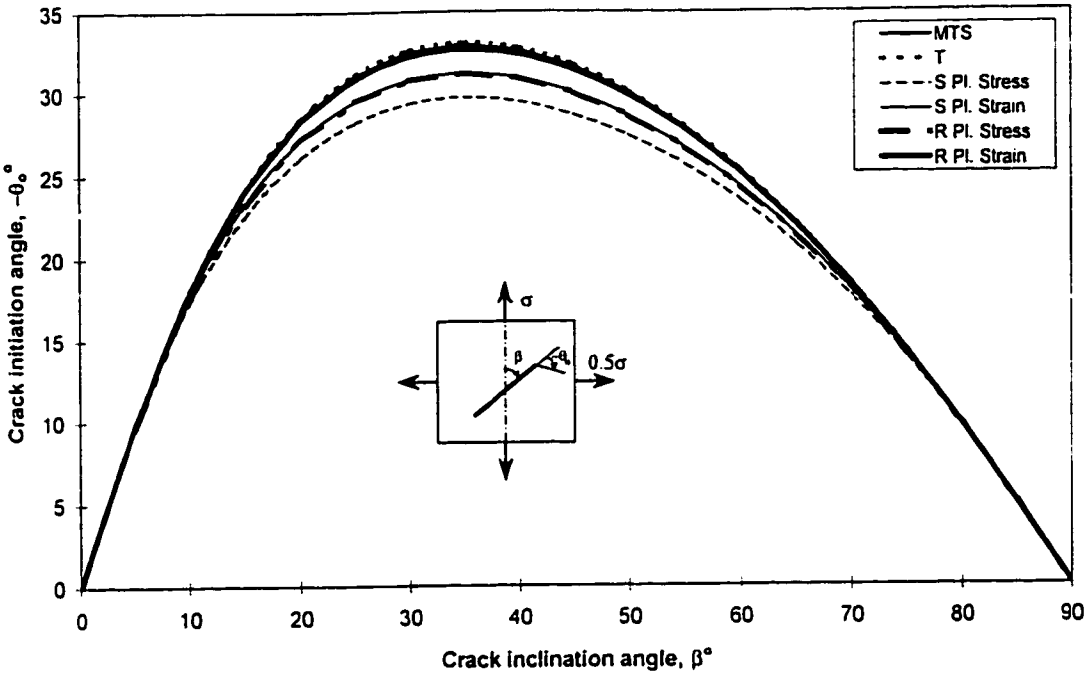

Fig. 3.11a: Biaxial loading loading, $\lambda = 0.5$

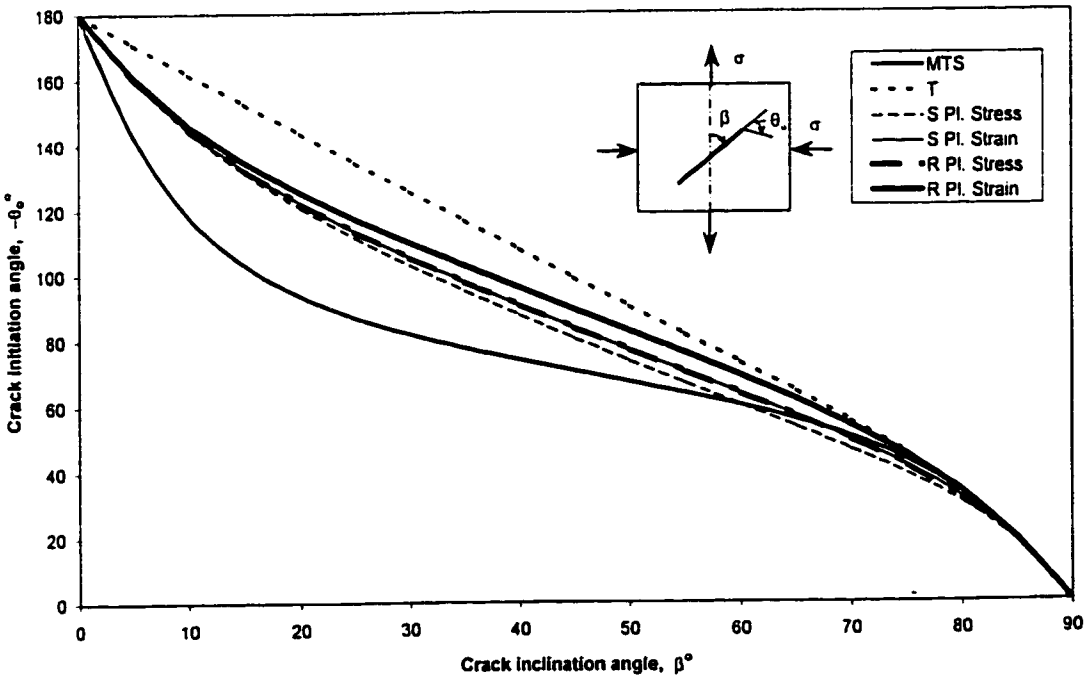

Fig. 3.11b: Biaxial loading, $\lambda = -1.0$

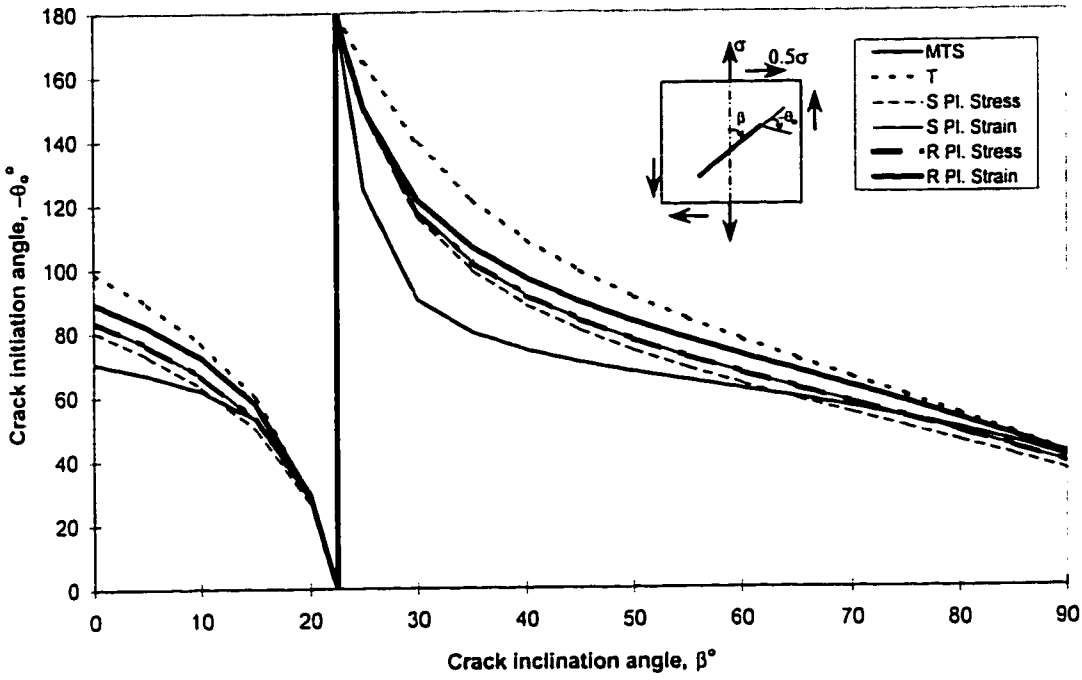

Fig. 3.12a: Proportional tension torsion loading, $\alpha = 0.5$

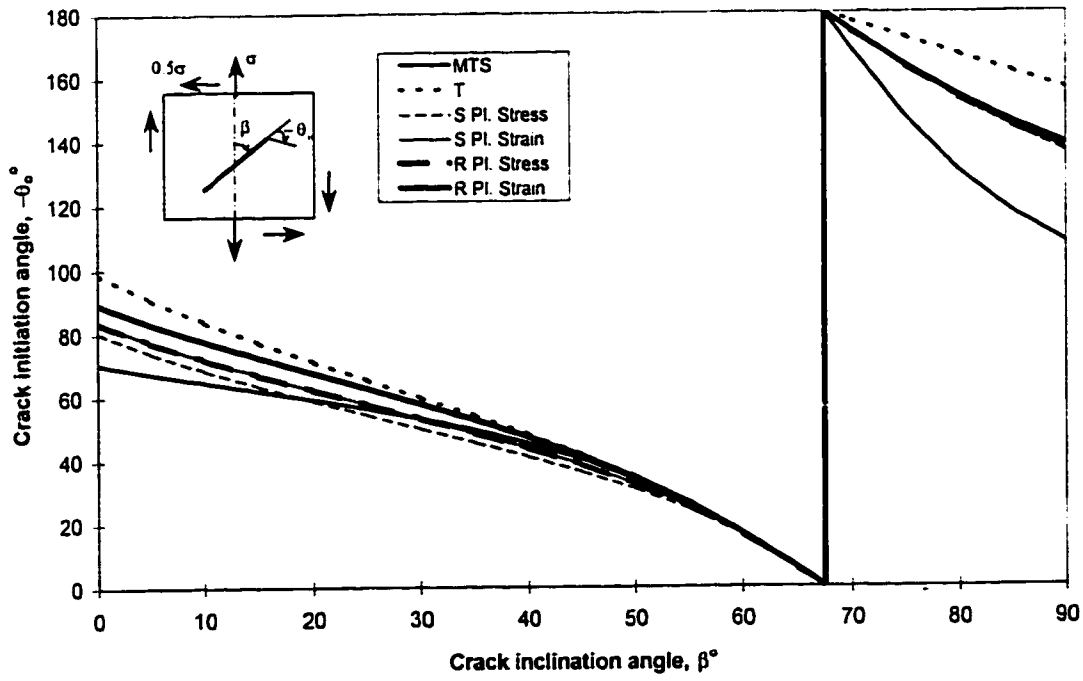

Fig. 3.12b: Proportional tension torsion loading, $\alpha = -0.5$

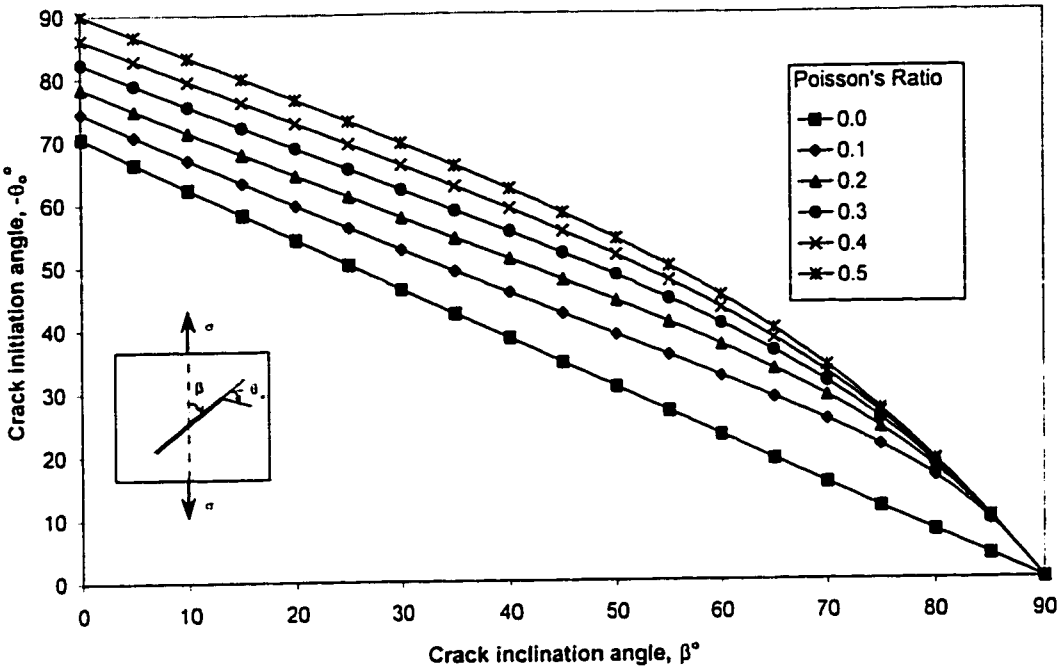

Fig. 3.13a: S-criterion, uniaxial tension, plane strain

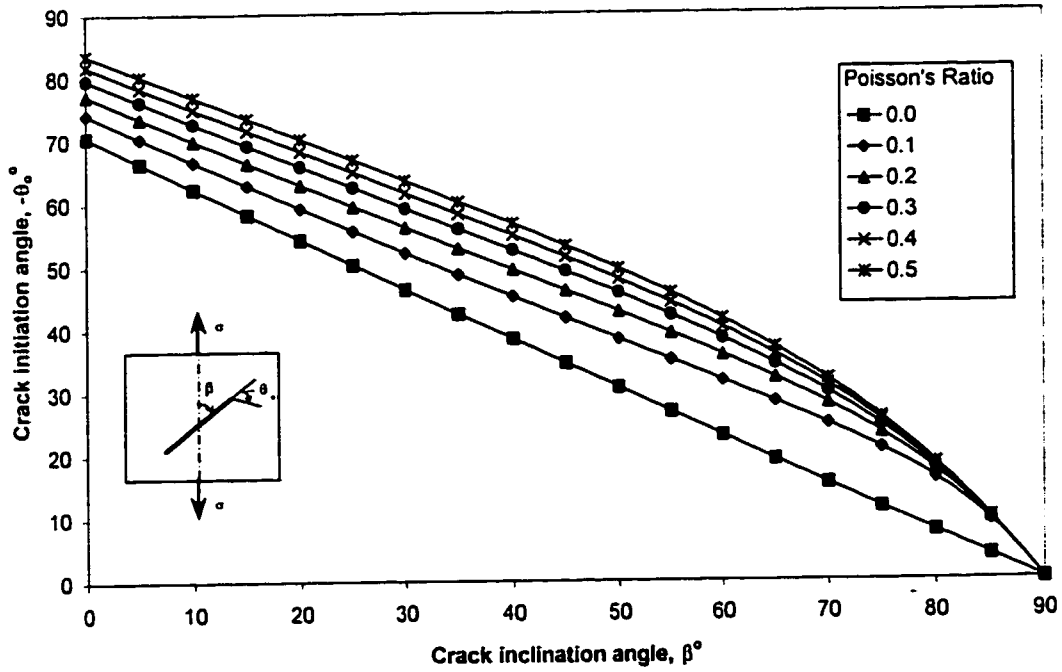

Fig. 3.13b: S-criterion, uniaxial tension, plane stress

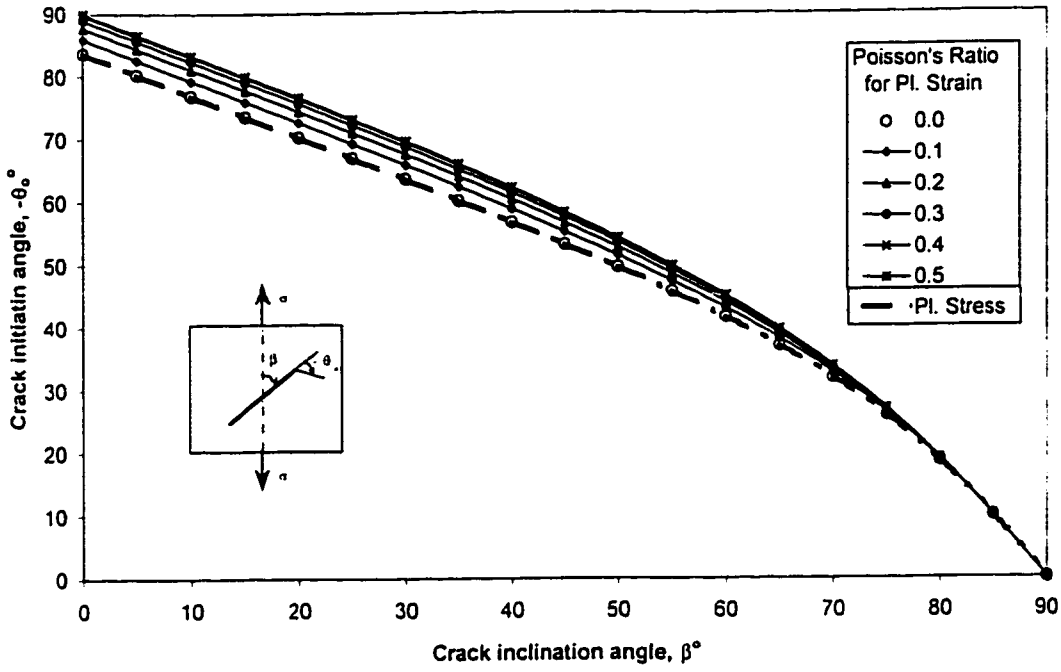

Fig. 3.14: R-criterion, uniaxial tension, plane strain and plane stress

Chapter 4

Crack Tip Core Region and Crack Initiation Angles for Anisotropic Materials

4.1 Introduction

Many engineering materials can be considered to have isotropic behavior, and results within reasonable accuracy can be generated. However, it is not always possible to assume an isotropic behavior. A large number of engineering materials have anisotropic properties. Composites of oriented fibers, composites of whisker reinforced, wood, rock and other materials are most often orthotropic and anisotropic from point to point. The fracture behavior of such materials under mixed mode loading, therefore, cannot be predicted by the criteria that are developed on the isotropic material behavior assumption. The modification of available criteria or new criteria based on anisotropic consideration are needed.

Several studies have been done to modify the available criteria for anisotropic materials. Saouma et al. (1987) modified the maximum tangential stress (MTS) theory. Gdoutos and

Zacharopoulos (1989) modified the minimum strain energy density criterion (S-criterion) to include anisotropy. The S-criterion is also modified by Zhiming and Ayari (1994). Instead of minimizing strain energy density factor S (as done by Gdoutos and Zacharopoulos, (1989)), they defined the S-criterion as minimizing the ratio of S to critical S (S_c), to include the effects of variation of toughness. Theorcaris and Philippidis (1991) have modified the T-criterion, by decomposing the anisotropic elastic potential into distinct components, for homogenous anisotropic materials.

The general way of dealing with anisotropic mixed mode fracture is to use the crack tip stress field for the anisotropic case, and then apply any available criterion for mixed mode fracture. The anisotropic stress field used by several researchers (Saouma et al., 1987; Gdoutos and Zacharopoulos, 1989; Zhiming and Ayari, 1994; Theorcaris and Philippidis, 1991) is given as:

$$\begin{aligned}
\sigma_x &= \frac{K_I}{\sqrt{2\pi r}} F_{Ix}(s_1, s_2, \theta) + \frac{K_{II}}{\sqrt{2\pi r}} F_{IIx}(s_1, s_2, \theta) \\
\sigma_y &= \frac{K_I}{\sqrt{2\pi r}} F_{Iy}(s_1, s_2, \theta) + \frac{K_{II}}{\sqrt{2\pi r}} F_{IIy}(s_1, s_2, \theta) \\
\tau_{xy} &= \frac{K_I}{\sqrt{2\pi r}} F_{Ixy}(s_1, s_2, \theta) + \frac{K_{II}}{\sqrt{2\pi r}} F_{IIxy}(s_1, s_2, \theta)
\end{aligned} \tag{4.1}$$

Where

$$
\begin{aligned}
F_{Ix}(s_1,s_2,\theta) &= \mathrm{Re}\left[\frac{s_1 s_2}{s_1-s_2}\left(\frac{s_2}{(\cos\theta+s_2\sin\theta)^{1/2}}-\frac{s_1}{(\cos\theta+s_1\sin\theta)^{1/2}}\right)\right]\\
F_{Iy}(s_1,s_2,\theta) &= \mathrm{Re}\left[\frac{1}{s_1-s_2}\left(\frac{s_1}{(\cos\theta+s_2\sin\theta)^{1/2}}-\frac{s_2}{(\cos\theta+s_1\sin\theta)^{1/2}}\right)\right]\\
F_{Ixy}(s_1,s_2,\theta) &= \mathrm{Re}\left[\frac{s_1 s_2}{s_1-s_2}\left(\frac{1}{(\cos\theta+s_1\sin\theta)^{1/2}}-\frac{1}{(\cos\theta+s_2\sin\theta)^{1/2}}\right)\right]\\
F_{IIx}(s_1,s_2,\theta) &= \mathrm{Re}\left[\frac{1}{s_1-s_2}\left(\frac{s_2^2}{(\cos\theta+s_2\sin\theta)^{1/2}}-\frac{s_1^2}{(\cos\theta+s_1\sin\theta)^{1/2}}\right)\right]\\
F_{IIy}(s_1,s_2,\theta) &= \mathrm{Re}\left[\frac{1}{s_1-s_2}\left(\frac{1}{(\cos\theta+s_2\sin\theta)^{1/2}}-\frac{1}{(\cos\theta+s_1\sin\theta)^{1/2}}\right)\right]\\
F_{IIxy}(s_1,s_2,\theta) &= \mathrm{Re}\left[\frac{s_1 s_2}{s_1-s_2}\left(\frac{s_1}{(\cos\theta+s_1\sin\theta)^{1/2}}-\frac{s_2}{(\cos\theta+s_2\sin\theta)^{1/2}}\right)\right]
\end{aligned}
\tag{4.2}
$$

This stress distribution at the crack tip depends on the configuration and loading of the anisotropic body as well as the material properties. s_1 and s_2 are the complex conjugate roots of the familiar characteristic equation:

$$a_{11}s^4 - 2a_{16}s^3 + (2a_{12}+a_{66})s^2 - 2a_{26}s + a_{22} = 0 \tag{4.3}$$

Where a_{ij} are the compliances related to engineering constants E_{ij}.

In order to investigate the crack tip core region for anisotropic case with crack initiation angles, and to extend the R-criterion (defined in Chapter 3) to include anisotropy, we are going to use a different approach. A yield function is used to define a core region. Therefore, we will use an anisotropic yield criterion to introduce the effects of anisotropy, and will use the same stress field as for isotropic bodies.

4.2 Analysis

The singular elastic stress field at the crack tip, is given as in Eq. (2.2), where r and θ are the polar co-ordinates with origin at the crack tip, and ν is the Poisson's ratio. The anisotropic yield function that we will use is the Hill's criterion (Hosford and Caddell, 1993). This yield function assumes that the material is homogenous and is characterized by three orthogonal axes of anisotropy, about which the properties have twofold symmetry. It also assumes that the tensile and compressive strengths are equal in any given direction. For a general state of stress, the Hill's anisotropic yield criterion has the form:

$$2f(\sigma_{ij}) = F(\sigma_y - \sigma_z)^2 + G(\sigma_z - \sigma_x)^2 + H(\sigma_x - \sigma_y)^2 + 2L\tau_{yz}^2 + 2M\tau_{xz}^2 + 2N\tau_{xy}^2 \qquad (4.4)$$

where F, G, H, L, M, and N are constants that characterize the anisotropy. For F=G=H and L=M=N=3F, Hill's criterion reduces to the isotropic von Mises criterion. The anisotropic constants F, G and H can be evaluated from simple tension tests, performed to obtain the yield stress in each direction. L, M and N can be evaluated from shear tests.

For a 2-D case, Eq. (4.4) reduces to:

$$2f(\sigma_{ij}) = F(\sigma_y - \sigma_z)^2 + G(\sigma_z - \sigma_x)^2 + H(\sigma_x - \sigma_y)^2 + 2N\tau_{xy}^2 \qquad (4.5)$$

where σ_z will depend on the state of stress, whether plane stress or plane strain, at the crack tip and is defined in Eq. (4.4). Four constants are left for a 2-D case, out of which 3 constants F, G, H define the degree of anisotropy in normal directions and N define the degree of anisotropy in shear direction.

Now expressing the stress intensity factors and stress field in the same way as for the isotropic case (Chapter 3), we have:

$$\begin{aligned} K_I &= \sigma_{app}\sqrt{\pi a} f_{K_I}(\beta) \\ K_{II} &= \sigma_{app}\sqrt{\pi a} f_{K_{II}}(\beta) \end{aligned} \tag{4.6}$$

where σ_{app} is the applied stress, which may be tensile, compressive, shear stress, or a combination of these, $f_{K_i}(\beta)$ is a function of the crack inclination angle, β, and the loading condition. We get the stress field as:

$$\begin{aligned} \sigma_x &= \frac{\sigma_{app}\sqrt{a}}{\sqrt{2r}} f_x(\theta, f_{K_i}) \\ \sigma_y &= \frac{\sigma_{app}\sqrt{a}}{\sqrt{2r}} f_y(\theta, f_{K_i}) \\ \tau_{xy} &= \frac{\sigma_{app}\sqrt{a}}{\sqrt{2r}} f_{xy}(\theta, f_{K_i}) \end{aligned} \tag{4.7}$$

where $f_x(\theta, f_{K_i})$, $f_y(\theta, f_{K_i})$, and $f_{xy}(\theta, f_{K_i})$ are defined as:

$$\begin{aligned} f_x(\theta, f_{K_i}) &= \left\{ f_{K_I}(\beta)\cos\frac{\theta}{2}\left(1 - \sin\frac{\theta}{2}\sin\frac{3\theta}{2}\right)\right\} - \left\{ f_{K_{II}}(\beta)\sin\frac{\theta}{2}\left(2 + \cos\frac{\theta}{2}\cos\frac{3\theta}{2}\right)\right\} \\ f_y(\theta, f_{K_i}) &= \left\{ f_{K_I}(\beta)\cos\frac{\theta}{2}\left(1 + \sin\frac{\theta}{2}\sin\frac{3\theta}{2}\right)\right\} + \left\{ f_{K_{II}}(\beta)\sin\frac{\theta}{2}\cos\frac{\theta}{2}\cos\frac{3\theta}{2}\right\} \\ f_{xy}(\theta, f_{K_i}) &= \left\{ f_{K_I}(\beta)\cos\frac{\theta}{2}\sin\frac{\theta}{2}\cos\frac{3\theta}{2}\right\} + \left\{ f_{K_{II}}(\beta)\cos\frac{\theta}{2}\left(1 - \sin\frac{\theta}{2}\sin\frac{3\theta}{2}\right)\right\} \end{aligned} \tag{4.8}$$

Substituting Eq. (4.7) in Eq. (4.5), we get:

$$2f(\sigma_{ij}) = \frac{\sigma_{app}^2 a}{2r}\left\{F(f_y - f_z)^2 + G(f_z - f_x)^2 + H(f_x - f_y)^2 + 2Nf_{xy}^2\right\} \tag{4.9}$$

Substituting Eq. (4.8) in Eq. (4.9), we get the anisotropic core region radius $R_{P,H}$ based on Hill's anisotropic yield function. For plane stress,

$$R_{P,H}(\theta, f_{K_I}) = \frac{r_{p,H}(\theta, f_{K_I})}{a\left[\frac{\sigma_{app}}{f(\sigma_{ij})}\right]^2} = \frac{1}{4}\left[f_{K_I}^2(\beta)g_1(\theta) + f_{K_{II}}^2(\beta)g_2(\theta) + f_{K_I}(\beta)f_{K_{II}}(\beta)g_{12}(\theta)\right] \quad (4.10a)$$

And for plane strain,

$$R_{P,H}(\theta, f_{K_I}) = \frac{r_{p,H}(\theta, f_{K_I})}{a\left[\frac{\sigma_{app}}{f(\sigma_{ij})}\right]^2} = \frac{1}{4}\left[\; f_{K_I}^2(\beta)(g_1(\theta) + h_1(\theta,\nu)) + f_{K_{II}}^2(\beta)(g_2(\theta) + h_2(\theta,\nu)) + f_{K_I}(\beta)f_{K_{II}}(\beta)(g_{12}(\theta) + h_{12}(\theta,\nu))\;\right] \quad (4.10b)$$

Where:

$$\begin{aligned}
g_1(\theta) &= \left(\frac{13F + 5G + 4H + 2N}{16}\right) + \left(\frac{25F + 9G + 4H - 2N}{32}\right)\cos\theta \\
&\quad + \left(\frac{-5F + 3G - 4H - 2N}{16}\right)\cos 2\theta + \left(\frac{-5F + 3G - 4H + 2N}{16}\right)\cos 3\theta \\
&\quad + \left(\frac{F + G + 4H - 2N}{32}\right)\cos 5\theta \\
g_2(\theta) &= \left(\frac{F + 25G + 20H + 10N}{16}\right) + \left(\frac{-F - 49G - 36H + 18N}{32}\right)\cos\theta \\
&\quad + \left(\frac{-F + 7G + 12H + 6N}{16}\right)\cos 2\theta + \left(\frac{F - 7G - 12H + 6N}{16}\right)\cos 3\theta \\
&\quad + \left(\frac{-F - G - 4H + 2N}{32}\right)\cos 5\theta \\
g_{12}(\theta) &= \left(\frac{-5F - 21G + 12H - 6N}{16}\right)\sin\theta + \left(\frac{F + G + 4H + 2N}{4}\right)\sin 2\theta \\
&\quad + \left(\frac{3F - 5G - 4H + 2N}{8}\right)\sin 3\theta + \left(\frac{-F - G - 4H + 2N}{16}\right)\sin 5\theta
\end{aligned} \quad (4.11a)$$

$$h_1(\theta)=\left(\frac{\nu(4\nu-5)F+\nu(4\nu-3)G}{2}\right)(1+\cos\theta)+\left(\frac{\nu(F-G)}{2}\right)(\cos 2\theta+\cos 3\theta)$$

$$h_2(\theta)=\left(\frac{\nu(4\nu-1)F+\nu(4\nu-7)G}{2}\right)(1-\cos\theta)+\left(\frac{\nu(F-G)}{2}\right)(\cos 2\theta-\cos 3\theta) \quad (4.11b)$$

$$h_{12}(\theta)=(\nu(3-4\nu)F+\nu(5-4\nu)G)\sin\theta+\nu(G-F)\sin 3\theta$$

These equations can be used to study the effect of anisotropic constants for any loading case for which the stress intensity factors are available.

4.3 Anisotropic R-criterion

The anisotropic R-criterion is defined in the same way as the isotropic R-criterion, except that the crack tip core region will be taken as defined by the Hill's function (as defined in previous section) instead of von Mises yield function. The direction of crack initiation coincides with the direction of minimum distance to the elastically loaded material around a variable core region, defined by Hill's anisotropic yield function. Mathematically, it can be stated as:

$$\frac{\partial R_{P,H}}{\partial\theta}=0$$
$$\frac{\partial^2 R_{P,H}}{\partial\theta^2}>0 \quad (4.12)$$

Applying the anisotropic R-criterion to Eq. (4.9), we get:

$$\omega_{10}\tan^{10}\frac{\theta}{2}+\omega_9\tan^9\frac{\theta}{2}+\omega_8\tan^8\frac{\theta}{2}+\omega_7\tan^7\frac{\theta}{2}+\omega_6\tan^6\frac{\theta}{2}+$$
$$\omega_5\tan^5\frac{\theta}{2}+\omega_4\tan^4\frac{\theta}{2}+\omega_3\tan^3\frac{\theta}{2}+\omega_2\tan^2\frac{\theta}{2}+\omega_1\tan\frac{\theta}{2}+\omega_0=0 \quad (4.13a)$$
$$w_1\cos\theta+w_2\cos 2\theta+w_3\cos 3\theta+w_4\cos 5\theta+$$
$$w_5\sin\theta+w_6\sin 2\theta+w_7\sin 3\theta+w_8\sin 5\theta>0$$

for plane stress, and

$$(\omega_{10}+\eta_{10})\tan^{10}\frac{\theta}{2}+(\omega_9+\eta_9)\tan^9\frac{\theta}{2}+(\omega_8+\eta_8)\tan^8\frac{\theta}{2}+(\omega_7+\eta_7)\tan^7\frac{\theta}{2}+$$
$$(\omega_6+\eta_6)\tan^6\frac{\theta}{2}+(\omega_5+\eta_5)\tan^5\frac{\theta}{2}+(\omega_4+\eta_4)\tan^4\frac{\theta}{2}+(\omega_3+\eta_3)\tan^3\frac{\theta}{2}+$$
$$(\omega_2+\eta_2)\tan^2\frac{\theta}{2}+(\omega_1+\eta_1)\tan\frac{\theta}{2}+(\omega_0+\eta_0)=0 \qquad (4.13b)$$
$$(w_1+n_1)\cos\theta+(w_2+n_2)\cos 2\theta+(w_3+n_3)\cos 3\theta+(w_4+n_4)\cos 5\theta+$$
$$(w_5+n_5)\sin\theta+(w_6+n_6)\sin 2\theta+(w_7+n_7)\sin 3\theta+(w_8+n_8)\sin 5\theta>0$$

for plane strain. The coefficients are defined as:

$$\begin{aligned}
\omega_{10} &= 4\mu(G+H)\\
\omega_9 &= 4\left[(4G+7H-2N)-\mu^2(G+H)\right]\\
\omega_8 &= 12\mu(-3G-7H+3N)\\
\omega_7 &= 2\left[(-9F-5G-36H+24N)+\mu^2(12G+32H-18N)\right]\\
\omega_6 &= \mu(75F+35G+212H-134N)\\
\omega_5 &= 3\left[(15F+7G+36H-18N)+\mu^2(-25F-9G-60H+30N)\right] \qquad (4.14a)\\
\omega_4 &= \mu(-89F-49G-268H+106N)\\
\omega_3 &= 2\left[(-8F-12G-48H+18N)+\mu^2(5F+9G+36H-16N)\right]\\
\omega_2 &= 3\mu(-F+11G+24H-14N)\\
\omega_1 &= \left[(F+9G+16H-14N)+\mu^2(5F-7G+2N)\right]\\
\omega_0 &= \mu(F-3G+2N)
\end{aligned}$$

$$
\begin{aligned}
\eta_{10} &= 4\mu\nu[-2G+(F+G)\nu] \\
\eta_9 &= 4\nu[(3F-5G)+2G\mu^2+\nu(F+G)(1-\mu^2)] \\
\eta_8 &= 12\mu\nu[2(-2F+G)+(F+G)\nu] \\
\eta_7 &= 8\nu[(-F-3G)+(5F-G)\mu^2+2\nu(F+G)(1-\mu^2)] \\
\eta_6 &= 8\mu\nu[2(-3F+2G)+(F+G)\nu] \\
\eta_5 &= 8\nu[-2F+(3F-G)\mu^2+\nu(F+G)(1-\mu^2)] \\
\eta_4 &= 8\mu\nu[2(3F-2G)-(F+G)\nu] \\
\eta_3 &= 8\nu[(-3F-G)+(3F+G)\mu^2+2\nu(F+G)(1-\mu^2)] \\
\eta_2 &= 12\mu\nu[2(2F-G)-(F+G)\nu] \\
\eta_1 &= 4\nu[(F-3G)+2(-F+2G)\mu^2+\nu(F+G)(1-\mu^2)] \\
\eta_0 &= 4\mu\nu[2G-(F+G)\nu]
\end{aligned}
\tag{4.14b}
$$

$$
\begin{aligned}
w_1 &= [(F+49G+36H-18N)+\mu^2(-25F-9G-4H+2N)] \\
w_2 &= 8[(F-7G-12H-6N)+\mu^2(5F-3G+4H+2N)] \\
w_3 &= 18[(-F+7G+12H-6N)+\mu^2(5F-3G+4H-2N)] \\
w_4 &= 25[(F+G+4H-2N)+\mu^2(-F-G-4H+2N)] \\
w_5 &= 2[(5F+24G-12H+6N)\mu] \\
w_6 &= 32[(-F-G-4H-2N)\mu] \\
w_7 &= 18[(-6F+10G+8H-4N)\mu] \\
w_8 &= 50[(F+G+4H-2N)\mu]
\end{aligned}
\tag{4.15a}
$$

$$
\begin{aligned}
n_1 &= 16\nu[-(F+7G)+\mu^2(5F+3G)+4\nu(F+G)(1-\mu^2)] \\
n_2 &= 64\nu[(-F+G)(1+\mu^2)] \\
n_3 &= 144\nu[(F-G)(1-\mu^2)] \\
n_4 &= 0 \\
n_5 &= 32\mu\nu[-(3F+5G)+4\nu(F+G)] \\
n_6 &= 0 \\
n_7 &= 288\mu\nu(F-G) \\
n_8 &= 0
\end{aligned}
\tag{4.15b}
$$

where μ is defined as:

$$\mu = \frac{K_I}{K_{II}} = \frac{f_{KI}(\beta)}{f_{KII}(\beta)} \tag{4.16}$$

$f_{KI}(\beta)$ and $f_{KII}(\beta)$ can be found for different loading conditions from Eqs. (3.12), (3.15), (3.19), and (3.22), (Refer to Fig. (2.3)).

4.4 Results and Discussions

The anisotropic crack tip core regions and results of the anisotropic R-criterion are plotted in Fig. 4.1 through Fig. 4.15 The isotropic R-criterion is also plotted with each figure for comparison. It is important to note that F defines the degree of anisotropy in normal direction in yz-plane, and G and H define it in xz- and zy-planes respectively. The constant N defines the degree of shear anisotropy in xy-plane. Several researchers (Zhiming, 1995; Zhang and Venugopalan, 1987) have shown the shapes of anisotropic core regions. The comparison of the crack tip core regions presented in this study with earlier studies will be done wherever possible, since not all of the studies use the same factors to define anisotropy. The results shown by Zhiming (1995) are somewhat ambiguous, since there is no mention of loading case geometry and these are plotted for different values of K_{II}/K_I ratios, without any consideration of how such ratio can be obtained in real situations. Moreover, there is no explanation as to why the shape of the core region for $K_{II}/K_I = 1$ is not symmetric, while it is symmetric for other ratios. Zhang and Venugopalan (1987) have shown the crack tip core regions only for pure mode-I. All the results presented in this study are comparable with those presented by Zhang and Venugopalan (1987) for pure mode-I.

Figures 4.1 to 4.5 show the core regions for uniaxial loading, both under plane stress and plane strain conditions at the crack tip, for different values of anisotropic factors F, G, H, and N. Figure 4.1 shows the core region for isotropic case (F=G=H, N=3F) and these are same as presented in Chapter 3, for isotropic von Mises yield function. Figure 4.2 shows that the anisotropic shear constant N effects the complete shape of the core region and distorts it proportionally as compared to the isotropic case. Theocaris and Philippidis (1991) have shown the shapes of strain energy component contours at the crack tip for various fiber composites. When these contours are compared with the shape of the crack tip core regions for different values of N, a reasonable resemblance is shown for $\beta = 30°, 60°, 90°$. A parametric analysis can help find the values of F, G, H, and N to fit a core region for a particular fiber composite.

Figures 4.3 to 4.5 show the effect of the normal anisotropic constants F, G, and H respectively, both in plane stress and plane strain under uniaxial loading. The factor F effects the core region more in the half of the crack (left half on the polar plot), whereas the factor G effects more in the other half ahead of the crack (right half on the polar plot). The factor H, effects the overall core region shape. In all the cases, the actual size of the core region is greater, roughly twice, than in the case of isotropic core region. Moreover, the size of the core regions for plane strain case is less than plane stress case, and the core region is symmetric about horizontal for pure mode-I ($\beta = 90°$) for all cases. Both of these observations the are same as for the isotropic case.

Figures 4.6 to 4.8 show the shape of the core regions for pure shear, biaxial ($\lambda = -0.5$), proportional tension torsion ($\alpha = -0.5$) loading, for different crack inclination angles, for both plane stress and plane strain condition at the crack tip.

The core regions show one global minimum and one local minimum, and in some cases for crack inclination angle β, one weak local minimum that is ignored for crack initiation angle.

Figures 4.9 and 4.10 show the effect of N on crack initiation angles under uniaxial tension and uniaxial compression for both plane stress and plane strain condition at the crack tip. The effect of N is more pronounced for plane strain case than for plane stress case. Overall, N shows little effect on crack initiation angles. Although the core region shape is affected considerably (Fig. 4.2) by the value of N, yet the orientation of minima do not change much.

Figures 4.11 and 4.12 show the effect of the normal anisotropic constants (F, G, H) for uniaxial loading for both plane stress and plane strain conditions, respectively. Same trend is observed for all the four cases, with uniaxial tension under plane stress (Fig. 4.11a) showing the largest variation for crack initiation angles. The crack initiation angles for different values of F show lower values for crack initiation angles than the isotropic case, while for different values of H, these show higher values than the isotropic case. The curves for different values of F can be compared with those shown by Theocaris and Philippidis (1991) for different fiber composites. A fit to experimental data for any anisotropic material can be obtained by using different values of F, G, H, and N. The cases for different values of G show a different behavior for uniaxial tension case.

This could be explained by considering the shape of the core region (Fig. 4.4). For plane stress case, the core region at $\beta = 90°$ (for G=4) do not show a local minimum, whereas for other crack inclination angles, the local minimum is observed in the same orientation. For plane strain condition, discrete global and local minimum are shown in the core region.

Figures 4.13 to 4.15 show the effect of F, G, and H on crack initiation angles for pure shear, biaxial ($\lambda = -0.5$), proportional tension torsion ($\alpha = -0.5$) loading, for both plane stress and plane strain condition at the crack tip. These results can be explained by comparing with the results for uniaxial loading cases under plane stress in the same way as discussed in Chapter 2. For pure shear case, for $\beta = 0° \sim 45°$, the behavior is like uniaxial tension and for $\beta = 45° \sim 90°$, the behavior is like mirrored uniaxial compression. Similarly for biaxial loading case, for $\beta = 0° \sim 35°$,the behavior is like mirrored uniaxial compression, and for $\beta = 35° \sim 90°$,it is like uniaxial tension. The results for proportional tension-torsion loading can be explained in a similar fashion as for to pure shear case. Due to the inclusion of a normal stress, the shape is shifted towards the left.

4.5 Conclusions

The anisotropic crack tip core region characteristics are analyzed using anisotropic Hill's criterion. Results show reasonable comparison with earlier theoretical studies. Parametric studies can be done to find values for anisotropic constants to fit experimental data for any anisotropic material.

The R-criterion is modified to include anisotropy. It is important to note here that the Y-criterion presented by Yehia (1991), which he believes to be formulated on basis on minimum core region radius, cannot be extended to include anisotropy in this way. This is due to the difficulties in decomposing anisotropic plastic potential into distinct components as indicated by Theocaris and Philippidis (1991).

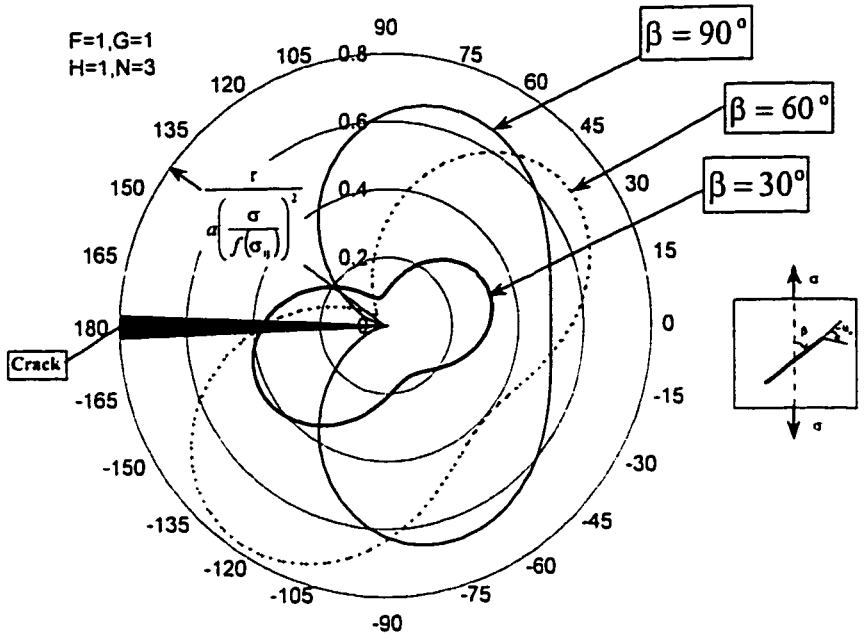

Fig. 4.1a: Core region, Uniaxial loading, plane stress, F=1,G=1,H=1,N=3

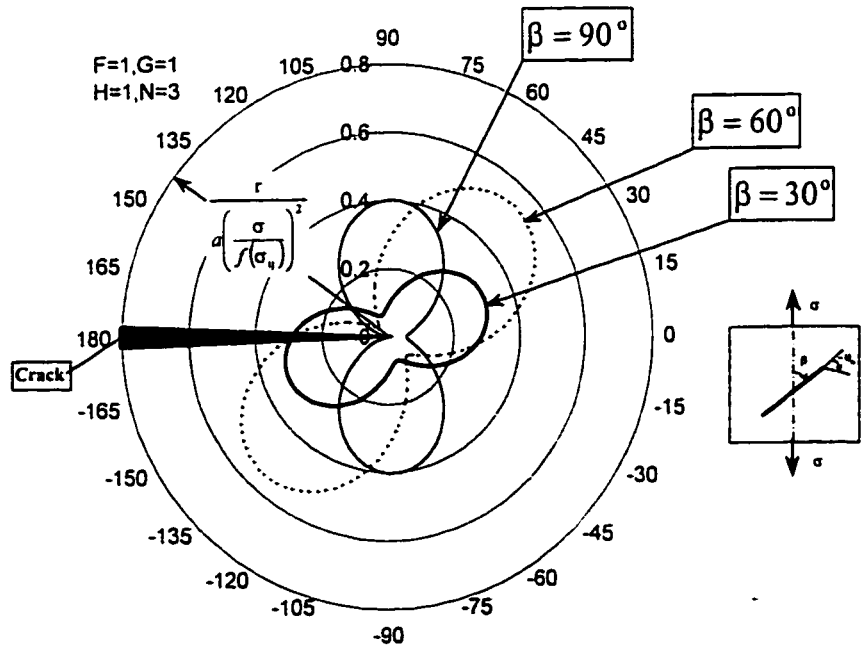

Fig. 4.1b: Core region, Uniaxial loading, plane strain, F=1,G=1,H=1,N=3

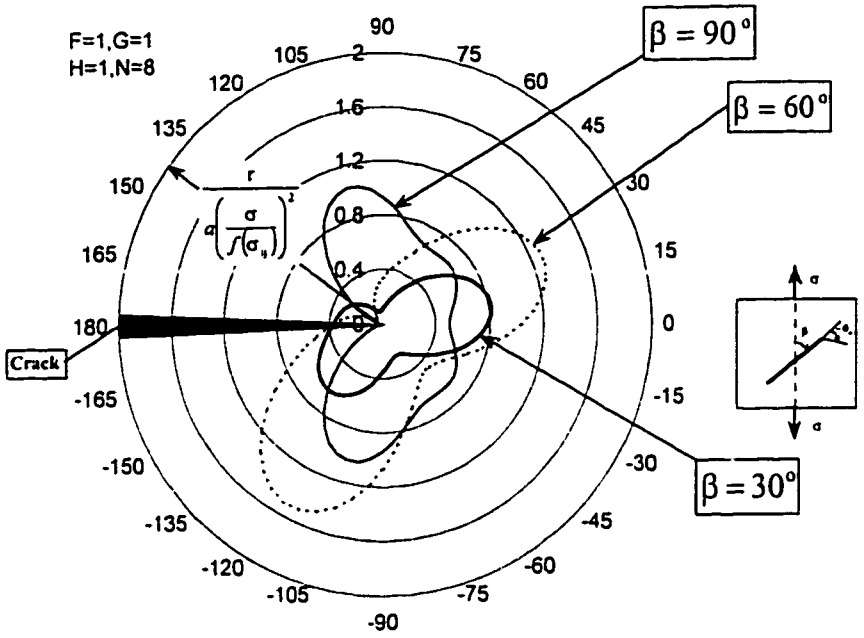

Fig. 4.2a: Core region, Uniaxial loading, plane stress, F=1,G=1,H=1,N=8

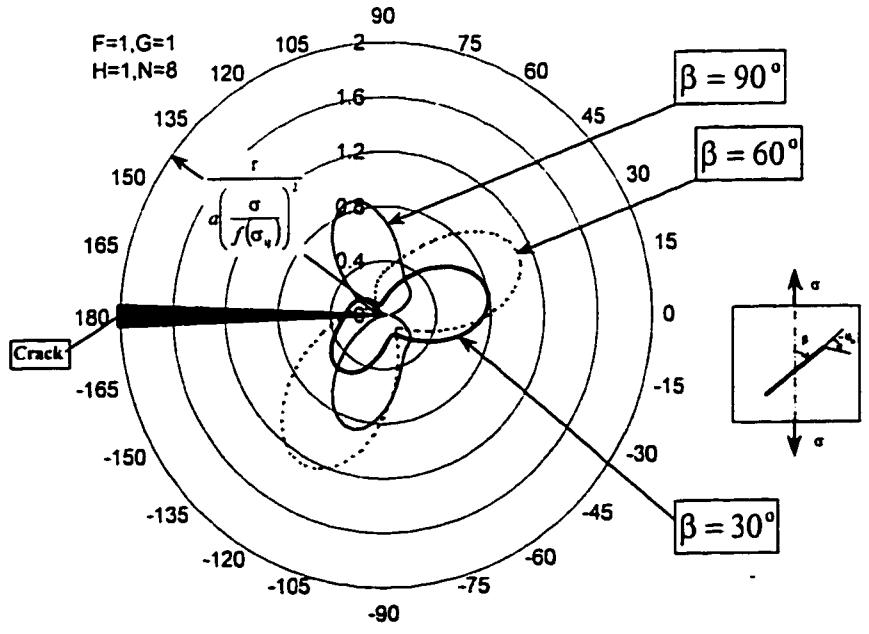

Fig. 4.2b: Core region, Uniaxial loading, plane strain, F=1,G=1,H=1,N=8

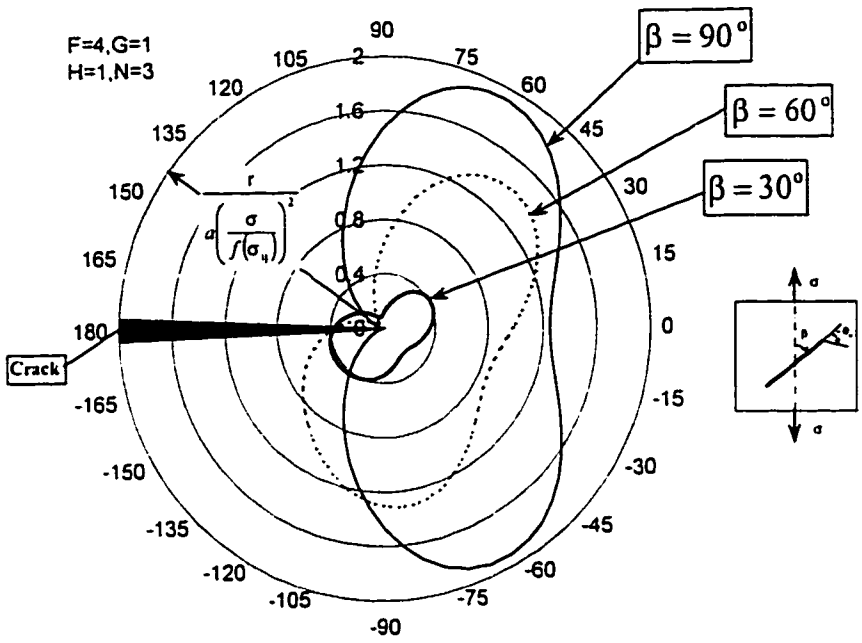

Fig. 4.3a: Core region, Uniaxial loading, plane stress, F=4,G=1,H=1,N=3

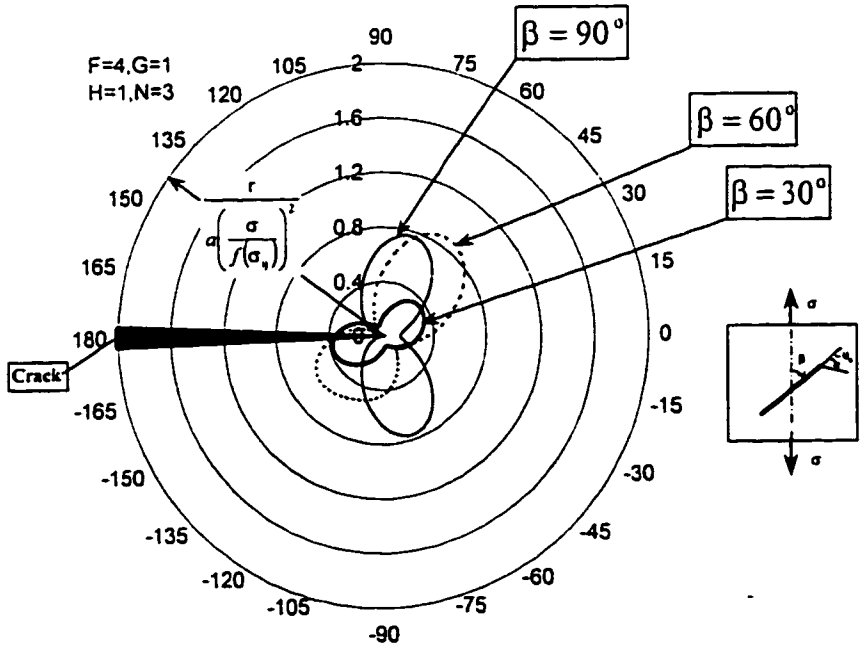

Fig. 4.3b: Core region, Uniaxial loading, plane strain, F=4,G=1,H=1,N=3

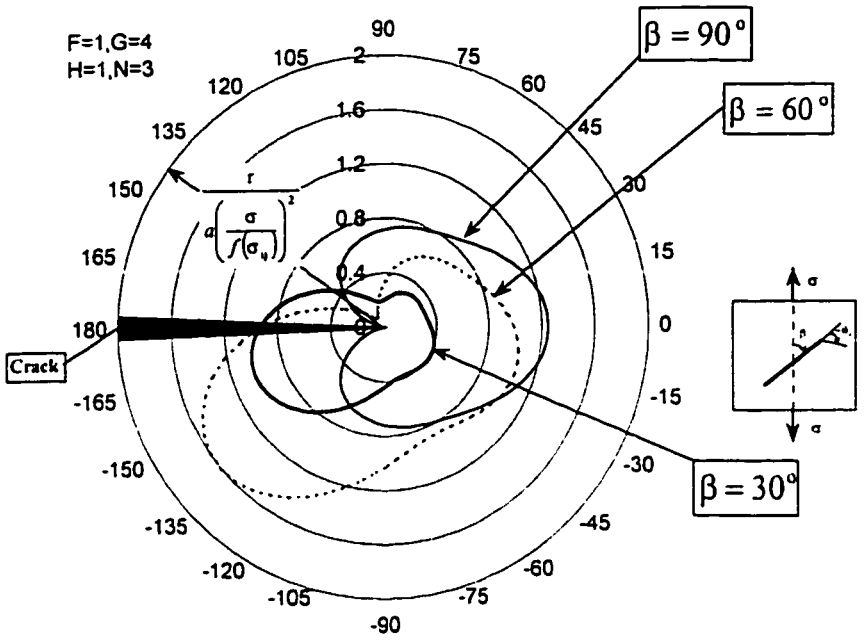

Fig. 4.4a: Core region, Uniaxial loading, plane stress, F=1,G=4,H=1,N=3

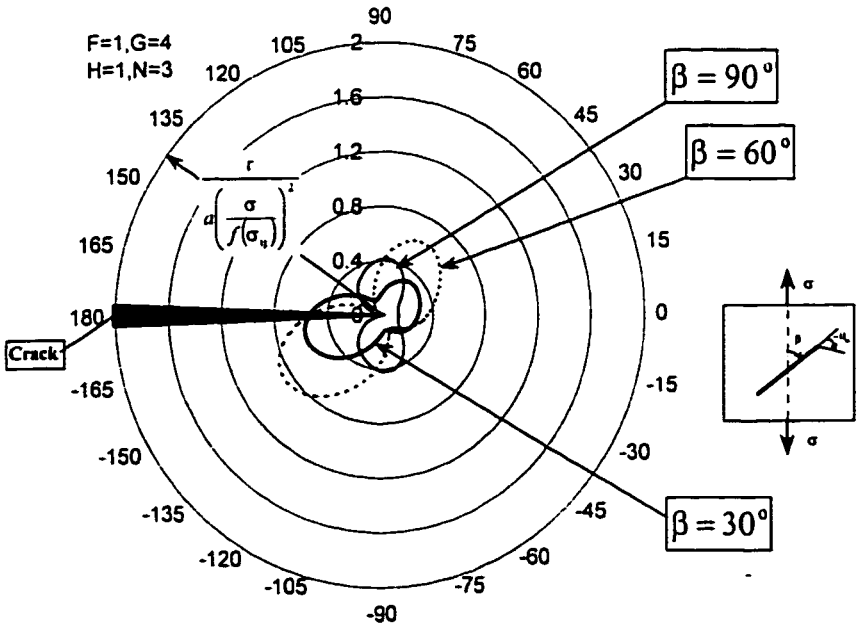

Fig. 4.4b: Core region, Uniaxial loading, plane strain, F=1,G=4,H=1,N=3

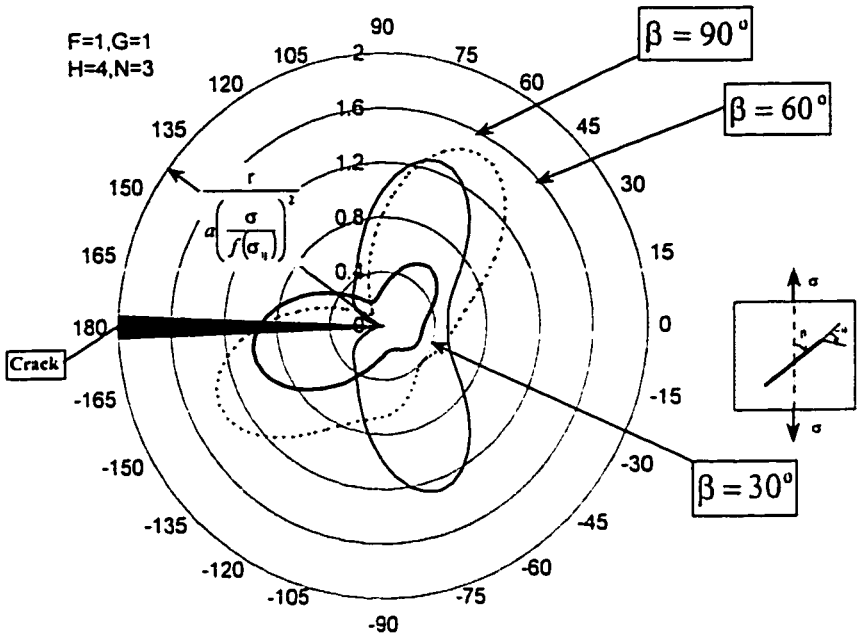

Fig. 4.5a: Core region, Uniaxial loading, plane stress, F=1,G=1,H=4,N=3

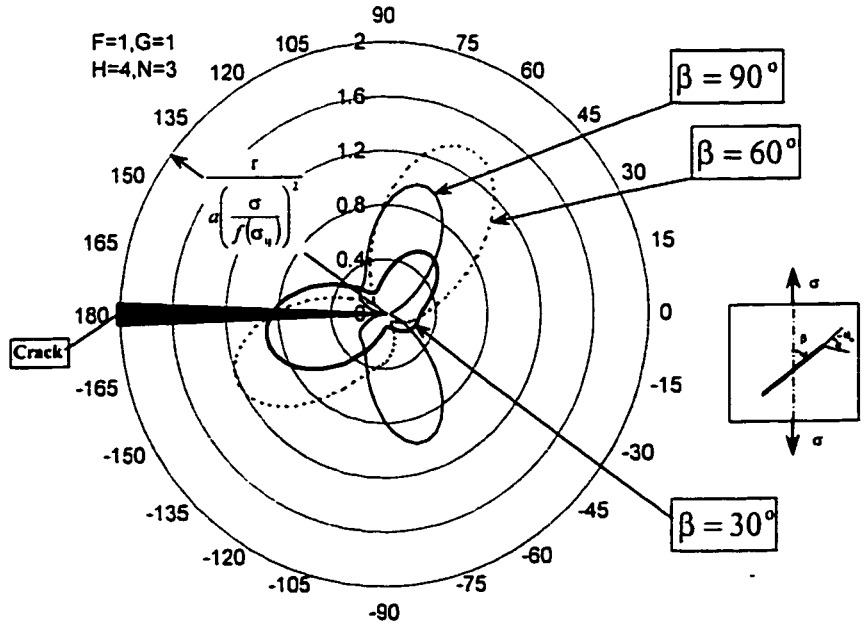

Fig. 4.5b: Core region, Uniaxial loading, plane strain, F=1,G=1,H=4,N=3

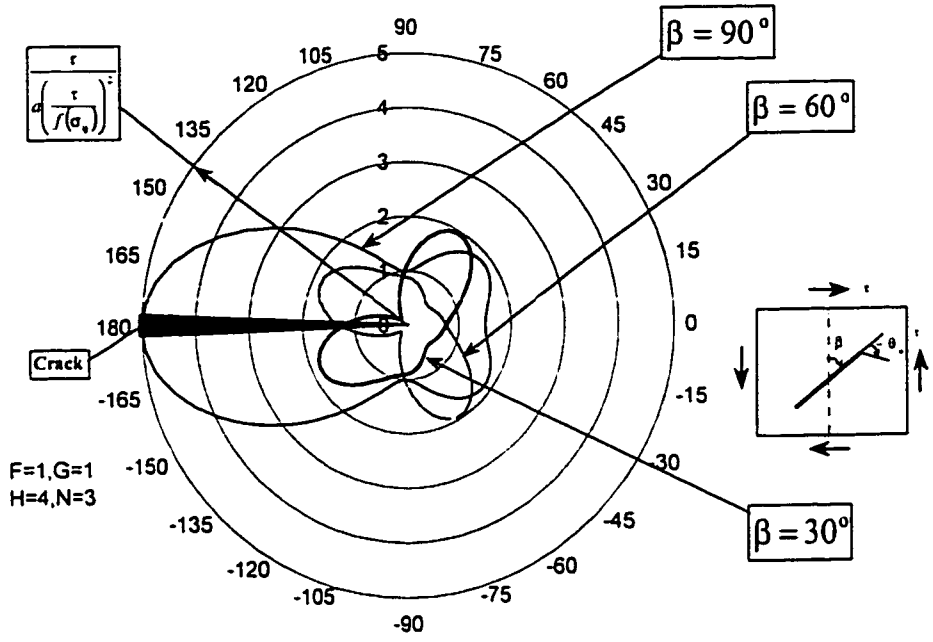

Fig. 4.6a: Core region, Pure shear loading, plane stress, , F=1,G=1,H=4,N=3

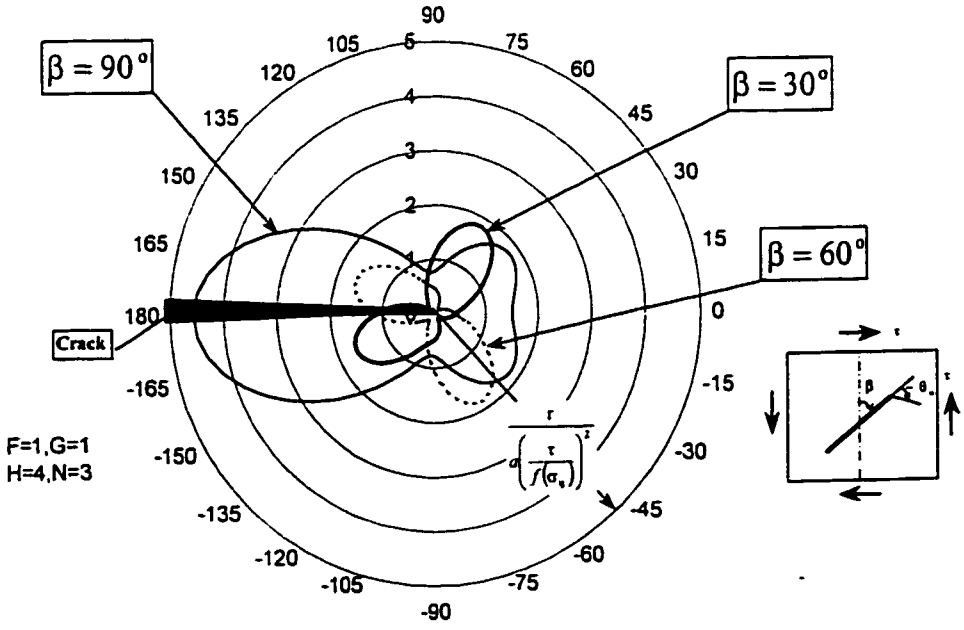

Fig. 4.6b: Core region, Pure shear loading, plane strain, , F=1,G=1,H=4,N=3

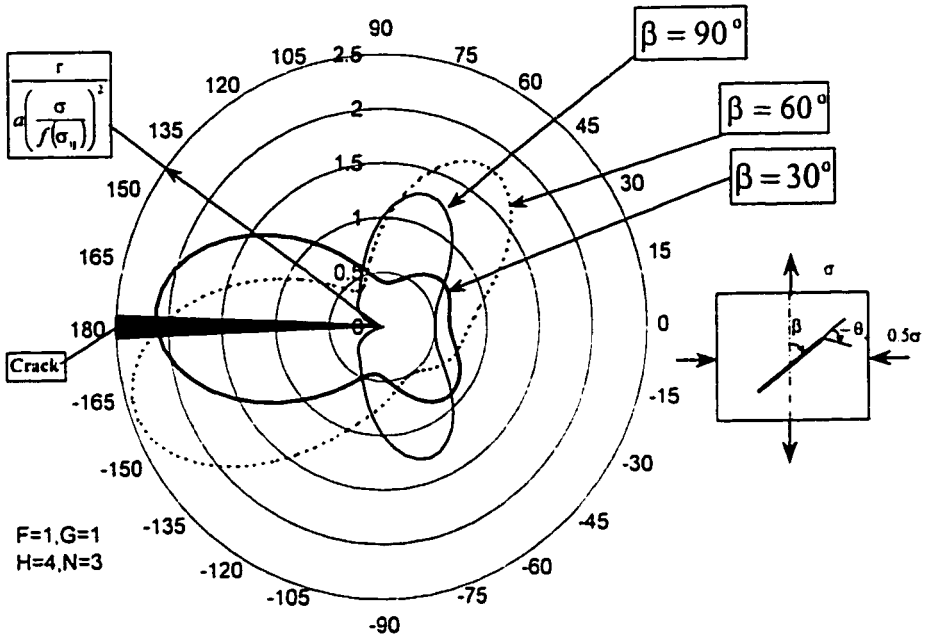

Fig. 4.7a: Core region, Biaxial loading λ = -0.5 , plane stress, F=1,G=1,H=4,N=3

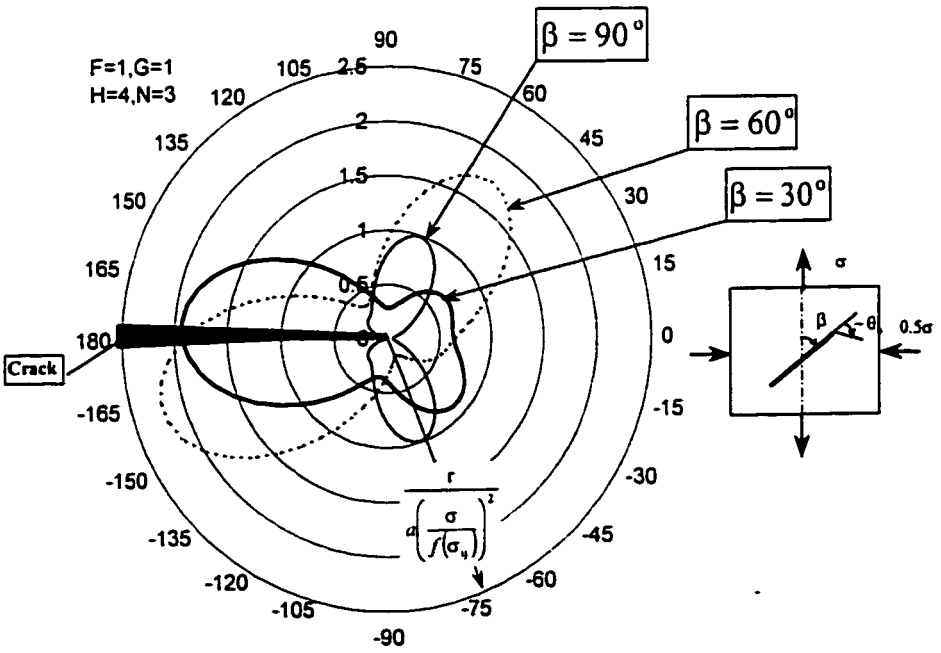

Fig. 4.7b: Core region, Biaxial loading λ = -0.5 , plane strain, F=1,G=1,H=4,N=3

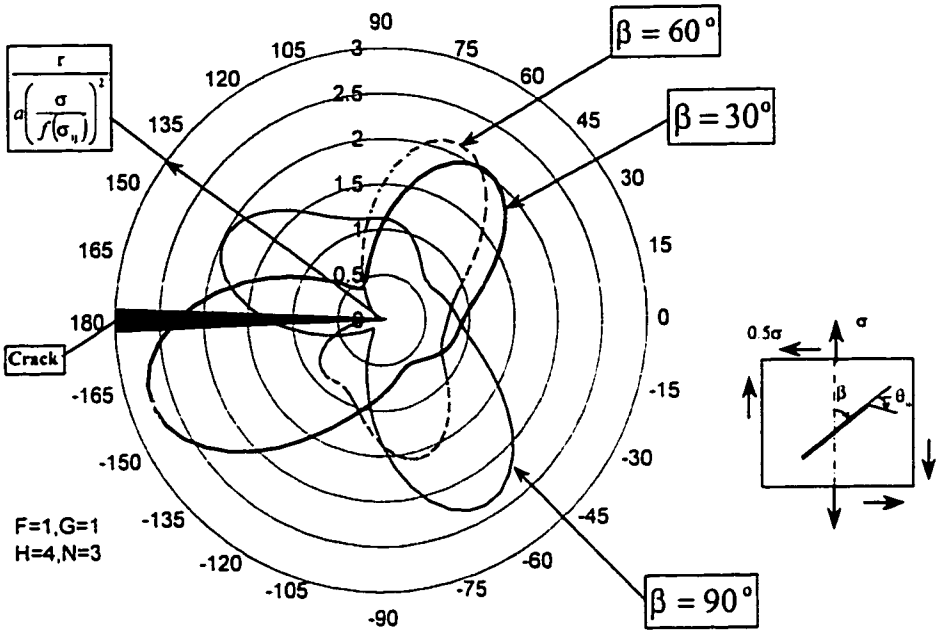

Fig. 4.8a: Core region, Proportional tension torsion loading α = -0.5 , plane stress, F=1,G=1,H=4,N=3

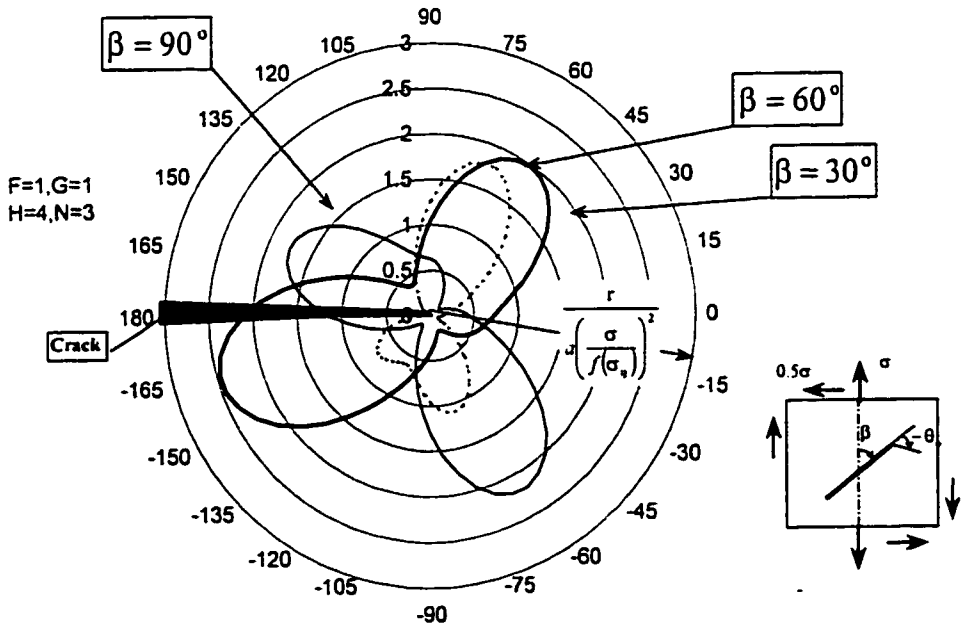

Fig. 4.8b: Core region, Proportional tension torsion loading α = -0.5 , plane strain, F=1,G=1,H=4,N=3

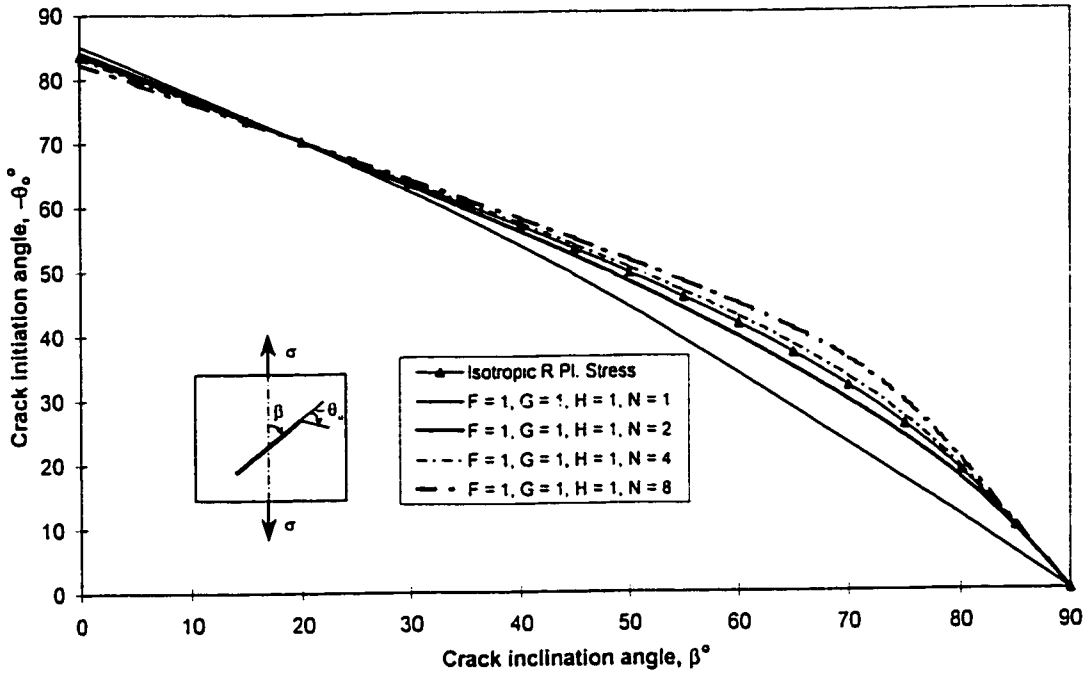

Fig. 4.9a: Uniaxial tension, plane stress, Effect of N

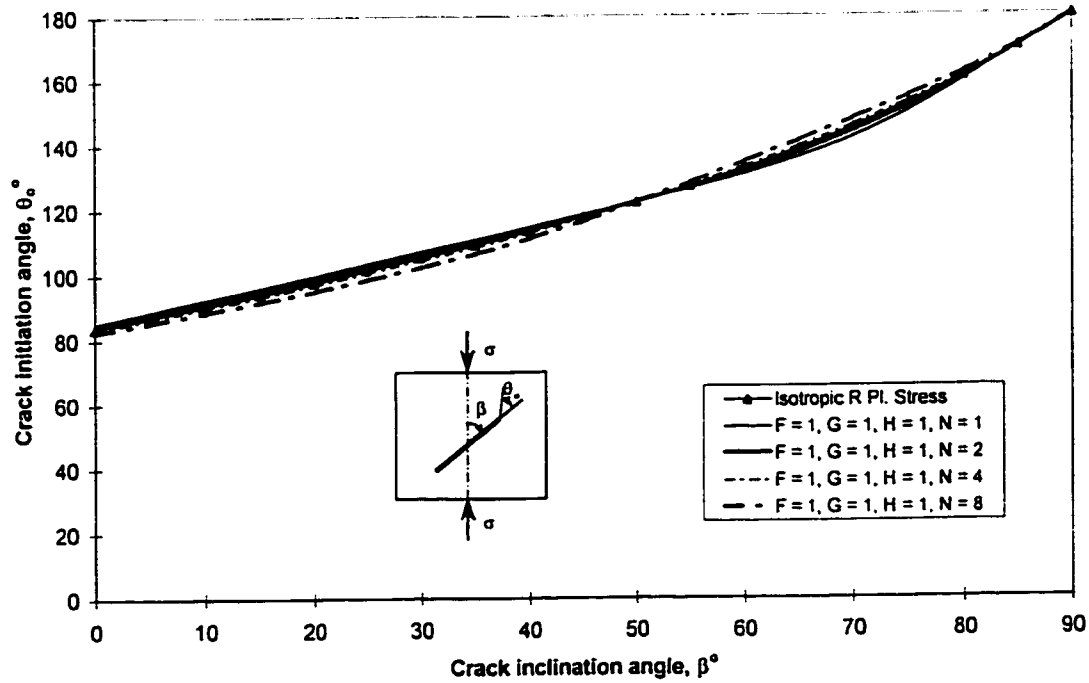

Fig. 4.9b: Uniaxial compression, plane stress, Effect of N

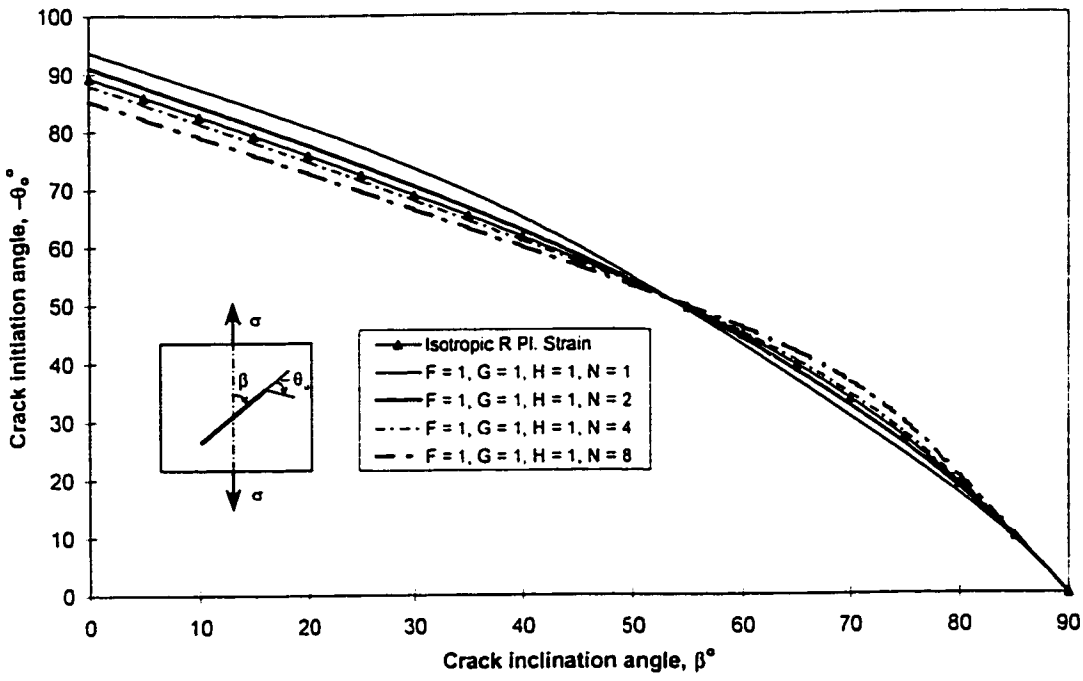

Fig. 4.10a: Uniaxial tension, plane strain, Effect of N

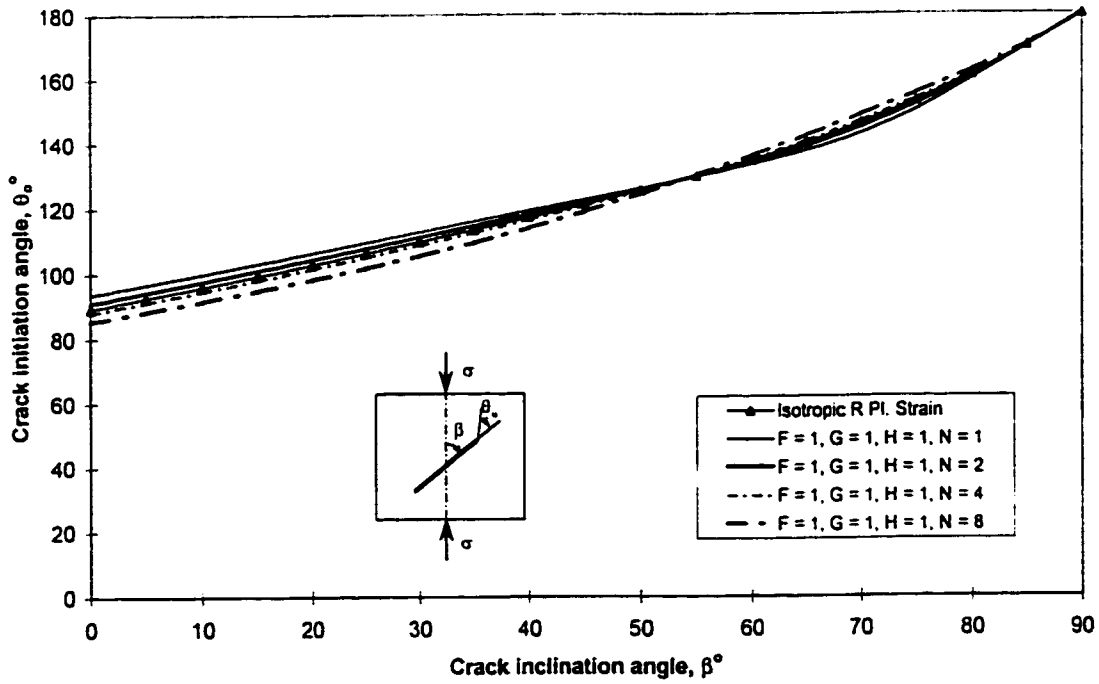

Fig. 4.10b: Uniaxial compression, plane strain, Effect of N

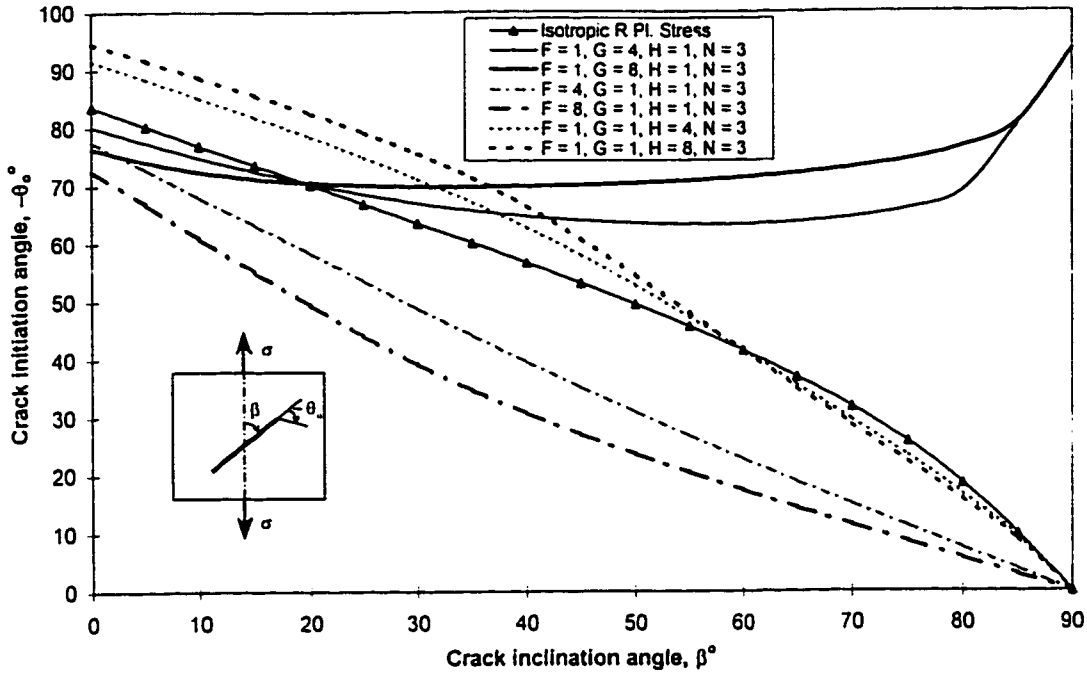

Fig. 4.11a: Uniaxial tension, plane stress, Effect of F, G, H

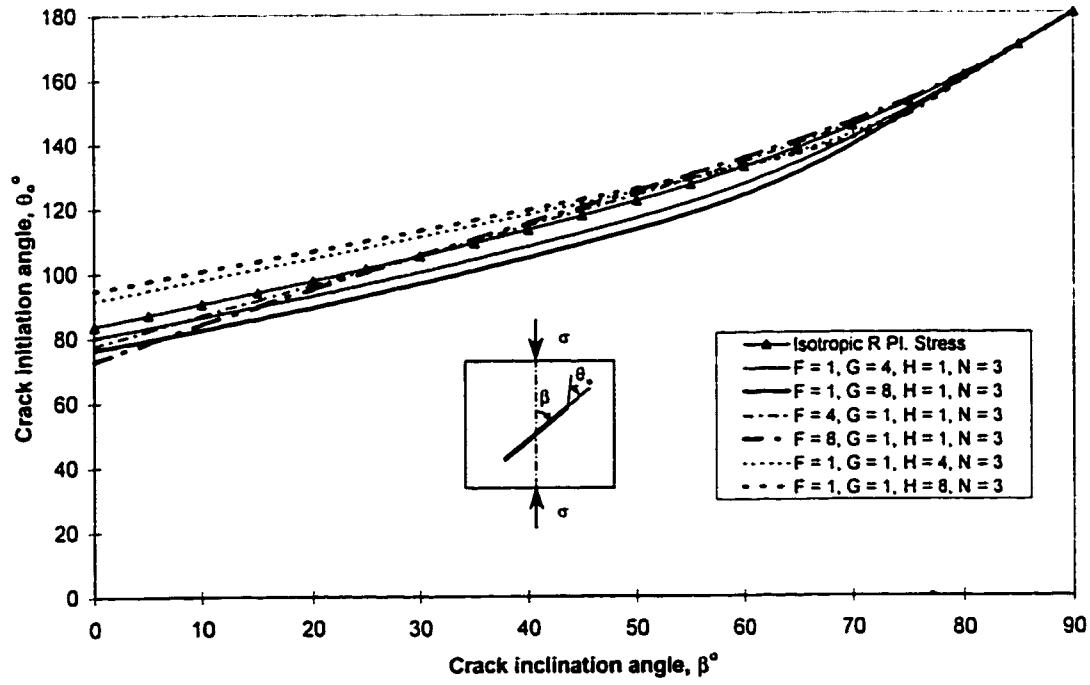

Fig. 4.11b: Uniaxial Compression, plane stress, Effect of F, G, H

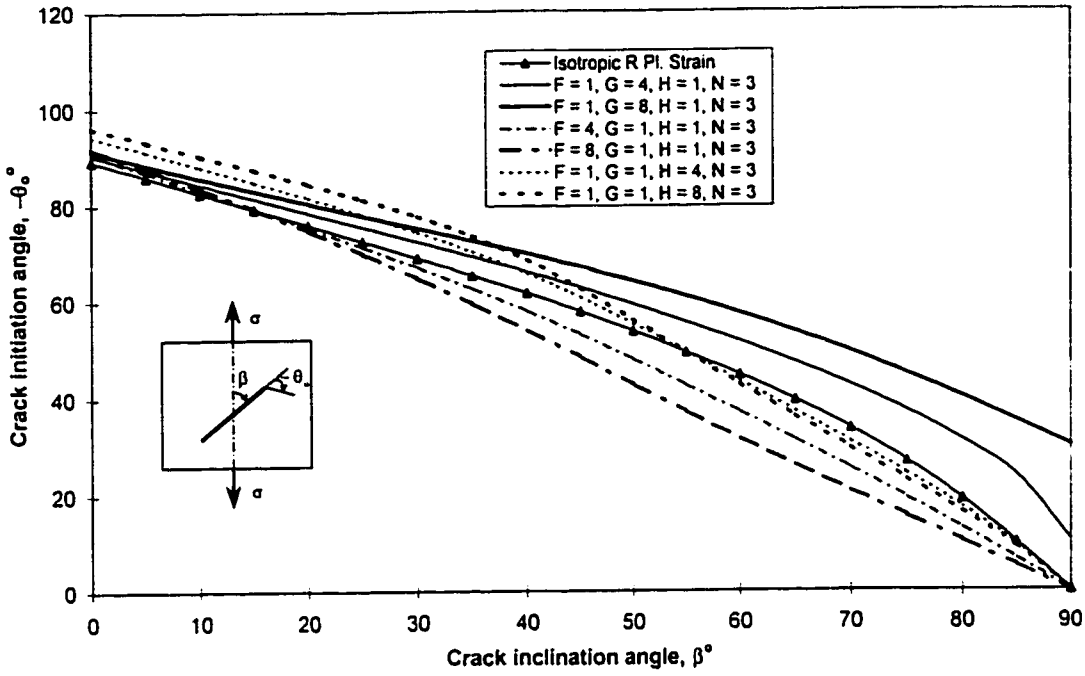

Fig. 4.12a: Uniaxial tension, plane strain, Effect of F, G, H

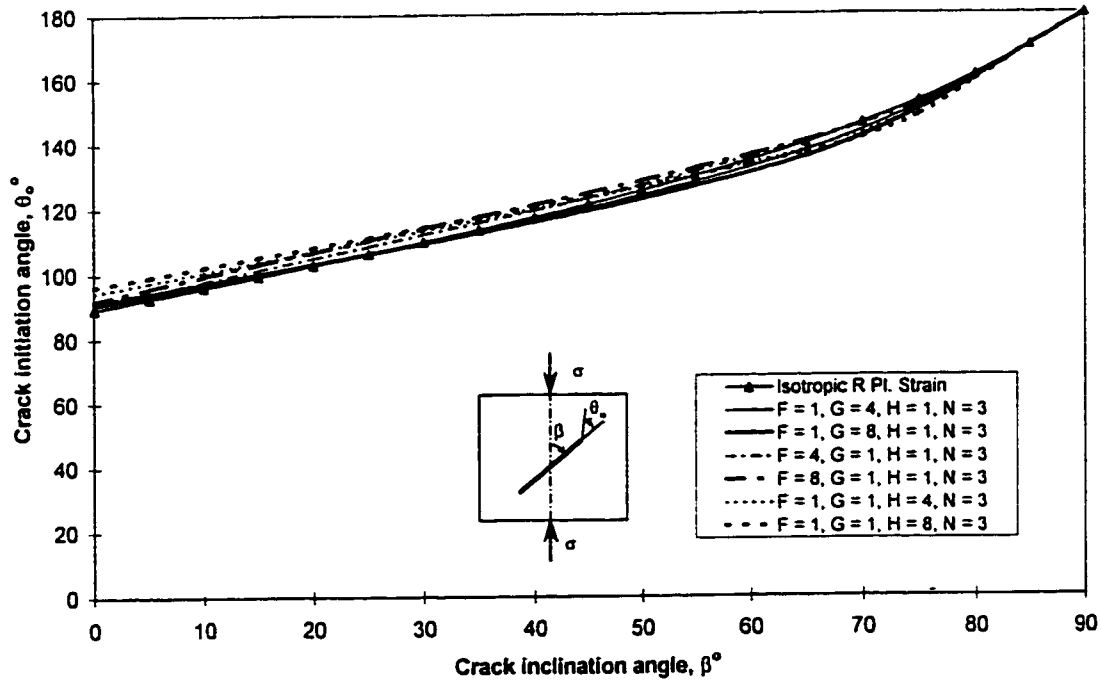

Fig. 4.12b: Uniaxial Compression, plane strain, Effect of F, G, H

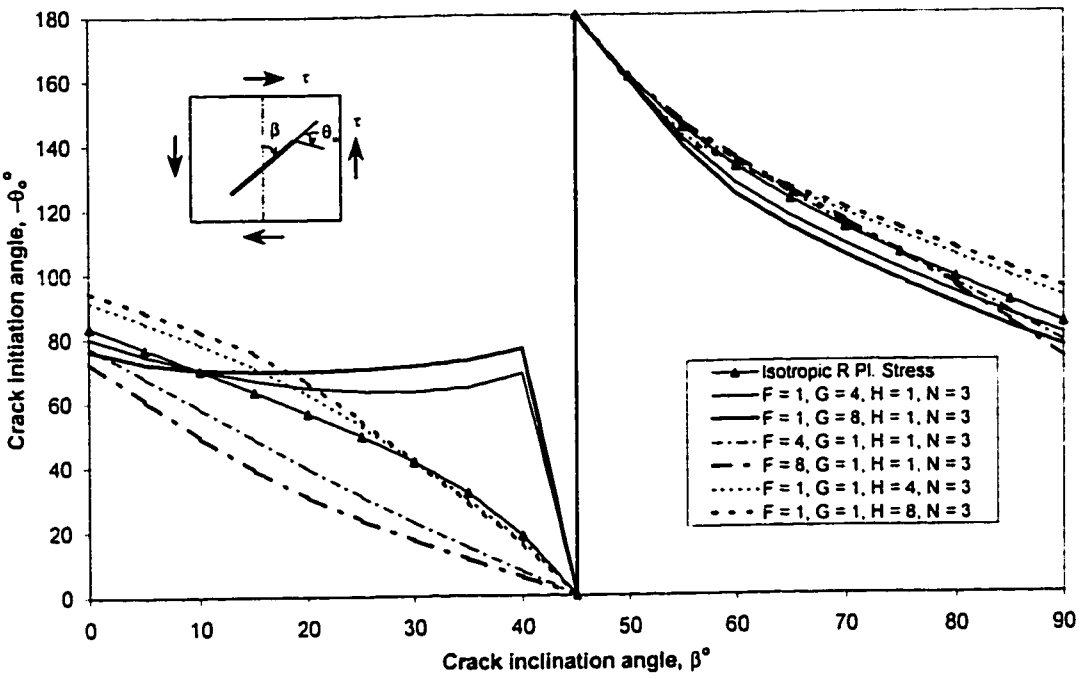

Fig. 4.13a: Pure shear, plane stress, Effect of F, G, H

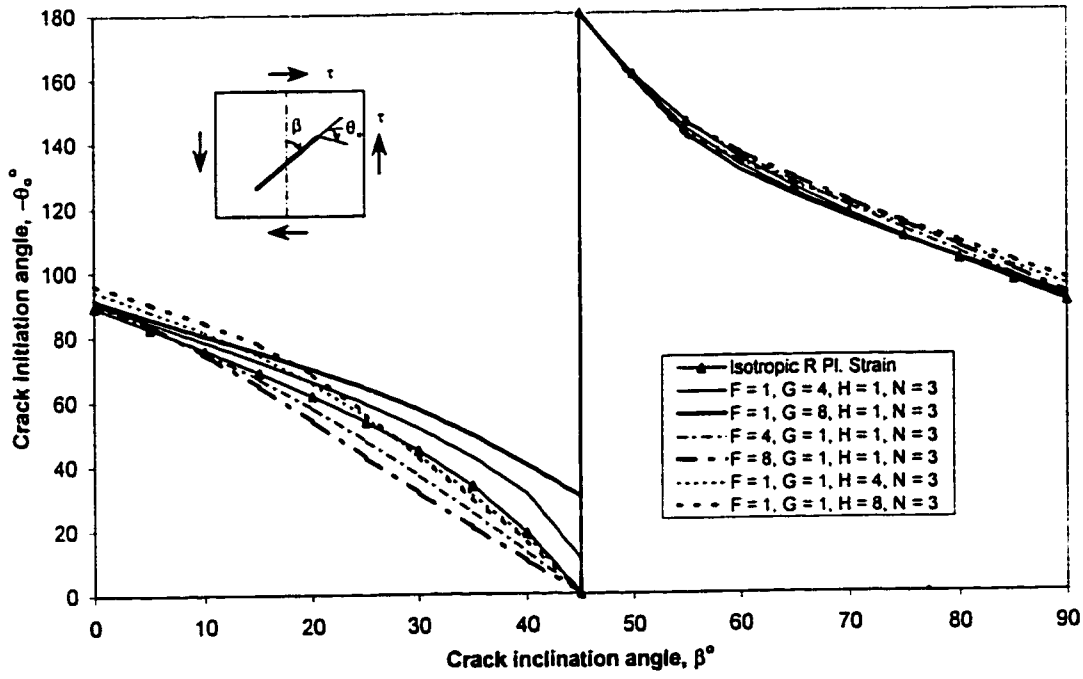

Fig. 4.13b: Pure shear, plane strain, Effect of F, G, H

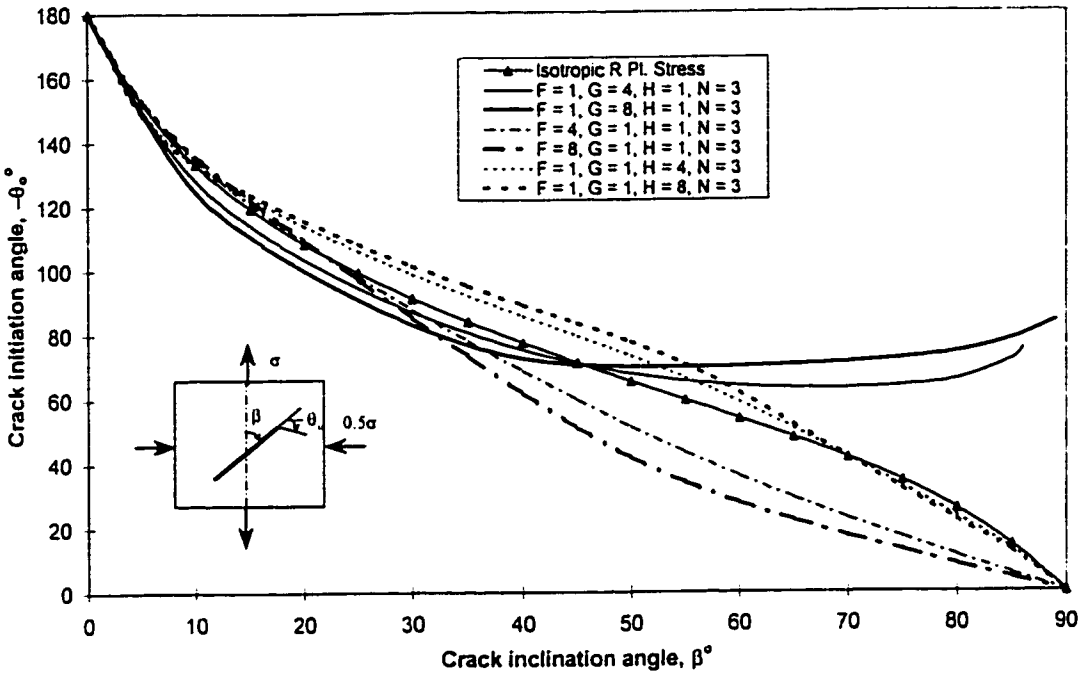

Fig. 4.14a: Biaxial loading $\lambda = -0.5$, plane stress, Effect of F, G, H

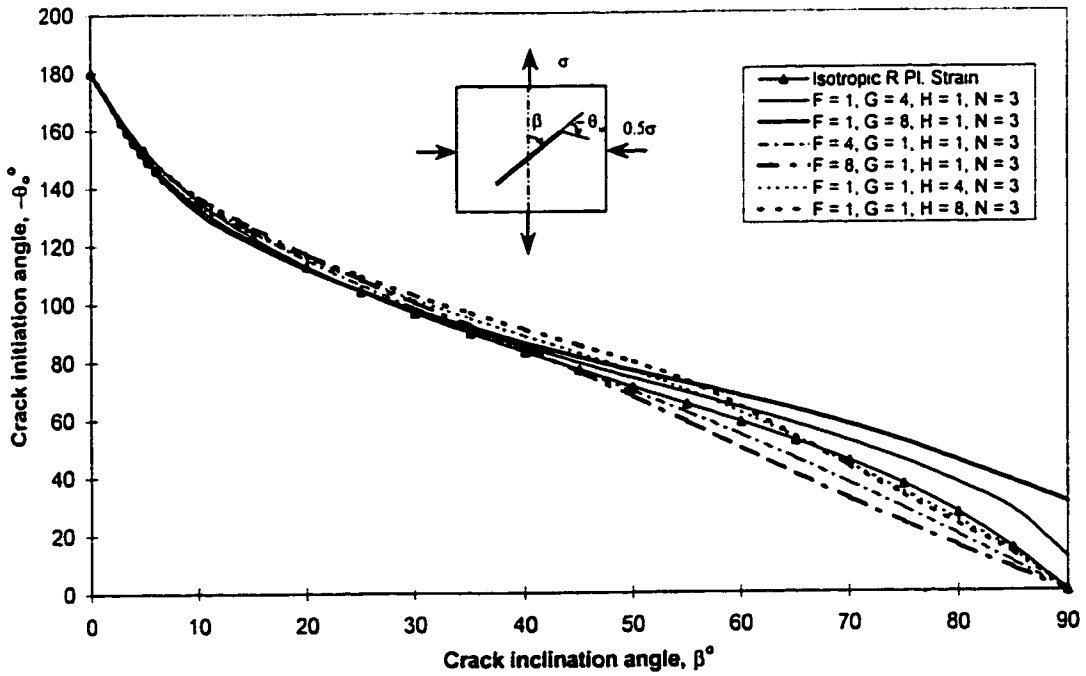

Fig. 4.14b: Biaxial loading $\lambda = -0.5$, plane strain, Effect of F, G, H

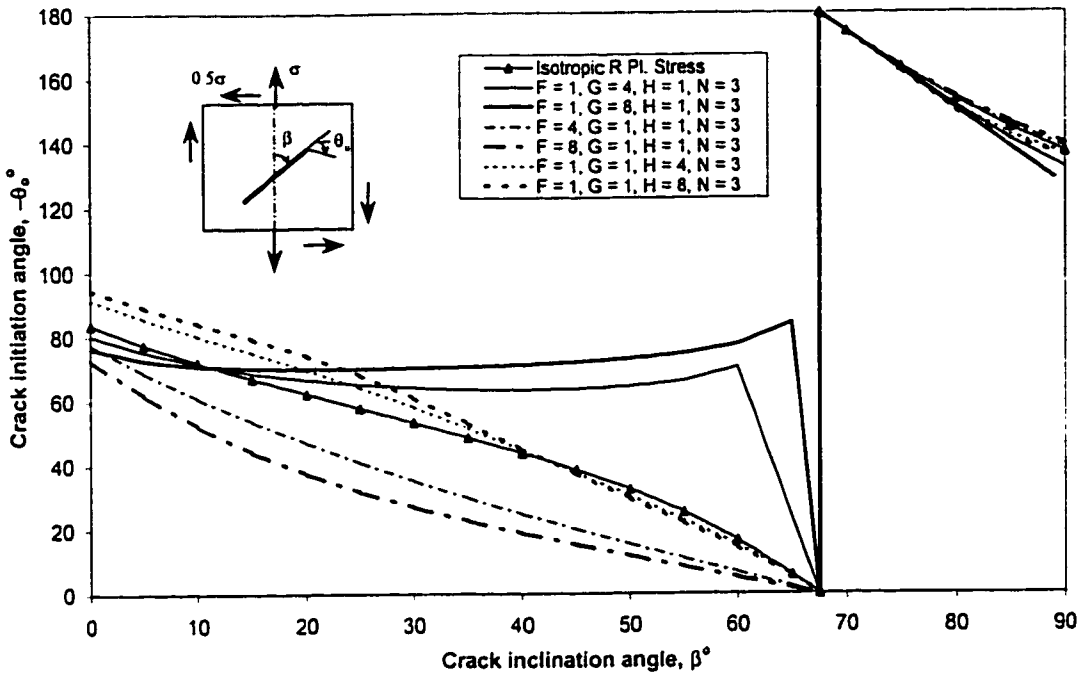

Fig. 4.15a: Proportional tension torsion loading α = -0.5, plane stress, Effect of F, G, H

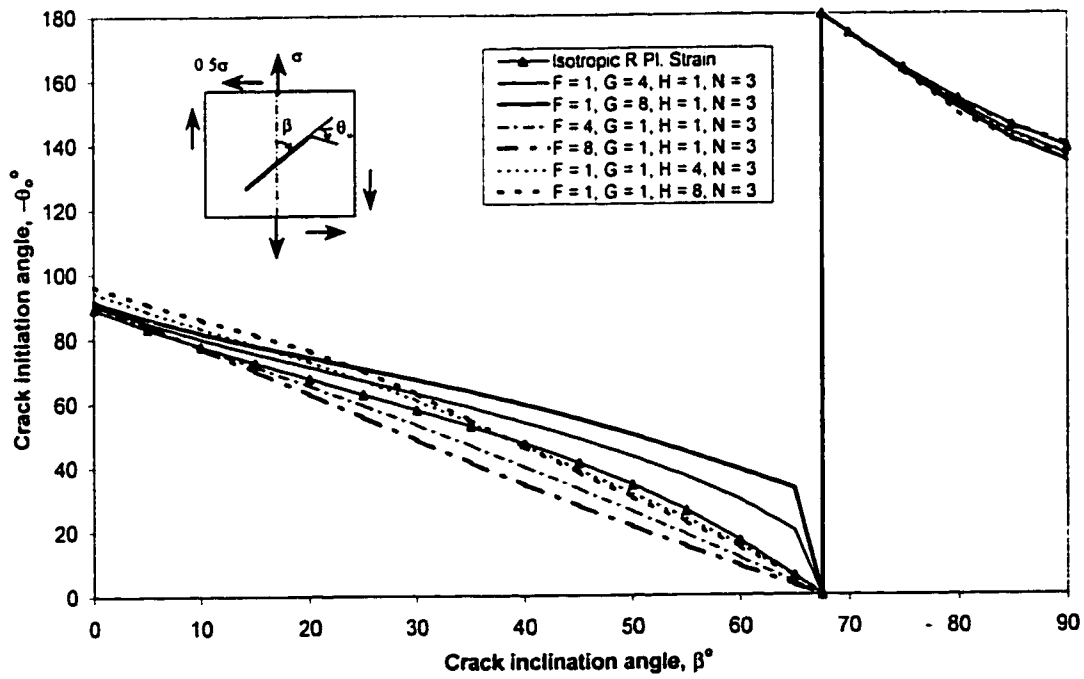

Fig. 4.15b: Proportional tension torsion loading α = -0.5, plane strain, Effect of F, G, H

Chapter 5

Investigation of Experimental Setups and Recommendations

5.1 Introduction

Theoretical and analytical analysis always need the support of experimental evidence to prove its engineering importance and stay alive in scientific literature. The field of experimentation have always been challenging for researchers in any field. There are no assumptions in experiments, one has to face the real situation. Theoretical analysis is always based on some assumptions. To be able to compare the experimental results with theoretical predictions, the assumptions made for theoretical analysis must be met by the experimental setup as close as possible.

The experiments for mixed mode fracture initiation present several problems from formation of initial crack to the measurement of initial direction of crack extension precisely. Many of such issues will be studied in this chapter. The experimental setups used by many researchers will be analyzed in details with reference to specimen

preparation, loading condition, initiation angle measurement, and crack type. At the end, some recommendations will be presented.

5.2 Available Experimental Setups

The first mixed mode crack initiation criterion was presented by Erdogan and Sih (1963), and the first set of experimental data for crack initiation angles with different crack inclination angles also comes from them. The experimental setup information is completed after consulting Erdogan et al. (1962) and Sih (1974), and is shown in Table 5.1.

Specimen material	Polymethylmethacrylate (PMMA) (Commercial name, plexiglass)
Specimen dimensions	18x9x3/16 inch^3 (458x229x5 mm^3)
Crack type	Central slit crack
Crack dimension	2 inch (51 mm) full crack length
Fracture state	Brittle
Crack inclination angles	30° to 80° with an increment of 10°
Testing machine	Not mentioned
Loading type	Uniaxial tension
Displacement rate	Not mentioned
Testing conditions	Not mentioned
Crack initiation angle measurement technique	Not mentioned

Table 5.1: Summary of experimental setup for Erdogan and Sih(1963)

Plexiglass was selected because of various reasons. It is a good approximation to a homogenous, isotropic, and linearly elastic ideal brittle material. Being a transparent material, it is easy to detect faulty crack tips, and to detect the crack initiation accurately.

Specimens are easy to prepare and put natural cracks in. Cracks were formed by cutting a slit with a jeweler's saw, placing a wedge in the slit, and tapping slightly to open a natural crack.

The second set of extensive experimental data is from Williams and Ewing (1972). Their experimental setup is summarized in Table 5.2.

Specimen material	Polymethylmethacrylate (PMMA)
Specimen dimensions	12x6x1/8 inch^3 (304x152x3 mm^3)
Crack type	Central slit crack
Crack dimension	Various dimensions
Fracture state	Brittle
Crack inclination angles	0^o to 90^o with an increment of 5^o
Testing machine	Instron
Loading type	Uniaxial tension - pin loaded via bolted clamps and universal joints
Displacement rate	0.2 inch/min (5 mm/min)
Testing conditions	20°C with 50% relative humidity
Crack initiation angle measurement technique	Projection microscope with 25x magnification

Table 5.2: Summary of experimental setup for Williams and Ewing(1972)

The initial cracks were formed by three different methods. The first set had a 1/4" (6.35 mm) diameter central hole with a 1/32" (0.8 mm) wide slits sawn in at the required angles, and forming cracks at the ends. The second set was made by milling in 1/16" (1.6 mm) wide slots and forming the ends of those into cracks. The third set was made by machining in with a 0.01" (0.254 mm) side slitting saw. In all cases, the ends of the cracks were formed by forcing a razor blade into the ends of the slits to form a natural

crack. Four different half lengths 0.3" , 0.5", 0.7", and 1.0" (7.62, 12.7, 17.8, 25.4 mm) were used with a 10% variations in these lengths due to difficulty in controlling the length. The value of crack inclination angle could not be fixed precisely, because the natural crack could never be grown at an angle identical with the initial slot, and differences of up to 2^{o} were found. In all cases, the angle of the crack, i.e., the tip was used.

The fracture angle was measured using a projection microscope with 25x magnification. The image showed a band with the upper and lower edges giving different values of crack initiation angle. These angles were measured within 1^{o}, and the variation between them was rarely more than 3^{o}. The reason for the difference is that if the initial crack front is not precisely normal to the sheet surface, then one edge moves before the other.

The only set of experiments under torsion comes from Ewing and Williams (1974). This does not cover much details on experimental setup. The tests were performed using a circular tube of PMMA loaded under torsion. The outside diameter of the tube was 89 mm and thickness was 6.35 mm, with cracks of different lengths set at various crack inclination angles to the tube axis. Both the crack length and crack inclination angles are not mentioned. The machine used was a conventional Avery Torsion machine, and the loading time was kept at approximately 75 seconds.

Ewing et al. (1976) presented the experimental results for edge cracks in plates under uniaxial tension and pure bending loading. The experimental technique is the same as for Williams and Ewing (1972), with specific values summarized in Table 5.3.

Specimen material	Polymethylmethacrylate (PMMA) ($E = 2x10^3$ MPa, $\nu = 0.43$)
Specimen dimensions	120x50x3 mm^3 for simple tension 200x50x6 mm^3 for pure bending
Crack type	Edge slit crack
Crack dimension	Not mentioned
Fracture state	Brittle
Crack inclination angles	15° to 86° for simple tension 14.25° to 88.6° for pure bending without any regular increment
Testing machine	Instron
Loading type	Uniaxial tension - pin loaded via bolted clamps and universal joints Pure bending - four point bending apparatus attached to the crosshead of the Instron machine
Displacement rate	5 mm/min
Testing conditions	20°C with 60% relative humidity
Crack initiation angle measurement technique	Projection microscope with 25x magnification

Table 5.3: Summary of experimental setup for Ewing et al.(1976)

The cracks were formed by sawing 1 mm wide slits at the required angles and forcing a razor blade into the end of the slit for forming a natural crack. The crack tip was symmetrically disposed with respect to the lengthwise dimension. The crack initiation angles were measured in the same way and with the same accuracy as for Williams and Ewing (1972).

The only set of experimental data for ductile fracture comes from Theocaris et al. (1982). They performed mixed mode crack initiation experiments in order to support their

proposed criterion, the T-criterion. The details of their experimental setup is given in Table 5.4.

Specimen material	Polycarbonate of Bisphenol A (PCBA)
Specimen dimensions	300x90x1.5 mm^3
Crack type	Central slit crack
Crack dimension	16 mm full crack length
Fracture state	Ductile
Crack inclination angles	10^o to 90^o with an increment of 10^o, with addition of 5^o and 45^o
Testing machine	Not mentioned
Loading type	Uniaxial tension
Displacement rate	Not mentioned
Testing conditions	Not mentioned
Crack initiation angle measurement technique	Projection lamp with 25x magnification

Table 5.4: Summary of experimental setup for Theocaris et al.(1982)

The crack was cut by 0.3 mm wide saw at the required angle of inclination. In all cases, the ends of cracks were smoothed by a diamond wire of 0.2 mm diameter in order to eliminate any initial directional preferences.

Kong et al. (1995) performed experiments on steel, but there is not enough information provided about the experimental setup. They used steel FeE 550, at -140°C and with high loading speed of 50 mm/sec to ensure brittle fracture. They used CCT-specimen.

Vallejo (1987) provided the experimental data for mixed mode crack initiation angles under uniaxial compression. The experimental setup is shown in Table 5.5.

Specimen material	Kaolinite Clay
Specimen dimensions	76.2x76.2x25.4 mm^3
Crack type	Central slit crack
Crack dimension	25 mm full crack length
Fracture state	Brittle and ductile
Crack inclination angles	15^o to 75^o with an increment of 15^o
Testing machine	Not mentioned
Loading type	Uniaxial compression
Displacement rate	5 mm/min
Testing conditions	Not mentioned
Crack initiation angle measurement technique	By taking photographs

Table 5.5: Summary of experimental setup for Vallejo(1987)

Dry kaolinite clay was mixed with distilled water to form a soft soil mass with a water content of 40%. After mixing, the clay water mixture was consolidated under a normal pressure of 25.7 kPa for a period of 5 days. The diameter of consolidometer was 300 mm. After unloading the consolidometer, specimen were cut from the clay block.

Immediately after cutting the prismatic samples, when the water content was about 30%, cracks were made in by a process of inserting and removing thin glass sheets 1 mm in thickness and 2.5 cm in width in a direction normal to the sample face. Five different water contents were developed in the samples by allowing these to air dry after the cracks were made. The water contents used are 27, 22, 15, 9, and 3 percent. Specimen with water content of greater than 20% behave like ductile materials while other with water content less than 20% showed brittle behavior.

To measure the angles, photographs were taken during and after the specimen were subjected to the compression tests. From these photos, the direction of crack initiation was measured.

Wu et al. (1977) performed uniaxial tension experiments on plates with angled elliptic notches. Experimental setup details are given in Table 5.6.

Specimen material	Polymethylmethacrylate (PMMA)
Specimen dimensions	380x152x3.2 mm^3
Crack type	Central elliptic notch
Crack dimension	12.7 mm semi-major length 2.5 mm semi-minor length
Fracture state	Brittle
Crack inclination angles	0° to 90° with an increment of 15°
Testing machine	Universal testing machine
Loading type	Uniaxial tension
Displacement rate	1.27 mm/min
Testing conditions	Room temperature
Crack initiation angle measurement technique	Microscope 50x magnification

Table 5.6: Summary of experimental setup for Wu et al.(1977)

Notches were machined using electric drills, files, 400 and 600 grades silicon carbide wet or dry paper. All specimen were annealed at 230°F for 2 hours, and overcooled for 45 minutes before testing. Strain gauges were glued to the specimen to insure that no misalignment of the tensile load is introduced.

5.3 Discussions and Recommendations

Many factors that influence the mixed mode crack initiation experiments can be summarized as:

Theoretical analysis assume the radius of the crack tip as zero, whereas for real specimen there is always a finite radius. Polymers offer the most suitable materials for mixed mode crack initiation problem, through their ease of machining. The most suitable method for producing a crack is to extend already formed slits using a sharp edge. The sharper the edge, the more the radius will approach zero. To make sure that cracks in all specimen are of same length and perpendicular to specimen surface, a fixture can be used.

It is relatively difficult to perform experiments using steels. Perhaps the most useful suitable method of creating a central crack is the electrochemical machining process, as used by Finnie and Weiss (1974).

Size of the crack is governed by the specimen size and manufacturing process accuracy. Smaller cracks are limited by the manufacturing problems, and larger cracks are limited due to finite width effects.

The specimen may have some residual stresses due to the crack formation process. These residual stresses can be removed by annealing the prepared specimen. In addition, the crack may show a preferred direction of initial extension due to irregularity/roughness at the crack tip. This problem can be solved by smoothing out the crack tip using some suitable filing process.

Cracks should be made perpendicular to the specimen surface all through the width otherwise the two crack tips will show different crack initiation angles on both sides of specimen surface. In such case, an average value of the four crack initiation angles may be used for small deviations.

Specimen must be loaded without any misalignment of the load. This can be done by using strain gauges on specimen. In addition, the crack initiation angle measuring technique must be thoroughly investigated. Latest technology of digital imaging may be used for accurate measurement of the crack initiation angles.

Another important issue is to perform pure mode-II experiments. In this respect the work of Erdogan and Sih(1963) and Williams and Birch(1976) can be consulted.

5.4 Conclusions

There are many issues regarding mixed mode crack initiation experiments that need attention. A standardization of typical parameters involved in experiments is needed.

1. The loading rate or strain may have an effect on crack initiation angle. A low strain rate employs a ductile fracture in most cases. Most of the experimental studies, available so far, have been done using polymers with low strain rates (~5mm/min). However, experiments using steels will definitely require a higher strain rate as used by Kong et al.(1995)

2. The dominant state of stress, whether plane stress or plane strain, should be specified with the experimental results, so that these may be compared with the criteria that depend on stress state at the crack tip, such as the S-criterion and the R-

criterion. In addition, the value of Poisson's ratio should be taken into account for comparison purposes.

3. The method of measurement of the crack initiation angle also need attention. Latest technology of digital imaging will provide more accurate measurement of the crack initiation angles as compared to conventional techniques such as projection microscope with magnification.

Chapter 6

Conclusions and Recommendations

6.1 Conclusions

A lot of research is going on in the field of fracture mechanics. This field of mechanics has now well based infrastructure, however, it still needs much work to be able to define, explain, and predict the behavior of engineering components and structure under general state of loading. The problem of crack initiation angle has received a lot of attention for uniaxial loading cases. However, there is scarce theoretical and experimental analysis, for explaining crack initiation under different loading conditions, including pure shear, biaxial, combined tension-torsion loading cases. This issue have been investigated in this research, and different factors that affect the crack initiation angles are analyzed. Several conclusions are drawn.

The crack behavior can be best explained on the basis of the resultant stresses, normal and tangential, to the crack face. Crack behavior under uniaxial loading is helpful in analyzing the other cases of loading.

The available experimental data is limited and does not favor any criterion over other for all loading conditions. For uniaxial case, the experimental results are in good agreement with most criteria for higher crack inclination angles. For low inclination angles, no particular criterion is favored. Also, the experimental data is somewhat confusing in terms of brittle and ductile behavior of materials used for testing. In addition, the loading rate, the state of stress at the crack tip, and material elastic properties are not reported for all the experimental results available in the open literature. Experimental setups used by different researchers are investigated. The method of introducing initial cracks in specimens vary largely, and this may affect the observed crack initiation angles between two studies.

Modified MTS-criterion, obtained by introducing a variable core region radius based on von Mises yield criterion in the formulation of the MTS-criterion, presents better fit to experimental data than the original MTS-criterion for uniaxial tension case. However, original MTS-criterion is better in case of uniaxial compression.

The core region radius is a function of crack inclination angle β, polar polar θ, and the loading ratio in case of proportional loading cases. It is also the function of the Poisson's ratio ν for plane strain case. The actual size of the core region depends on the initial half crack length, and the ratio of the applied stress to the yield strength of the material.

Based on the observation that crack initiation angles tend to follow the minima of the core region obtained by employing con Mises yield function, the R-criterion is proposed, which predicts crack initiation in direction of minimum core region radius. The R-criterion is simple as compared to other criterion for ductile behavior such as the T-criterion.

Core regions are investigated for anisotropic behavior using the Hill's anisotropic yield function, and good results are obtained. The R-criterion is also modified using Hill's anisotropic yield function to be applicable to anisotropic behavior of materials. Specific values of anisotropic constants, appearing in Hilll's anisotropoic yield function, can be obtained for any particular material through parametric studies.

6.2 Recommendations

Every research is intended to resolve some issues, and at the same time, some new issues are also unveiled. Some of the factors, that are considered to need attention in this field of research are as follows.

For uniaxial loading and for crack inclination angle equal to 0°, the crack is aligned with the applied load. The crack initiation angles predicted for this configuration are same as for pure mode-II. However, this configuration does not present a pure mode-II loading case. This needs explanation.

For biaxial loading case and for crack inclination angle either equal to 0°-or 90°, the crack is perpendicular to either of the axes. For this configuration, the crack behavior is completely under the stress perpendicular to it, and it seems that the normal stress on other face has no effect on crack initiation angles this needs to be investigated.

Experimental studies need to be done under different loading conditions, and in relation to material elastic properties such as the Poisson's ratio. In addition, the effect of the loading rate and the state of stress (plane stress or plane strain) must be considered. The method of specimen preparation, especially the method of introducing a sharp inclined crack, needs to be standardization for a central crack configuration.

The effect of initial half crack length a on crack initiation angles has not been investigated. From a mathematical point of view, the crack length has no effect on the crack initiation angles, when a singular elastic stress field is used. However, if the higher order terms (non-singular) are considered in the stress function described by Williams(1957), then the crack length a does not vanishes from the final equations for any criterion. Therefore, one can use such equations to study the effect of the crack length on the crack initiation angle. As an example, to use MTS-criterion, one can use the following equation for tangential stress. The second and higher terms are non-singular.

$$\sigma_\theta = \left(\frac{a}{2r}\right)^{\frac{1}{2}} \cos\frac{\theta}{2}\left(p_y \cos^2\frac{\theta}{2} - \frac{3p_{xy}}{2}\sin\theta\right) + p_x \sin^2\theta + \left(\frac{2r}{a}\right)^{\frac{1}{2}} F(p_x, p_{xy}, \theta) + \ldots\ldots$$

(Williams and Ewing, 1972)

The R-criterion, so far, predicts only the direction of crack initiation. More work is needed to make the R-criterion capable of predicting the fracture load. Many researchers (Theocaris et al.,1982; Yehia, 1991) have proposed that critical load for crack initiation can be obtained by equating the minimum radius of the elastic-plastic core region to a critical radius r_{cr}, which is defined on pure mode-I loading as:

$$r_{cr} = \frac{K_I^2}{2\pi\sigma^2} \qquad \text{plane stress}$$

$$r_{cr} = \frac{K_I^2}{2\pi\sigma^2}(1-2\nu)^2 \qquad \text{planestrain}$$

This seems incorrect since the critical condition for a crack under mixed mode loading must be derived by a critical value based on mixed mode loading. Using the R-criterion, the critical load may be related to the actual distance from the crack tip to the elastically loaded material. This actual distance can be calculated by using the non-dimensional relation for the core region as given in this research. By calculating the energy required by the crack tip to travel through this distance, one can relate to the critical load for crack initiation.

After we get crack initiation angle, another important issue is to simulate the crack propagation path. First of all, the initial direction of crack extension and the amount of extension (incremental increase in crack length) is calculated, using the elastic stress field. Based on new crack length and load, the stress intensity factors are updated, and the new crack initiation angle and crack extension is calculated based on updated elastic stress field. In this way, the crack propagation path can be simulated

References

1. Anderson, T. L., 1991, "Fracture Mechanics: Fundamentals and Applications", CRC Press.

2. Andrianopolous, N. P., 1986, "Discussion on the use of the T-criterion in fracture mechanics", Eng. Fracture Mech., Vol.24, No.4, pp.635-636.

3. Andrianopolous, N. P., 1992, "Discussion, Author's closure on the discussion by N. A. B. Yiehia of LEFM brittle and ductile fractures as described by the T-criterion", Eng. Fracture Mech., Vol.41, No.5, pp.785.

4. Andrianopolous, N. P., and Theocaris, P. S., 1988, " LEFM brittle and ductile fractures as described by the T-criterion", Eng. Fracture Mech., Vol.30, No.1, pp.5-12.

5. Awaji, H., 1998, "The Griffith criterion for mode II fracture", Int. J. of Fracture, Vol.89, pp.L3-L7.

6. Broek, D., 1982, "Elementary Engineering Fracture Mechanics", Martinus Nijhoff Publishers.

7. Chang, K. J., 1982, "A further examination on the application of the strain energy density theory to the angled crack problem", J. of Applied Mechanics, Vol.49, pp.377-382.

8. Erdogan, F., and Sih, G. C., 1963, "On the crack extension in plates under plane loading and transverse shear", J. of Basic Eng., Vol.85, pp.519-527.

9. Erdogan, F., Tuncel, O., and Paris, P. C., 1962, "An experimental investigation of the crack tip stress intensity factors in plates under cylindrical bending", J. of Basic Eng., Vol.84, pp.542-546.

10. Ewing, P. D., and Williams, J. G., 1974, "The fracture of spherical shells under pressure and circular tubes with angled cracks in torsion", Int. J. of Fracture, Vol.10, No.4, pp.537-544.

11. Ewing, P. D., Swedlow, J. L., and Williams, J., G., 1976, "Further results on the angled crack problem", Int. J. of Fracture, Vol.12, No.1, pp.85-93.

12. Finnie, I., and Weiss, H. D., 1974, " Some observations on Sih's strain energy density approach for fracture prediction", Int. J. of Fracture, Vol.10, pp.136-139.

13. Gdoutos, E. E., 1984, "Problems of mixed mode crack propagation", Martinus Nijhoff Publishers.

14. Gdoutos, E. E., and Zacharopoulos, D. A., 1989, "Mixed-Mode crack growth in anisotropic media", Vol.34, No.2, pp.337-346.

15. Griffith, A. A., 1921, "The phenomenon of rupture and flow in solids", Phil. Trans. Royal Soc., Vol.A221, pp.163-198.

16. Hartranft, R. J., Sih, G. C., 1977, "Stress singularity for a crack with an arbitrarily curved front", Engng Fracture Mechanics, Vol.9, pp.705-718.

17. Hertzberg, R. W., 1996, "Deformation and fracture mechanics of engineering materials", John Wiley & Sons Inc.

18. Hosford, W. F., and Caddell, R. M., 1993, "Metal Forming", Prentice-Hall Inc.

19. Hussain, M. A., Pu, S. L., and Underwood, J., 1974, "Strain energy release rate for a crack under combined mode I and Mode II", Fracture Analysis ASTM STP 560, pp.2-28.

20. Jendoubi, K., Ranganathan, N., and Merah, N., 1991, "Effect of thickness on elasto-plastic deformation and hysteretic energy dissipated at crack tip", J. of Testing and Evaluation, Vol.19, No.3, pp.201-209.

21. Kassir, M. K., Sih, G. C., 1966, "Three-dimensional stress distribution around an elliptical crack under arbitrary loadings", J. of Applied Mechanics, Vol.33, pp.601-611.

22. Kipp, M. E., Sih, G. C., 1975, "The strain energy density failure criterion applied to notched elastic solids", Int. J. Solids Structures, Vol.11, pp.153-173.

23. Kong, X. M., Schluter, N., and Dahl, W., 1995, "Effect of triaxial stress on mixed-mode fracture", Eng. Fracture Mech.,Vol.52, No.2, pp.379-388.

24. Maiti, S. K., and Smith, R. A., 1983, "Comparison of the criteria for mixed mode brittle fracture based on the preinstability stress-strain field, Part I: Slit and elliptical cracks under uniaxial tensile loading", Int. J. of Fracture, Vol.23, pp.281-295.

25. Plank, R., and Kuhn, G., 1999, "Fatigue crack propagation under non-proportional mixed mode loading", Eng. Fracture Mech., Vol.62, pp.203-229.

26. Ranganathan, N., Jendoubi, K., and Merah, N., 1994, "Experimental characterization of the elastic-plastic strain fields at the crack tip due to cyclic loading", J. of Eng. Mat. and Technology, Vol.116, pp.187-192.

27. Saouma, V. E., Ayari, M. L., and Leavell, D. A., 1987, "Mixed mode crack propagation in homogeneous anisotropic solids", Eng. Fracture Mech., Vol.27, No.2, pp.171-184.

28. Selcuk, S., Hurd, D. S., Crouch S. L., and Gerberich, W. W., 1994, "Prediction of interfacial crack path: a direct boundary integral approach and experimental study", Int. J. of Fracture, Vol.67, pp.1-20.

29. Sih, G. C., 1973, "Some basic problems in fracture mechanics and new concepts", Eng. Fracture Mech., Vol.5, pp.365-377.

30. Sih, G. C., 1974, "Strain-energy-density factor applied to mixed mode crack problems", Int. J. of Fracture, Vol.10, No.3, pp.305-321.

31. Sih, G. C., Paris, P. C., and Erdogan, F., 1962, "Crack-tip stress intensity factors for plane extension and plate bending problems", J. of Applied Mechanics, Vol.29, pp.306-312.

32. Theocaris, P. S., 1986, "Discussion of 'On the use of the T-criterion in fracture mechanics' by N. A. B. Yehia", Eng. Fracture Mech., Vol.24, No.3, pp.371-382.

33. Theocaris, P. S., and Andrianopoulos, N. P., 1982, "The Mises elastic-plastic boundary as the core region in fracture criteria", Eng. Fracture Mech., Vol.16, No.3, pp.425-432.

34. Theocaris, P. S., and Andrianopoulos, N. P., 1982, "The T-criterion applied to ductile fracture", Int. J. of Fracture,Vol.20, pp.R125-R130.

35. Theocaris, P. S., and Philippidis, T. P., 1991, "Mixed-mode fracture mechanics of anisotropic plates by means of the T-criterion", Vol.52, pp.223-237.

36. Theocaris, P. S., Kardomateas, G. A., and Andrianopoulos, N. P., 1982, "Experimental study of the T-criterion in ductile fracture", Eng. Fracture Mech.,Vol.17, No.5, pp.439-447.

37. Ukadgaonker, V. G., and Awasare, P. J., 1995, "A new criterion for fracture initiation", Eng. Fracture Mech., Vol.51, No.2, pp.265-274.

38. Vallejo, L. E., 1987, "The brittle and ductile behavior of a material containing a crack under mixed-mode loading", 28th US symposium on Rock Mechanics, Tucson 29June-1July 1987, pp383-390.

39. Williams, J. G., 1984, "Fracture Mechanics of Polymers", John Wiley and Sons Inc.

40. Williams, J. G., and Birch, M. W., 1976, "Mixed mode fracture anisotropic media", Cracks and Fracture, ASTM STP 601, pp.125-137.

41. Williams, J. G., and Ewing, P. D., 1972, "Fracture under complex stress – The angled crack problem", Int. J. of Fracture Mechanics, Vol.8, No.4, pp.441-446.

42. Williams, M. L., 1957, "On the stress distribution at the base of a stationary crack", J. of Applied Mechanics", Vol.24, pp.109-114.

43. Wu, H. C., Yao, R. F., and Yip, M. C., 1977, "Experimental investigation of the angled elliptic notch problem in tension", J. of Applied Mech., Vol., pp.455-461.

44. Yan, X., Zhang, Z., and Du, S., 1992, "Mixed-mode fracture criteria for the materials with different yield strengths in tension and compression", Eng. Fracture Mech., Vol.42, No.1, pp.109-116.

45. Yehia, N. A. B,. and Shephard, M. S., 1987, "The NT-criterion for predicting crack growth increments", Eng. Fracture Mech., Vol.26, No.3, pp.371-382.

46. Yehia, N. A. B., 1986, " Crack tip region - could it be a fracture criterion?", Int. J. of Fracture, Vol.31, pp.R25-R28.

47. Yehia, N. A. B., 1990, "Discussion 'LEFM brittle and ductile fractures as described by the T-criterion' by N. P. Andrianopolous and P. S. Theocaris", Eng. Fracture Mech., Vol.35, No.6, pp.1117-1120.

48. Yehia, N. A. B., 1991, "Distortional strain energy density criterion: The Y-criterion", Eng. Fracture Mech., Vol.39, No.3, pp.477-485.

49. Zengtao, C., and Duo, W., 1994, "A note on the fracture criteria for mixed-mode crack problems of materials with different yield strengths in tension and compression", Int. J. of Fracture, Vol.69, pp.R11-R14.

50. Zhang, J. P., and Venugopalan, D., 1987, "Effects of notch radius and anisotropy on the crack tip plastic zone", Eng. Fracture Mech., Vol.26, No.6, pp.913-925.

51. Zhiming, Y., 1995, "Plastic zone characteristics of crack tip in anisotropic solids", Int. J. of Fracture, Vol.74, pp.R3-R10.

52. Zhiming, Y., and Ayari, M. L., 1994, "Prediction of crack propagation in anisotropic solids", Eng. Fracture Mech., Vol.49, No.6, pp.797-808.